

Physics at a Neutrino Factory

C. Albright,^{8,22} G. Anderson,¹⁴ V. Barger,²¹ R. Bernstein,⁸
 G. Blazey,⁸ A. Bodek,²⁰ E. Buckley-Geer,⁸ A. Bueno,⁷
 M. Campanelli,⁷ D. Carey,⁸ D. Casper,¹⁸ A. Cervera,⁶ C. Crisan,⁸
 F. DeJongh,⁸ S. Eichblatt,¹⁴ A. Erner,¹⁴ R. Fernow,³ D. Finley,⁸
 J. Formaggio,⁵ J. Gallardo,³ S. Geer,⁸ M. Goodman,¹ D. Harris,⁸
 E. Hawker,¹¹ J. Hill,¹⁶ R. Johnson,⁹ D. Kaplan,⁹ S. Kahn,³
 B. Kayser,¹³ E. Kearns,² B.J. King,³ H. Kirk,³ J. Krane,¹⁰
 D. Krop,¹⁴ Z. Ligeti,⁸ J. Lykken,⁸ K. McDonald,¹⁵
 K. McFarland,²⁰ I. Mocioiu,¹⁶ J. Morfin,⁸ H. Murayama,¹⁷
 J. Nelson,¹⁹ D. Neuffer,⁸ P. Nienaber,¹² R. Palmer,³ S. Parke,⁸
 Z. Parsa,³ R. Plunkett,⁸ E. Prebys,¹⁵ C. Quigg,⁸ R. Raja,⁸
 S. Rigolin,⁴ A. Rubbia,⁷ H. Schellman,^{14,8} M. Shaevitz,⁸
 P. Shanahan,⁸ R. Shrock,^{3,16} P. Spentzouris,⁸ R. Stefanski,⁸
 J. Stone,² L. Sulak,² G. Unel,¹⁴ M. Velasco,¹⁴ K. Whisnant¹⁰,
 J. Yu⁸, E.D. Zimmerman⁵

¹ Argonne National Laboratory, Argonne, IL 60439

² Boston University, Boston, MA 02215

³ Brookhaven National Laboratory, Upton, NY 11973

⁴ University of Michigan, Ann Arbor, MI 48105

⁵ Columbia University, New York, NY 10027

⁶ Dept. de Física Atomica y Nuclear and IFIC, Universidad de Valencia, Spain

⁷ Institut für Teilchenphysik, ETHZ, CH-8093, Zürich, Switzerland

⁸ Fermi National Accelerator Laboratory, Batavia, IL 60510

⁹ Illinois Institute of Technology, Chicago, IL 60616

¹⁰ Iowa State University, Ames, IA 50011

- 11 *Los Alamos National Laboratory, Los Alamos, NM 87545*
- 12 *Marquette University, Milwaukee, WI 53233*
- 13 *National Science Foundation, Arlington, VA 22230*
- 14 *Northwestern University, Evanston, IL 60208*
- 15 *Princeton University, Princeton, NJ 08544*
- 16 *State University of New York Stony Brook, Stony Brook, NY 11794*
- 17 *Univ. of California Berkeley, Berkeley, CA 94720*
- 18 *University of California Irvine, Irvine, CA 92697*
- 19 *University of Minnesota, Minneapolis, MN 55455*
- 20 *University of Rochester, Rochester, NY 14627*
- 21 *University of Wisconsin, Madison, WI 53706*
- 22 *Northern Illinois University, DeKalb, IL 60115*

Preface

In response to the growing interest in building a *Neutrino Factory* to produce high intensity beams of electron- and muon-neutrinos and antineutrinos, in October 1999 the Fermilab Directorate initiated two six-month studies. The first study, organized by N. Holtkamp and D. Finley, was to investigate the technical feasibility of an intense neutrino source based on a muon storage ring. This design study has produced a report in which the basic conclusion is that a Neutrino Factory is technically feasible, although it requires an aggressive R&D program. The second study, which is the subject of this report, was to explore the physics potential of a Neutrino Factory as a function of the muon beam energy and intensity, and for oscillation physics, the potential as a function of baseline.

The work presented in this report is the result of the enthusiastic contributions of many people from many institutions. This enthusiasm made the organizers job fun. We also want to thank our local sub-group organizers and sub-editors for their many effective contributions, ranging from running the study groups to editing the report: Bob Bernstein, Debbie Harris, Eric Hawker, Stephen Parke, Panagiotis Spentzouris, and Chris Quigg.

Neutrino Factories seem to have caught the imagination of the community. We hope that this report goes some way towards documenting why.

Steve Geer and Heidi Schellman

Executive Summary

In the Fall of 1999, the Fermilab Directorate chartered a study group to investigate the physics motivation for a *neutrino factory* based on a muon storage ring that would operate in the era beyond the current set of neutrino-oscillation experiments. We were charged to evaluate the prospective physics program as a function of the stored muon energy (up to 50 GeV), the number of useful muon decays per year (in the range from 10^{19} to 10^{21} decays per year), and the distance from neutrino source to detector. A companion study evaluated the technical feasibility of a neutrino factory and identified an R&D program that would lead to a detailed design. Our conclusion is that there is a compelling physics case for a neutrino factory with a beam energy of about 20 GeV or greater, that initially provides at least $O(10^{19})$ muon decays per year.

The principal motivation for a neutrino factory is to provide the intense, controlled, high-energy beams that will make possible incisive experiments to pursue the mounting evidence for neutrino oscillations. The composition and spectra of intense neutrino beams from a muon storage ring will be determined by the charge, momentum, and polarization of the stored muons, through the decays $\mu^- \rightarrow e^- \nu_\mu \bar{\nu}_e$ or $\mu^+ \rightarrow e^+ \bar{\nu}_\mu \nu_e$. There is no other comparable source of electron neutrinos and antineutrinos. In addition, a neutrino factory would provide well collimated muon neutrino and antineutrino beams. The uncertainties on the beam composition and flux are expected to be significantly better than those for conventional neutrino beams. If the neutrino factory energy exceeds about 20 GeV the neutrino beam intensity greatly exceeds the corresponding intensity provided by conventional wide band beams. The neutrino factory therefore offers unprecedented opportunities for precise measurements of nucleon structure and of electroweak parameters. The intense muon source needed for the neutrino factory would make possible exquisitely sensitive searches for muon-electron conversion and other rare processes.

Experiments carried out at a neutrino factory within the next decade can add crucial new information to our understanding of neutrino oscillations. By studying the oscillations of ν_μ , ν_e , $\bar{\nu}_\mu$, and $\bar{\nu}_e$, it will be possible to measure, or put stringent limits on, all of the appearance modes $\nu_e \rightarrow \nu_\tau$, $\nu_e \rightarrow \nu_\mu$, and $\nu_\mu \rightarrow \nu_\tau$. This is a necessary step beyond the measurements provided by the next generation of neutrino experiments, and will provide a basic test of our understanding of neutrino oscillations. It will also be possible to determine precisely (or place stringent limits on) all of the leading oscillation parameters, including the mixing angle θ_{13} which appears to be difficult to determine precisely with conventional neutrino beams. In addition, a neutrino factory would enable us to infer the pattern of neutrino masses; and, under the right circumstances, to observe CP violation in the lepton sector. Baselines greater than about 2000 km will enable a quantitative study of matter effects and a determination of the mass

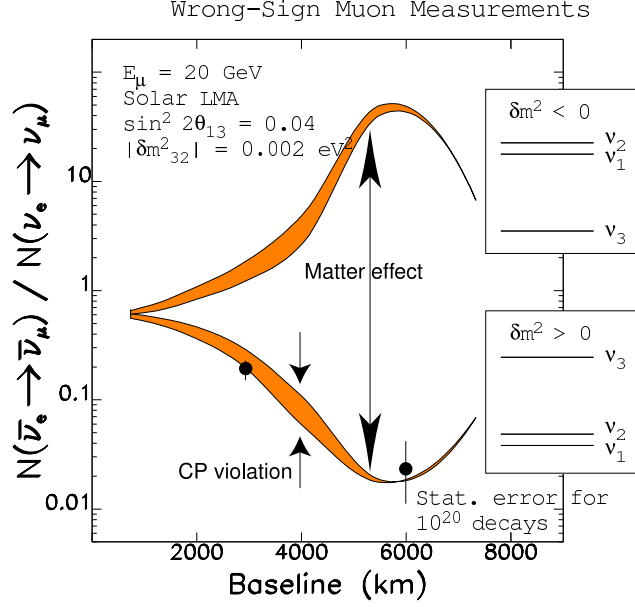


Figure I: Predicted ratios of $\bar{\nu}_e \rightarrow \bar{\nu}_\mu$ to $\nu_e \rightarrow \nu_\mu$ rates at a 20 GeV neutrino factory. The upper (lower) band is for $\delta m_{32}^2 < 0$ ($\delta m_{32}^2 > 0$). The range of possible CP violation determines the widths of the bands. The statistical error shown corresponds to 10^{20} muon decays of each sign and a 50 kt detector. Results are from Ref. 51.

hierarchy. If the MiniBOONE experiment confirms the $\nu_\mu \leftrightarrow \nu_e$ effect reported by the LSND experiment, experiments with rather short baselines (a few tens of km) could be extremely rewarding, and enable, for example, the search for $\nu_e \rightarrow \nu_\tau$ oscillations.

If the atmospheric neutrino deficit is correctly described by three flavor oscillations with δm^2 in the range favored by the SuperKamionkande data, and if the parameter $\sin^2 2\theta_{13}$ is not smaller than ~ 0.01 , then exciting cutting-edge long baseline oscillation physics could begin with an ~ 50 kt detector at a neutrino factory with muon energies as low as 20 GeV delivering as few as 10^{19} muon decays per year. This “entry-level” facility would be able to measure $\nu_e \rightarrow \nu_\mu$ and $\bar{\nu}_e \rightarrow \bar{\nu}_\mu$ oscillations. For baselines of a few thousand km the ratio of rates $N(\bar{\nu}_e \rightarrow \bar{\nu}_\mu)/N(\nu_e \rightarrow \nu_\mu)$ is sensitive to the sign of δm^2 , and hence to the pattern of neutrino masses (Fig. I). With 10^{19} decays and a 50 kt detector a unique and statistically significant measurement of the neutrino mass spectrum could be made. In addition, the $\nu_e \rightarrow \nu_\mu$ event rate is approximately proportional to the parameter $\sin^2 2\theta_{13}$, which could therefore be measured.

With higher beam intensities and/or higher beam energies the physics potential of a neutrino factory is enhanced (Fig. II). In particular, as the intensity is increased to $O(10^{20})$ decays/year $\nu_e \rightarrow \nu_\tau$ oscillations might be measured, and eventually CP violation in the lepton sector observed if the large mixing angle MSW solution is the correct description of the solar neutrino deficit. Higher beam intensities would also allow smaller values of $\sin^2 2\theta_{13}$ to be probed (Fig.

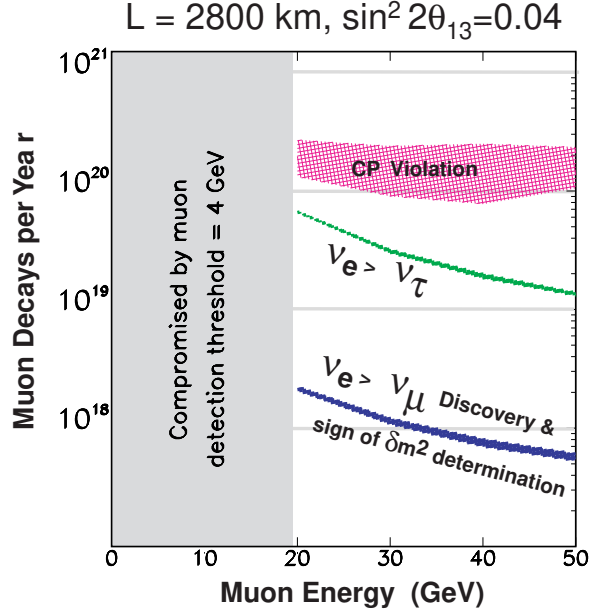


Figure II: The required number of muon decays needed in a neutrino factory to observe $\nu_e \rightarrow \nu_\mu$ oscillations in a 50 kt detector and determine the sign of δm^2 , and the number of decays needed to observe $\nu_e \rightarrow \nu_\tau$ oscillations in a few kt detector, and ultimately put stringent limits on (or observe) CP violation in the lepton sector with a 50 kt detector. Results are from Ref. 51.

III), and higher precision measurements of the oscillation parameters to be made. An example of the improvement of measurement precision with neutrino factory intensity is shown in Fig. IV for the determinations of $\sin^2 \theta_{23}$ and $\sin^2 2\theta_{13}$.

The physics program at detectors located close to the neutrino factory is also compelling. The neutrino fluxes are four orders of magnitude higher than those from existing beams. Such intense beams make experiments with high precision detectors and low mass targets feasible for the first time. Using these detectors and the unique ability of neutrinos to probe particular flavors of quarks will allow a precise measurement of the individual light quark contents of the nucleon in both an isolated and nuclear environment. In addition, neutrinos provide an elegant tool for probing the spin structure of the nucleon and may finally enable resolution of the nucleon spin among its partonic components. The high event rates at a neutrino factory would also enable a new generation of tagged heavy quark production experiments, precision measurements of electro-weak and strong interaction parameters, and searches for exotic phenomena other than oscillations.

Recommendations

The physics program we have explored for a neutrino factory is compelling. We recommend a sustained effort to study both the physics opportunities and the

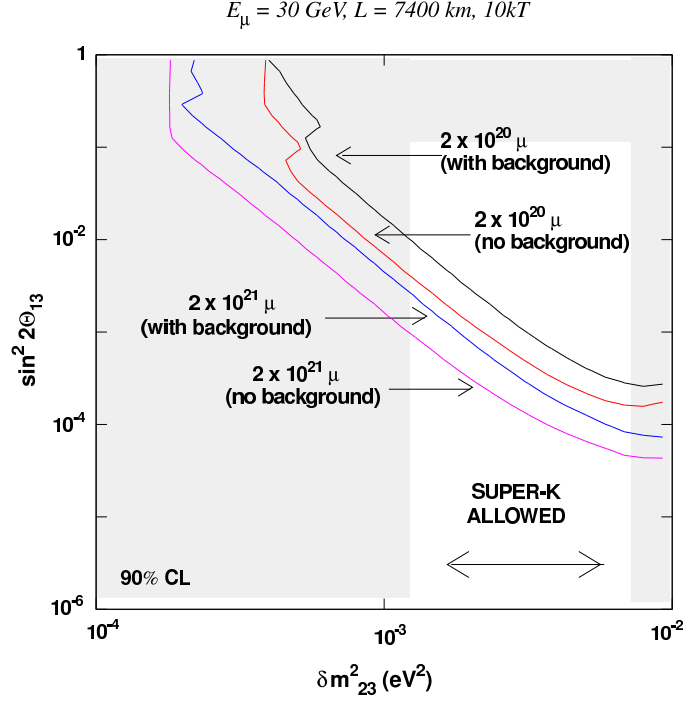


Figure III: Limits on $\sin^2 2\theta_{13}$ that would result from the absence of a $\nu_e \rightarrow \nu_\mu$ signal in a 10 kt detector 7400 km downstream of a 30 GeV neutrino factory in which there are 10^{20} and $10^{21} \mu^+$ decays, followed by the same number of μ^- decays. The limits are shown as a function of δm^2_{32} . The impact of including backgrounds in the analysis is shown. Note that the unshaded band shows the δm^2 region favored by the SuperK atmospheric neutrino deficit results. Results are from Ref. 50.

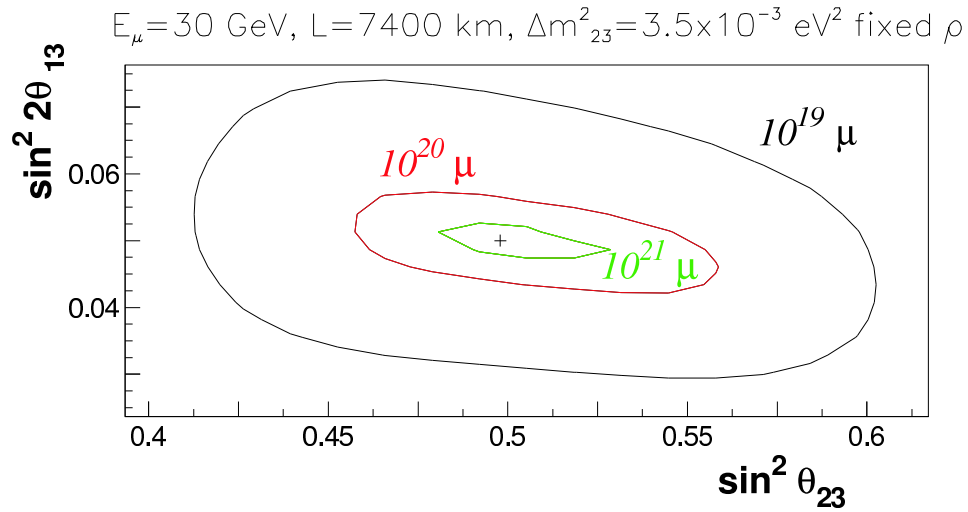


Figure IV: Precision with which the oscillation parameters $\sin^2 \theta_{23}$ and $\sin^2 2\theta_{13}$ can be measured in a 10 kt detector 7400 km downstream of a 30 GeV neutrino factory in which there are 10^{19} , 10^{20} , and $10^{21} \mu^+$ decays. Results are from Ref. 50.

machine realities.

- (i) We encourage support for the R&D needed to learn whether a neutrino factory can be a real option in the next decade.
- (ii) We propose further studies of detector technologies optimized for a neutrino factory, including both novel low mass detectors for near experiments and very high mass detectors for long baselines. For long baseline experiments detectors should have masses of a few times 10 kt or more that are able to detect and measure wrong-sign muons, and detectors of a few kt or more able to observe tau-lepton appearance with high efficiency. It is also desirable to identify electrons, and if possible measure the sign of their charge. Both the detector technologies themselves and the civil engineering issues associated with the construction of such massive detectors need to be addressed.
- (iii) We recommend continued studies to better compare the physics potential of upgraded conventional neutrino beams with the corresponding potential at a neutrino factory, and also studies to better understand the benefits of muon polarization.
- (iv) The present study concentrated on the muon storage ring as a neutrino source and did not cover the additional physics programs which would use the proton driver and the high intensity muon beams. We recommend a further study directed at these other facets of physics at a muon storage ring facility.

Contents

1	Introduction	11
2	Beam properties	14
2.1	Interaction rates	14
2.2	Tau neutrino interactions	19
2.3	Systematic uncertainties on the muon beam and neutrino flux . .	19
2.4	Event distributions at a near site	20
3	Oscillation physics	24
3.1	Theoretical framework	24
3.1.1	Neutrino Oscillations in Vacuum	26
3.1.2	Three Active Neutrinos Only	27
3.1.3	Three Active Flavor Oscillation Scenarios	30
3.1.4	Three Active and One Sterile Neutrinos	33
3.1.5	Scenarios with Three Active plus One Sterile Neutrino . .	36
3.2	Where will we be in 5-10 years ?	37
3.2.1	$\nu_\mu \rightarrow \nu_\tau, \nu_s$	37
3.2.2	$\nu_\mu \leftrightarrow \nu_e$	39
3.2.3	$\nu_e \rightarrow \nu_\mu, \nu_\tau, \nu_s$	40
3.2.4	Summary	40
3.3	The neutrino factory oscillation physics program	45
3.4	Detector considerations	47
3.4.1	Muon identification and measurement	49
3.4.2	τ -lepton identification and measurement	51
3.4.3	A Liquid Argon neutrino detector	53
3.4.4	A magnetized Steel/Scintillator neutrino detector	54
3.4.5	A Water Cerenkov detector	57
3.4.6	Specialized τ -lepton detectors	60
3.4.7	Detector summary	63
3.5	Oscillation measurements	65
3.5.1	Observation of $\nu_e \rightarrow \nu_\mu$ oscillations and the pattern of neutrino masses	65
3.5.2	Observation of $\nu_e \rightarrow \nu_\tau$ oscillations	70
3.5.3	Measurement of $\nu_\mu \rightarrow \nu_\tau$ oscillations	74
3.5.4	Determination of $\sin^2 2\theta_{13}$, $\sin^2 2\theta_{23}$, and δm_{32}^2	74

3.5.5	Search for CP violation	85
3.6	Summary	89
4	Non–Oscillation Physics	91
4.1	Possible detector configurations and statistics	92
4.2	Neutrino Scattering Kinematics	93
4.3	Total cross section Measurements	96
4.4	Structure function measurements	97
4.5	Perturbative QCD	98
4.6	Nuclear Effects	99
4.7	Spin Structure	101
4.8	Charm Production and $D^0 - \overline{D}^0$ Mixing	105
4.9	Precision Electroweak Measurements	107
4.10	Heavy Lepton Mixing	112
4.11	Neutrino Magnetic Moments	114
4.12	Exotic processes	119
4.13	Summary	121
5	Summary and Recommendations	123

1 Introduction

New accelerator technologies offer the possibility of building, not too many years in the future, an accelerator complex to accumulate more than 10^{19} , and perhaps more than 10^{20} , muons per year [1]. It has been proposed [2] to build a *Neutrino Factory* by accelerating the muons from this intense source to energies of several GeV or more, injecting the muons into a storage ring having long straight sections, and exploiting the intense neutrino beams that are produced by muons decaying in the straight sections. If the challenge of producing, capturing, accelerating, and storing a millimole of unstable muons can be met, the decays

$$\mu^- \rightarrow e^- \nu_\mu \bar{\nu}_e, \quad \mu^+ \rightarrow e^+ \bar{\nu}_\mu \nu_e \quad (1)$$

offer exciting possibilities for the study of neutrino interactions and neutrino properties [2, 3, 4, 5]. In a Neutrino Factory the composition and spectra of intense neutrino beams will be determined by the charge, momentum, and polarization of the stored muons. The prospect of intense, controlled, high-energy beams of electron neutrinos and antineutrinos—for which we have no other plausible source—is very intriguing.

Neutrinos—weakly interacting, nearly massless elementary fermions—have long been objects of fascination, as well as reliable probes. One of the most dramatic recent developments in particle physics is the growing evidence that neutrinos may oscillate from one species to another during propagation, which implies that neutrinos have mass.

If neutrinos ν_1, ν_2, \dots have different masses m_1, m_2, \dots , each neutrino flavor state may be a mixture of different mass states. Let us consider two species for simplicity, and take

$$\begin{pmatrix} \nu_e \\ \nu_\mu \end{pmatrix} = \begin{pmatrix} \cos \theta & \sin \theta \\ -\sin \theta & \cos \theta \end{pmatrix} \begin{pmatrix} \nu_1 \\ \nu_2 \end{pmatrix}. \quad (2)$$

The probability for a neutrino born as ν_μ to oscillate into a ν_e ,

$$P(\nu_\mu \rightarrow \nu_e) = \sin^2 2\theta \sin^2 \left(1.27 \frac{\delta m^2}{1 \text{ eV}^2} \cdot \frac{L}{1 \text{ km}} \cdot \frac{1 \text{ GeV}}{E} \right), \quad (3)$$

depends on two parameters related to experimental conditions: L , the distance from the neutrino source to the detector, and E , the neutrino energy. It also depends on two fundamental neutrino parameters: the difference of masses squared, $\delta m^2 = m_1^2 - m_2^2$, and the neutrino mixing parameter, $\sin^2 2\theta$. The probability that a neutrino born as ν_μ remain a ν_μ at distance L is

$$P(\nu_\mu \rightarrow \nu_\mu) = 1 - \sin^2 2\theta \sin^2 \left(1.27 \frac{\delta m^2}{1 \text{ eV}^2} \cdot \frac{L}{1 \text{ km}} \cdot \frac{1 \text{ GeV}}{E} \right). \quad (4)$$

Many experiments have now used natural sources of neutrinos, neutrino radiation from fission reactors, and neutrino beams generated in particle accelerators

to look for evidence of neutrino oscillation. The positive indications for neutrino oscillations fall into three classes:[6]

1. Five solar-neutrino experiments report deficits with respect to the predictions of the standard solar model: Kamiokande and Super-Kamiokande (SuperK) using water-Cerenkov techniques, SAGE and GALLEX using chemical recovery of germanium produced in neutrino interactions with gallium, and Homestake using radiochemical separation of argon produced in neutrino interactions with chlorine. These results suggest the oscillation $\nu_e \rightarrow \nu_x$, with $|\delta m^2|_{\text{solar}} \approx 10^{-5} \text{ eV}^2$ and $\sin^2 2\theta_{\text{solar}} \approx 1$ or a few $\times 10^{-3}$, or $|\delta m^2|_{\text{solar}} \approx 10^{-10} \text{ eV}^2$ and $\sin^2 2\theta_{\text{solar}} \approx 1$.
2. Five atmospheric-neutrino experiments report anomalies in the arrival of muon neutrinos: Kamiokande, IMB, and SuperK using water-Cerenkov techniques, and Soudan 2 and MACRO using sampling calorimetry. The most striking result is the zenith-angle dependence of the ν_μ rate reported last year by SuperK [7, 8]. These results suggest the oscillation $\nu_\mu \rightarrow \nu_\tau$ or ν_s , with $\sin^2 2\theta_{\text{atm}} \approx 1$ and $|\delta m^2|_{\text{atm}} = 10^{-3}$ to 10^{-2} eV^2 . The oscillation $\nu_\mu \rightarrow \nu_\tau$ is increasingly the favored interpretation.
3. The LSND experiment [9] reports the observation of $\bar{\nu}_e$ -like events in what should be an essentially pure $\bar{\nu}_\mu$ beam produced at the Los Alamos Meson Physics Facility, suggesting the oscillation $\bar{\nu}_\mu \rightarrow \bar{\nu}_e$. This result has not yet been reproduced by any other experiment. The favored region lies along a band from $(\sin^2 2\theta_{\text{LSND}} = 10^{-3}, |\delta m^2|_{\text{LSND}} \approx 1 \text{ eV}^2)$ to $(\sin^2 2\theta_{\text{LSND}} = 1, |\delta m^2|_{\text{LSND}} \approx 7 \times 10^{-2} \text{ eV}^2)$.

A host of other experiments have failed to turn up evidence for neutrino oscillations in the regimes of their sensitivity. These results limit neutrino mass-squared differences and mixing angles. In more than a few cases, positive and negative claims are in conflict, or at least face off against each other. Over the next five years, many experiments will seek to verify, further quantify, and extend these claims. If all of the current experimental indications of neutrino oscillation survive, there are apparently three different mass-squared-difference scales, which cannot be accommodated with only three neutrino types. New *sterile* neutrinos may be required. This would be a profound discovery.

From the era of the celebrated two-neutrino experiment [10] to modern times, high-energy neutrino beams have played a decisive role in the development of our understanding of the constituents of matter and the fundamental interactions among them. Major landmarks include the discovery of weak neutral-current interactions [11], and incisive studies of the structure of the proton and the quantitative verification of perturbative quantum chromodynamics as the theory of the strong interactions [12]. The determinations of the weak mixing parameter $\sin^2 \theta_W$ and the strong coupling constant α_s in deeply inelastic neutrino interactions are comparable in precision to the best current measurements. Though experiments with neutrino beams have a long history, beams

of greatly enhanced intensity would bring opportunities for dramatic improvements. Because weak-interaction cross sections are small, high-statistics studies have required massive targets and coarse-grained detectors. Until now, it has been impractical to consider precision neutrino experiments using short liquid hydrogen targets, or polarized targets, or active semiconductor target-detectors. All of these options are opened by a muon storage ring, which would produce neutrinos at approximately 10^4 times the flux of existing neutrino beams.

At the energies best suited for the study of neutrino oscillations—tens of GeV, by our current estimates—the muon storage ring is compact. We could build it at one laboratory, pitched at a deep angle, to illuminate a laboratory on the other side of the globe with a neutrino beam whose properties we can control with great precision. By choosing the right combination of energy and destination, we can tune future neutrino-oscillation experiments to the physics questions we will need to answer, by specifying the ratio of path length to neutrino energy and determining the amount of matter the neutrinos traverse. Although we can use each muon decay only once, and we will not be able to select many destinations, we may be able to illuminate two or three well-chosen sites from a muon-storage-ring neutrino source. That possibility—added to the ability to vary the muon charge, polarization, and energy—may give us just the degree of experimental control it will take to resolve the outstanding questions about neutrino oscillations. Experiments at a Neutrino Factory would seek to verify the number of neutrino types participating in the oscillations, precisely determine the mixing parameters that relate the flavor states to the mass states, determine the pattern of neutrino masses, and look for CP violation in the lepton sector.

The prodigious flux of neutrinos close to the muon storage ring raises the prospect of neutrino-scattering experiments of unprecedented sensitivity and delicacy. Experiments that might be pursued at a Neutrino Factory include precise measurements of the nucleon structure (including changes that occur in a nuclear environment), measurements of the spin structure of the nucleon using a new and powerful technique, charm measurements with several million tagged particles, precise measurements of Standard Model parameters, and searches for exotic phenomena.

We believe that the physics program at a Neutrino Factory is compelling and encourage support for a vigorous R&D program to make neutrino factories a real option for the future.

2 Beam properties

Consider an ensemble of polarized negatively-charged muons. When the muons decay they produce muon neutrinos with a distribution of energies and angles in the muon rest-frame described by [13]:

$$\frac{d^2 N_{\nu_\mu}}{dx d\Omega_{cm}} \propto \frac{2x^2}{4\pi} [(3 - 2x) + (1 - 2x)P_\mu \cos \theta_{cm}] , \quad (5)$$

where $x \equiv 2E_\nu/m_\mu$, θ_{cm} is the angle between the neutrino momentum vector and the muon spin direction, and P_μ is the average muon polarization along the beam direction. The electron antineutrino distribution is given by:

$$\frac{d^2 N_{\bar{\nu}_e}}{dx d\Omega_{cm}} \propto \frac{12x^2}{4\pi} [(1 - x) + (1 - x)P_\mu \cos \theta_{cm}] , \quad (6)$$

and the corresponding distributions for $\bar{\nu}_\mu$ and ν_e from μ^+ decay are obtained by the replacement $P_\mu \rightarrow -P_\mu$. Only neutrinos and antineutrinos emitted in the forward direction ($\cos \theta_{lab} \simeq 1$) are relevant to the neutrino flux for long-baseline experiments; in this limit $E_\nu = xE_{max}$ and at high energies the maximum E_ν in the laboratory frame is given by $E_{max} = \gamma(1 + \beta \cos \theta_{cm})m_\mu/2$, where β and γ are the usual relativistic factors. The ν_μ and $\bar{\nu}_e$ distributions as a function of the laboratory frame variables are then given by:

$$\frac{d^2 N_{\nu_\mu}}{dx d\Omega_{lab}} \propto \frac{1}{\gamma^2(1 - \beta \cos \theta_{lab})^2} \frac{2x^2}{4\pi} [(3 - 2x) + (1 - 2x)P_\mu \cos \theta_{cm}] , \quad (7)$$

and

$$\frac{d^2 N_{\bar{\nu}_e}}{dx d\Omega_{lab}} \propto \frac{1}{\gamma^2(1 - \beta \cos \theta_{lab})^2} \frac{12x^2}{4\pi} [(1 - x) + (1 - x)P_\mu \cos \theta_{cm}] . \quad (8)$$

Thus, for a high energy muon beam with no beam divergence, the neutrino and antineutrino energy- and angular- distributions depend upon the parent muon energy, the decay angle, and the direction of the muon spin vector. With the muon beam intensities that could be provided by a muon-collider type muon source [1] the resulting neutrino fluxes at a distant site would be large. For example, Fig. 1 shows as a function of muon energy and polarization, the computed fluxes per 2×10^{20} muon decays at a site on the other side of the Earth ($L = 10000$ km). Note that the ν_e ($\bar{\nu}_e$) fluxes are suppressed when the muons have $P = +1$ (-1). This can be understood by examining Eq. (8) and noting that for $P = -1$ the two terms cancel in the forward direction for all x .

2.1 Interaction rates

Neutrino charged current (CC) scattering cross-sections are shown as a function of energy in Fig. 2. At low energies the neutrino scattering cross section is

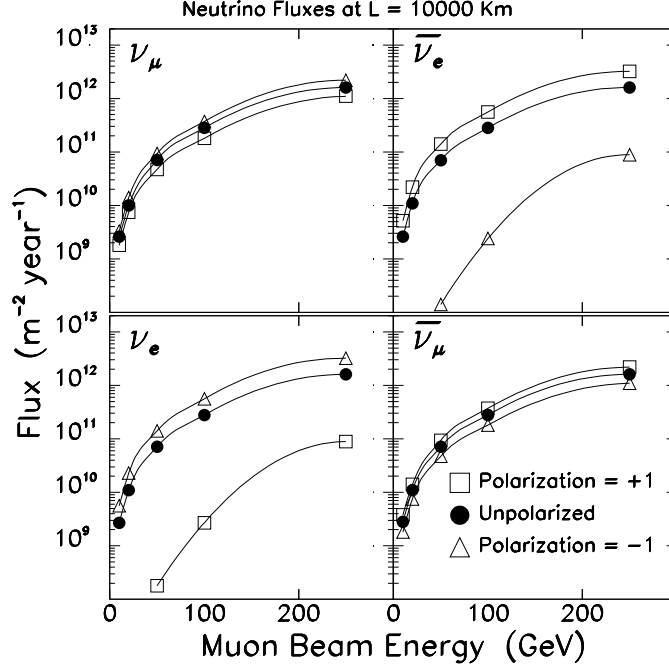


Figure 1: Calculated ν and $\bar{\nu}$ fluxes in the absence of oscillations at a far site located 10000 km from a neutrino factory in which 2×10^{20} muons have decayed in the beam-forming straight section. The fluxes are shown as a function of the energy of the stored muons for negative muons (top two plots) and positive muons (bottom two plots), and for three muon polarizations as indicated. The calculated fluxes are averaged over a circular area of radius 1 km at the far site. Calculation from Ref. 2.

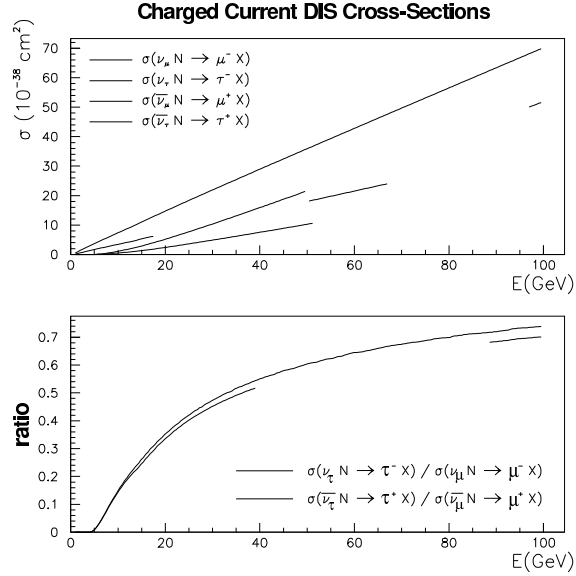


Figure 2: The total cross section for charged current neutrino scattering by muon and tau neutrinos (top plot), and the ratio of tau to muon neutrino cross sections as a function of neutrino energy (bottom plot).

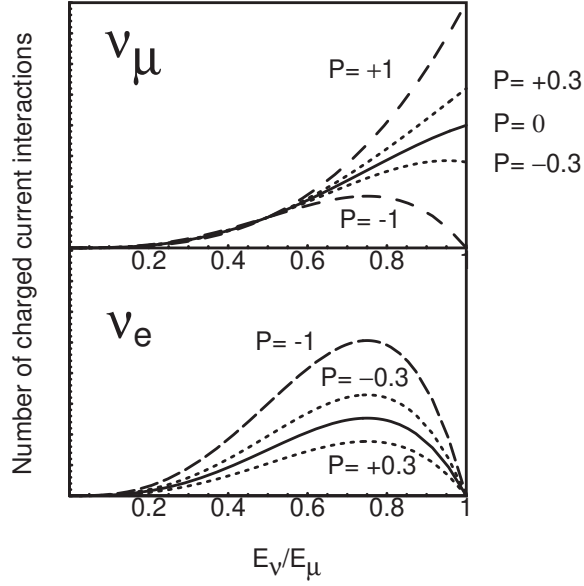


Figure 3: Charged current event spectra at a far detector. The solid lines indicate zero polarization, the dotted lines indicate polarization of ± 0.3 and the dashed lines indicate full polarization. The $P = 1$ case for electron neutrinos results in no events and is hidden by the x axis.

dominated by quasi-elastic scattering and resonance production. However, if E_ν is greater than ~ 10 GeV, the total cross section is dominated by deep inelastic scattering and is approximately [14]:

$$\sigma(\nu + N \rightarrow \ell^- + X) \approx 0.67 \times 10^{-38} \text{ cm}^2 \times (E_\nu, \text{GeV}), \quad (9)$$

$$\sigma(\bar{\nu} + N \rightarrow \ell^+ + X) \approx 0.34 \times 10^{-38} \text{ cm}^2 \times (E_{\bar{\nu}}, \text{GeV}). \quad (10)$$

The number of ν and $\bar{\nu}$ CC events per incident neutrino observed in an isoscalar target is given by:

$$N(\nu + N \rightarrow \ell^- + X) = 4.0 \times 10^{-15} (E_\nu, \text{GeV}) \text{ events per gr/cm}^2, \quad (11)$$

$$N(\bar{\nu} + N \rightarrow \ell^+ + X) = 2.0 \times 10^{-15} (E_{\bar{\nu}}, \text{GeV}) \text{ events per gr/cm}^2. \quad (12)$$

Using this simple form for the energy dependence of the cross section, the predicted energy distributions for ν_e and ν_μ interacting in a far detector ($\cos \theta = 1$) at a neutrino factory are shown in Fig. 3. The interacting ν_μ energy distribution is compared in Fig. 4 with the corresponding distribution arising from the high-energy NUMI wide band beam. Note that neutrino beams from a neutrino factory can be considered narrow band beams. In practice, CC interactions can only be cleanly identified when the final state lepton exceeds a threshold energy. The calculated final state lepton distributions are shown in Fig. 5. Integrating over the energy distribution, the total ν and $\bar{\nu}$ interaction rates per muon decay are given by:

$$N_\nu = 1.2 \times 10^{-14} \left[\frac{(E_\mu, \text{GeV})^3}{(L, \text{km})^2} \right] \times C(\nu) \text{ events per kt} \quad (13)$$

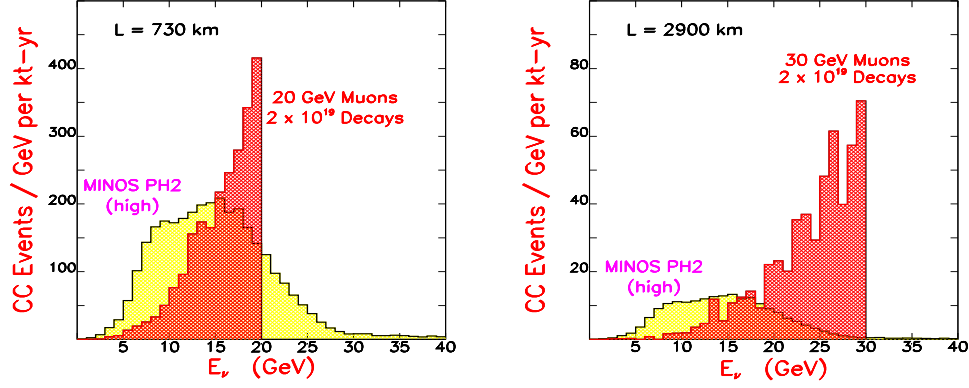


Figure 4: Comparison of interacting ν_μ energy distributions for the NUMI high energy wide band beam (Ref. 15) with a 20 GeV neutrino factory beam (Ref. 2) at $L = 730$ km and a 30 GeV neutrino factory beam at $L = 2900$ km. The neutrino factory distributions have been calculated based on Eq. (5) (no approximations), and include realistic muon beam divergences and energy spreads.

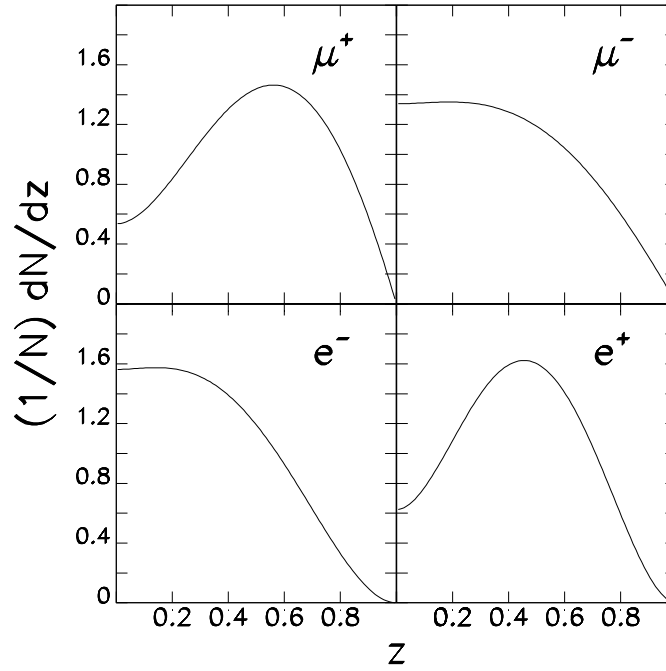


Figure 5: Lepton energy spectra for CC $\bar{\nu}_\mu$ (top left), ν_μ (top right), ν_e (bottom left), and $\bar{\nu}_e$ (bottom right) interactions. Note that z is the energy normalized to the primary muon energy $z = E_\ell/E_\mu$. Calculation from Ref. 16.

Table 1: Muon neutrino and electron antineutrino CC interaction rates in the absence of oscillations, calculated for baseline length $L = 732$ km (FNAL \rightarrow Soudan), for MINOS using the wide band beam and a muon storage ring delivering 10^{20} decays with $E_\mu = 10, 20$, and 50 GeV at 3 baselines. The neutrino factory calculation includes a realistic muon beam divergence and energy spread.

Experiment		Baseline (km)	$\langle E_{\nu_\mu} \rangle$ (GeV)	$\langle E_{\bar{\nu}_e} \rangle$ (GeV)	N(ν_μ CC) (per kt-yr)	N($\bar{\nu}_e$ CC) (per kt-yr)
MINOS	Low energy	732	3	–	458	1.3
	Medium energy	732	6	–	1439	0.9
	High energy	732	12	–	3207	0.9
Muon ring	E_μ (GeV)					
	10	732	7.5	6.6	1400	620
	20	732	15	13	12000	5000
	50	732	38	33	1.8×10^5	7.7×10^4
Muon ring	E_μ (GeV)					
	10	2900	7.6	6.5	91	41
	20	2900	15	13	740	330
	50	2900	38	33	11000	4900
Muon ring	E_μ (GeV)					
	10	7300	7.5	6.4	14	6
	20	7300	15	13	110	51
	50	7300	38	33	1900	770

and

$$N_{\bar{\nu}} = 0.6 \times 10^{-14} \left[\frac{(E_\mu, \text{GeV})^3}{(L, \text{km})^2} \right] \times C(\nu) \text{ events per kt}, \quad (14)$$

where

$$C(\nu_\mu) = \frac{7}{10} + P_\mu \frac{3}{10}, \quad C(\nu_e) = \frac{6}{10} - P_\mu \frac{6}{10} \quad (15)$$

$$(16)$$

The calculated ν_e and ν_μ CC interaction rates resulting from 10^{20} muon decays in the beam-forming straight-section of a neutrino factory are compared in Table 1 with expectations for the corresponding rates at the next generation of accelerator-based neutrino experiments. Note that event rates at a neutrino factory increase as E_μ^3 , and are significantly larger than expected for the next generation of approved experiments if $E_\mu > 20$ GeV. The radial dependence of the event rate is shown in Fig. 6 for a 20 GeV neutrino factory and three baselines.

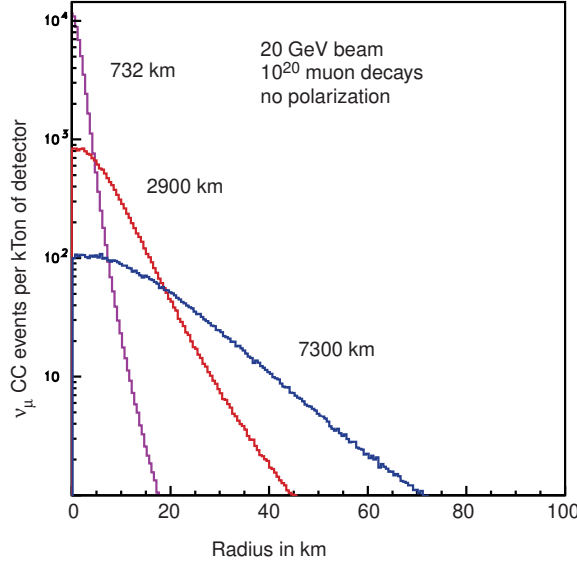


Figure 6: Events/kT of detector as a function of distance from the beam center for a 20 GeV muon beam.

Finally, for an isoscalar target the neutral current (NC) cross sections are approximately 0.4 of the CC cross sections[17], and are given by:

$$\sigma(\nu + N \rightarrow \nu + X) \approx 0.3 \times 10^{-38} \text{ cm}^2 \times (E_\nu, \text{GeV}), \quad (17)$$

$$\sigma(\bar{\nu} + N \rightarrow \bar{\nu} + X) \approx 0.15 \times 10^{-38} \text{ cm}^2 \times (E_{\bar{\nu}}, \text{GeV}). \quad (18)$$

2.2 Tau neutrino interactions

Tau neutrino CC interaction rates are substantially less than the corresponding ν_e and ν_μ rates, especially near the tau production threshold of ~ 3.3 GeV. The NC rates should be the same as those for electron and muon neutrinos. Figure 2 shows the calculated [18] ratio of ν_τ/ν_μ CC interaction rates as a function of the neutrino energy. Near threshold, contributions from quasi-elastic and resonance production dominate. If the ν_τ cross sections from Ref. [19] are used, the predicted event rates are 5–7% lower.

2.3 Systematic uncertainties on the muon beam and neutrino flux

In the neutrino beam-forming straight section the muon beam is expected to have an average divergence given by $\sigma_\theta = O(0.1/\gamma)$. The neutrino beam divergence will therefore be dominated by muon decay kinematics, and uncertainties on the beam direction and divergence will yield only small uncertainties in the neutrino flux at a far site. However, if precise knowledge of the flux is required, the uncertainties on θ and σ_θ must be taken into account, along with uncertainties on the flux arising from uncertainties on the muon energy distribution and

Table 2: Dependence of predicted charged current event rates on muon beam properties at a neutrino factory. The last column lists the required precisions with which each beam property must be determined if the uncertainty on the neutrino flux at the far site is to be less than $\sim 1\%$. Here Δ denotes uncertainty while σ denotes the spread in a variable. Table from Ref. 20.

Muon Beam property	Beam Type	Rate Dependence	Target Precision
Energy (E_μ)	ν (no osc)	$\Delta N/N = 3 \Delta E_\mu/E_\mu$	$\Delta(E_\mu)/E_\mu < 0.003$
	$\nu_e \rightarrow \nu_\mu$	$\Delta N/N = 2 \Delta E_\mu/E_\mu$	$\Delta(E_\mu)/E_\mu < 0.005$
Direction ($\Delta\theta$)	ν (no osc)	$\Delta N/N \leq 0.01$ (for $\Delta\theta < 0.6 \sigma_\theta$)	$\Delta\theta < 0.6 \sigma_\theta$
Divergence (σ_θ)	ν (no osc)	$\Delta N/N \sim 0.03 \Delta\sigma_\theta/\sigma_\theta$ (for $\sigma_\theta \sim 0.1/\gamma$)	$\Delta\sigma_\theta/\sigma_\theta < 0.2$ (for $\sigma_\theta \sim 0.1/\gamma$)
Momentum spread (σ_p)	ν (no osc)	$\Delta N/N \sim 0.06 \Delta\sigma_p/\sigma_p$	$\Delta\sigma_p/\sigma_p < 0.17$
Polarization (P_μ)	ν_e (no osc)	$\Delta N_{\nu_e}/N_{\nu_e} = \Delta P_\mu$	$\Delta P_\mu < 0.01$
	ν_μ (no osc)	$\Delta N_{\nu_\mu}/N_{\nu_\mu} = 0.4 \Delta P_\mu$	$\Delta P_\mu < 0.025$

polarization. The relationships between the uncertainties on the muon beam properties and the resulting uncertainties on the neutrino flux are summarized in Table 2. If, for example, we wanted to know the ν_e and ν_μ fluxes at a far site with a precision of 1%, we would need to know the beam divergence σ_θ to 20% (Fig. 7), and ensure that the beam direction was within $0.6 \sigma_\theta$ of the nominal direction [20] (Fig. 8).

2.4 Event distributions at a near site

The event distributions measured in a detector close to the neutrino factory will be quite different from the corresponding distributions at a far site. There are two main reasons for this difference. First, the near detector accepts neutrinos over a large range of muon decay angles θ , not just those neutrinos traveling in the extreme forward direction. This results in a broader neutrino energy distribution that is sensitive to the radial size of the detector (Fig. 9). Second, if the distance of the detector from the end of the beam forming straight section is of the order of the straight section length, then the θ acceptance of the detector varies with the position of the muon decay along the straight section. This results in a more complicated radial flux distribution than expected for a far detector. However, since the dominant effects are decay length and muon decay kinematics, it should be modeled quite accurately. (Fig. 10).

Note that, even in a limited angular range, the event rates in a near detector

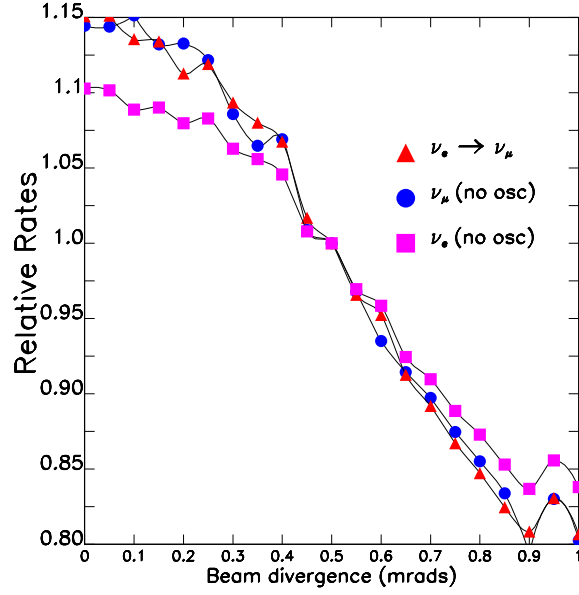


Figure 7: Dependence of CC interaction rates on the muon beam divergence for a detector located at $L = 2800$ km from a muon storage ring containing 30 GeV unpolarized muons. Rates are shown for ν_e (boxes) and ν_μ (circles) beams in the absence of oscillations, and for $\nu_e \rightarrow \nu_\mu$ oscillations (triangles) with the three-flavor oscillation parameters IA1. The calculation is from Ref. 20.

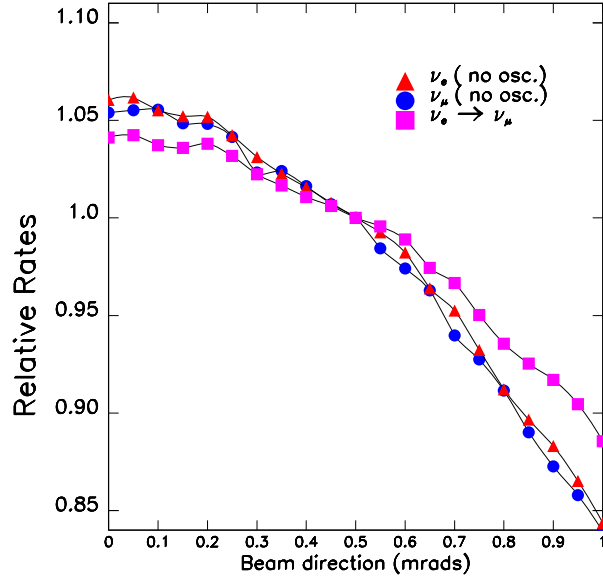


Figure 8: Dependence of CC interaction rates on the neutrino beam direction. Relative rates are shown for a detector at a far site located downstream of a storage ring containing 30 GeV unpolarized muons, and a muon beam divergence of 0.33 mr. Rates are shown for ν_e (triangles) and ν_μ (circles) beams in the absence of oscillations, and for $\nu_e \rightarrow \nu_\mu$ oscillations (boxes) with the three-flavor oscillation parameters IA1. The calculation is from Ref. 20.

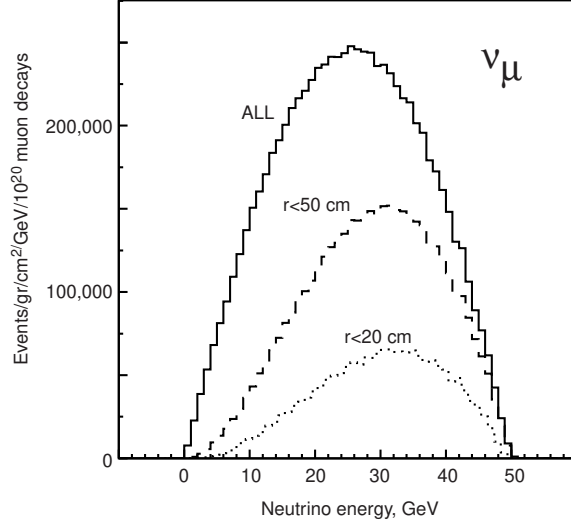


Figure 9: Events per gr/cm^2 per GeV for a detector 40 m from a muon storage ring with a 600 m straight section. The 3 curves show all events and those falling within 50 and 20 cm of the beam center.

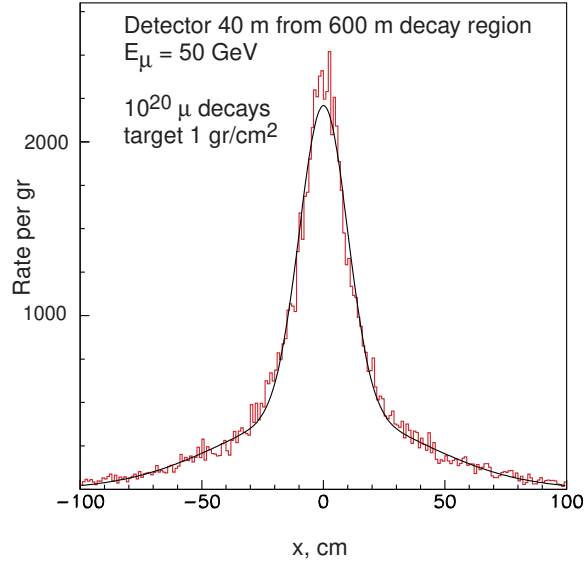


Figure 10: Events per gr/cm^2 as a function of the transverse coordinate x 50 m downstream of a 50 GeV neutrino factory providing 10^{20} muon decays. The central peak is mainly due to decays in the last hundred meters of the decay pipe while the large tails are due to upstream decays.

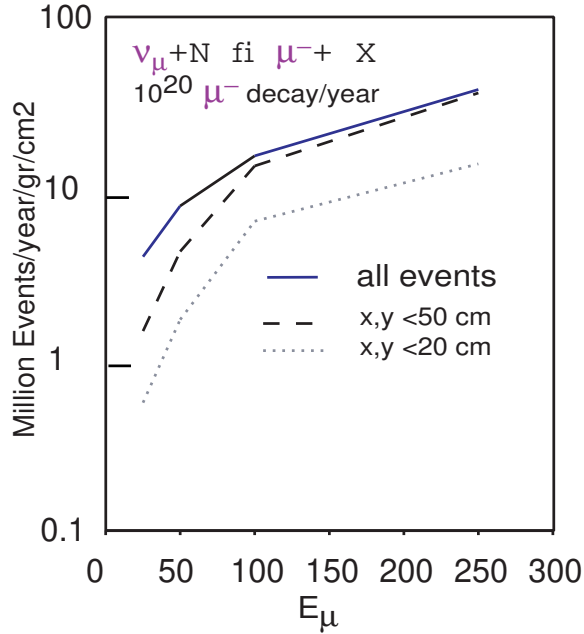


Figure 11: Events per gr/cm^2 at a near detector as a function of muon beam energy. The curves indicate (solid) all events, the dashed and dotted curves show the effects of radial position cuts.

are very high. Figure 11 illustrates the event rates per gram/cm^2 as a function of energy. Because most of the neutrinos produced forward in the center of mass traverse the detector fiducial volume, the factor of γ^2 present in the flux for $\theta \sim 0$ is lost and the event rate increases linearly with E_μ . For a 50 GeV muon storage ring, the interaction rate per 10^{20} muon decays is 7 million events/ gram/cm^2 . Rate calculations are discussed further in the context of specific experiments in the section on non-oscillation experiments. Finally, in the absence of special magnetized shielding, the high neutrino event rates in any material upstream of the detector will cause substantial backgrounds. The event rate in the last 3 interaction lengths ($300 \text{ gr}/\text{cm}^2$) of the shielding between the detector and the storage ring would be 30 interactions per beam spill at a 15 Hz machine delivering 2×10^{20} muon decays per year. These high background rates will require clever magnetized shielding designs and fast detector readout to avoid overly high accidental rates in low mass experiments.

3 Oscillation physics

The recent impressive atmospheric neutrino results from the SuperK experiment have gone a long way towards establishing the existence of neutrino oscillations [21]. Up to the present era, neutrino oscillation experiments at accelerators were searches for a phenomenon that might or might not be within experimental reach. The situation now is quite different. The atmospheric neutrino deficit defines for us the δm^2 and oscillation amplitude that future long-baseline oscillation experiments must be sensitive to, namely $\delta m^2 = \mathcal{O}(10^{-3}) \text{ eV}^2$ and $\sin^2 2\theta = \mathcal{O}(1)$. Experiments that achieve these sensitivities are guaranteed an excellent physics program that addresses fundamental physics questions. We can hope that future neutrino oscillation experiments will provide the keys we need to understand really fundamental questions, for example: the origin of the minute neutrino masses and the reason why there are three lepton families. We cannot guarantee that these insights will be forthcoming from neutrino oscillation measurements, but they might be. For this reason it is important to understand how our community can get detailed experimental information on the neutrino oscillation scheme, the mass splittings between the neutrino mass eigenstates, and the leptonic mixing matrix that controls the oscillation probabilities. A neutrino factory would be a new tool, providing a beam of energetic electron neutrinos. In the following we address how this new tool might be exploited to go well beyond the capabilities of the next generation of neutrino oscillation experiments.

In this section we begin by describing the theoretical basis for neutrino oscillations, and then define a selection of oscillation parameter sets that can be used in assessing the physics program at a neutrino factory. This is followed by a summary of the current experimental status and how it can be expected to change in the next few years. We then discuss the parameters and the performance of candidate detectors at a neutrino factory. The section is completed with a survey of the physics measurements that can be performed at a neutrino factory as a function of beam energy, intensity, and baseline, and finally, a summary of our conclusions.

3.1 Theoretical framework

There exist three known flavors of active neutrinos which form left-handed doublets with their associated charged leptons. The interaction of these active neutrinos with the electroweak gauge bosons is described by the Standard Model (SM). In principle there can be additional flavors of neutrino which are singlets under the electroweak gauge group. These electroweak singlet neutrinos do not have electroweak couplings, and their interactions are not described by the SM. Let us denote the flavor vector of the $SU(2) \times U(1)$ active neutrinos as $\nu = (\nu_e, \nu_\mu, \nu_\tau)$ and the vector of electroweak-singlet neutrinos as $\chi = (\chi_1, \dots, \chi_{n_s})$.

The Dirac and Majorana neutrino mass terms can then be written compactly as

$$-\mathcal{L}_m = \frac{1}{2}(\bar{\nu}_L \ \overline{\chi}_L^c) \begin{pmatrix} M_L & M_D \\ (M_D)^T & M_R \end{pmatrix} \begin{pmatrix} \nu_R^c \\ \chi_R \end{pmatrix} + h.c. \quad (19)$$

where M_L is the 3×3 left-handed Majorana mass matrix, M_R is a $n_s \times n_s$ right-handed Majorana mass matrix, and M_D is the 3-row by n_s -column Dirac mass matrix. In general, all of these are complex, and $(M_L)^T = M_L$, $(M_R)^T = M_R$. Without further theoretical input, the number n_s of “sterile” electroweak-singlet neutrinos is not determined. For example, in the SM, minimal supersymmetric standard model (MSSM), or minimal SU(5) grand unified theory (GUT), $n_s = 0$, while in the SO(10) GUT, $n_s = 3$. (This is true for both the original non-supersymmetric and the current supersymmetric versions of these GUTs.) Since the terms $\chi_{jR}^T C \chi_{kR}$ are electroweak singlets, the elements of the matrix M_R , would not be expected to be related to the electroweak symmetry breaking scale, but instead, would be expected to be much larger, plausibly of the order of the GUT scale.

Mechanisms involving M_L only for the generation of neutrino masses without the presence of electroweak-singlet neutrinos exist. The simplest scenarios, in which one or more Higgs triplets are introduced to couple to a pair of left-handed neutrinos, are excluded by measurements of the ρ parameter. Therefore, other extensions of the SM must be considered, for example the addition of one or more Higgs singlets, non-renormalizable terms involving a large mass scale such as the GUT scale, or R-parity-violating terms in the context of supersymmetry.

The most natural explanation for the three known ultra-light neutrino masses is generally regarded to be the seesaw mechanism [22], which involves M_R , and arises from Eq. (19) in the case of $n_s = 3$ electroweak singlet neutrinos. This leads to neutrino masses generically of order

$$m_\nu \sim \frac{m_D^2}{m_R} \quad (20)$$

where m_D and m_R denote typical elements of the corresponding matrices. With $m_D \sim m_t$ and $m_R \sim 10^{16}$ GeV, as suggested in a (supersymmetric) SO(10) grand unified theory framework, a scale of $m_\nu \sim 10^{-3}$ eV is readily obtained. In this case the three light neutrino masses are obtained by diagonalization of the effective 3×3 light neutrino mass matrix

$$M_\nu = -M_D M_R^{-1} M_D^T \quad (21)$$

while the super-heavy neutrinos are determined from the right-handed Majorana matrix M_R .

Additional electroweak-singlet neutrinos may arise in string theory with the existence of supersymmetric partners of moduli fields, resulting in the appearance of n_ℓ light sterile neutrinos. But the presence of these light sterile neutrinos may undermine the seesaw mechanism and, for this reason, is not very appealing.

However, if one tries to fit all of the data from the oscillation experiments, to obtain a reasonable χ^2 it is necessary to include light sterile neutrinos. We shall illustrate some of the effects of sterile neutrinos with a toy model in which one studies the minimal number, $n_\ell = 1$.

3.1.1 Neutrino Oscillations in Vacuum

The presence of non-zero masses for the light neutrinos introduces a leptonic mixing matrix, U , which is the analogue of the CKM quark mixing matrix, and which in general is not expected to be diagonal. The matrix U connects the flavor eigenstates with the mass eigenstates:

$$|\nu_\alpha\rangle = \sum_i U_{\alpha i} |\nu_i\rangle, \quad (22)$$

where α denotes one of the active neutrino flavors, e , μ or τ or one of the n_ℓ light sterile flavors, while i runs over the light mass eigenstate labels. The number of flavor states considered here is equal to the number of light mass eigenstates, so U is a square unitary matrix.

The neutrino mass differences and the mixing parameters can be probed by studying oscillations between different flavors of neutrinos, as a function of the neutrino energy E and the distance traversed L . The oscillation probability $P(\nu_\alpha \rightarrow \nu_\beta)$ is given by the absolute square of the overlap of the observed flavor state, $|\nu_\beta\rangle$, with the time-evolved initially-produced flavor state, $|\nu_\alpha\rangle$. In vacuum, the evolution operator involves just the Hamiltonian H_0 of a free particle, yielding the well-known result:

$$\begin{aligned} P(\nu_\alpha \rightarrow \nu_\beta) &= \left| \langle \nu_\beta | e^{-iH_0 L} | \nu_\alpha \rangle \right|^2 = \sum_{i,j} U_{\alpha i} U_{\beta i}^* U_{\alpha j}^* U_{\beta j} e^{-i\delta m_{ij}^2 L/2E} \\ &= P_{\text{CP-even}}(\nu_\alpha \rightarrow \nu_\beta) + P_{\text{CP-odd}}(\nu_\alpha \rightarrow \nu_\beta). \end{aligned} \quad (23)$$

The CP-even and CP-odd contributions are

$$\begin{aligned} P_{\text{CP-even}}(\nu_\alpha \rightarrow \nu_\beta) &= P_{\text{CP-even}}(\bar{\nu}_\alpha \rightarrow \bar{\nu}_\beta) \\ &= \delta_{\alpha\beta} - 4 \sum_{i>j} \text{Re} (U_{\alpha i} U_{\beta i}^* U_{\alpha j}^* U_{\beta j}) \sin^2\left(\frac{\delta m_{ij}^2 L}{4E}\right) \\ P_{\text{CP-odd}}(\nu_\alpha \rightarrow \nu_\beta) &= -P_{\text{CP-odd}}(\bar{\nu}_\alpha \rightarrow \bar{\nu}_\beta) \\ &= 2 \sum_{i>j} \text{Im} (U_{\alpha i} U_{\beta i}^* U_{\alpha j}^* U_{\beta j}) \sin\left(\frac{\delta m_{ij}^2 L}{2E}\right) \end{aligned} \quad (24)$$

so that

$$P(\bar{\nu}_\alpha \rightarrow \bar{\nu}_\beta) = P(\nu_\beta \rightarrow \nu_\alpha) = P_{\text{CP-even}}(\nu_\alpha \rightarrow \nu_\beta) - P_{\text{CP-odd}}(\nu_\alpha \rightarrow \nu_\beta) \quad (25)$$

where, by CPT invariance, $P(\nu_\alpha \rightarrow \nu_\beta) = P(\bar{\nu}_\beta \rightarrow \bar{\nu}_\alpha)$. In vacuum the CP-even and CP-odd contributions are even and odd, respectively, under time reversal:

$\alpha \leftrightarrow \beta$. In Eq. (24), $\delta m_{ij}^2 = m(\nu_i)^2 - m(\nu_j)^2$, and the combination $\delta m_{ij}^2 L / (4E)$ in $\hbar = c = 1$ units can be replaced by $1.2669 \cdots \delta m_{ij}^2 L / E$ with δm_{ij}^2 in eV^2 and (L, E) in (km, GeV) . In disappearance experiments $\beta = \alpha$ and no CP-violation can appear since the product of the mixing matrix elements is inherently real. At distances L large compared to all the individual oscillation lengths, $\lambda_{ij}^{\text{osc}} \sim E / \delta m_{ij}^2$, the sine squared terms in $P_{\text{CP-even}}$ average to 0.5 whereas the sine terms in $P_{\text{CP-odd}}$ average to zero. Therefore CP violating effects are largest and hence easiest to observe at distances between the smallest and largest oscillation lengths.

3.1.2 Three Active Neutrinos Only

With three neutrinos, the mixing matrix U is the 3×3 unitary Maki-Nagawa-Sakata (MNS) matrix [23]. We parameterize U by

$$U = \begin{pmatrix} c_{13}c_{12} & c_{13}s_{12} & s_{13}e^{-i\delta} \\ -c_{23}s_{12} - s_{13}s_{23}c_{12}e^{i\delta} & c_{23}c_{12} - s_{13}s_{23}s_{12}e^{i\delta} & c_{13}s_{23} \\ s_{23}s_{12} - s_{13}c_{23}c_{12}e^{i\delta} & -s_{23}c_{12} - s_{13}c_{23}s_{12}e^{i\delta} & c_{13}c_{23} \end{pmatrix}, \quad (26)$$

where $c_{jk} \equiv \cos \theta_{jk}$ and $s_{jk} \equiv \sin \theta_{jk}$. For Majorana neutrinos, U contains two further multiplicative phase factors, but these do not enter in oscillation phenomena.

With the plausible hierarchical neutrino mass spectrum $m_1 < m_2 \ll m_3$ and the assumption that the LSND effect is not a neutrino oscillation phenomena, we can identify the largest δm^2 scale with the atmospheric neutrino deficit: $\delta M^2 = \delta m_{atm}^2 = \delta m_{32}^2 \simeq \delta m_{31}^2$. In the approximation that we neglect oscillations driven by the small δm^2 scale, the ν_e oscillation probabilities can be written as

$$\begin{aligned} P(\nu_e \rightarrow \nu_e) &\simeq 1 - 4|U_{e3}|^2(1 - |U_{e3}|^2) \sin^2\left(\frac{\delta m_{atm}^2 L}{4E}\right) \\ &= 1 - \sin^2(2\theta_{13}) \sin^2\left(\frac{\delta m_{atm}^2 L}{4E}\right), \end{aligned} \quad (27)$$

$$\begin{aligned} P(\nu_e \rightarrow \nu_\mu) &\simeq 4|U_{e3}|^2|U_{\mu 3}|^2 \sin^2\left(\frac{\delta m_{atm}^2 L}{4E}\right) \\ &= \sin^2(2\theta_{13}) \sin^2(\theta_{23}) \sin^2\left(\frac{\delta m_{atm}^2 L}{4E}\right), \end{aligned} \quad (28)$$

$$\begin{aligned} P(\nu_e \rightarrow \nu_\tau) &\simeq 4|U_{\tau 3}|^2|U_{e3}|^2 \sin^2\left(\frac{\delta m_{atm}^2 L}{4E}\right) \\ &= \sin^2(2\theta_{13}) \cos^2(\theta_{23}) \sin^2\left(\frac{\delta m_{atm}^2 L}{4E}\right) \end{aligned} \quad (29)$$

and the ν_μ oscillation probabilities are

$$\begin{aligned} P(\nu_\mu \rightarrow \nu_\mu) &\simeq 1 - 4|U_{\mu 3}|^2(1 - |U_{\mu 3}|^2) \sin^2\left(\frac{\delta m_{atm}^2 L}{4E}\right) \\ &= 1 - 4 \sin^2(\theta_{23}) \cos^2(\theta_{13})(1 - \sin^2(\theta_{23}) \cos^2(\theta_{13})) \sin^2\left(\frac{\delta m_{atm}^2 L}{4E}\right), \end{aligned} \quad (30)$$

$$\begin{aligned}
P(\nu_\mu \rightarrow \nu_e) &\simeq 4|U_{e3}|^2|U_{\mu3}|^2 \sin^2\left(\frac{\delta m_{atm}^2 L}{4E}\right) \\
&= \sin^2(2\theta_{13}) \sin^2(\theta_{23}) \sin^2\left(\frac{\delta m_{atm}^2 L}{4E}\right),
\end{aligned} \tag{31}$$

$$\begin{aligned}
P(\nu_\mu \rightarrow \nu_\tau) &\simeq 4|U_{\mu3}|^2|U_{\tau3}|^2 \sin^2\left(\frac{\delta m_{atm}^2 L}{4E}\right) \\
&= \sin^2(2\theta_{23}) \cos^4(\theta_{13}) \sin^2\left(\frac{\delta m_{atm}^2 L}{4E}\right).
\end{aligned} \tag{32}$$

The CP-odd contribution to the atmospheric neutrino oscillation probability vanishes in the one-mass-scale-dominant approximation. However if we include the effects of the small mass scale, δm_{21}^2 , then

$$\begin{aligned}
P_{\text{CP-odd}}(\nu_\mu \rightarrow \nu_\tau) &= -4c_{12}c_{13}^2c_{23}s_{12}s_{13}s_{23}(\sin \delta) \\
&\quad \left[\sin\left(\frac{\delta m_{21}^2 L}{2E}\right) \sin^2\left(\frac{\delta m_{atm}^2 L}{4E}\right) + \sin\left(\frac{\delta m_{atm}^2 L}{2E}\right) \sin^2\left(\frac{\delta m_{21}^2 L}{4E}\right) \right].
\end{aligned} \tag{33}$$

At distances significantly larger than the atmospheric neutrino oscillation length, $E/\delta m_{atm}^2$, the second term in brackets averages to zero whereas the sin squared part of the first term averages to one half, leaving

$$P_{\text{CP-odd}}(\nu_\mu \rightarrow \nu_\tau) \simeq -2c_{12}c_{13}^2c_{23}s_{12}s_{13}s_{23}(\sin \delta) \sin\left(\frac{\delta m_{21}^2 L}{2E}\right). \tag{34}$$

The Jarlskog factor [24], J , is given by $J = c_{12}c_{13}^2c_{23}s_{12}s_{13}s_{23}(\sin \delta)$ and is a convenient measure of the size of the CP violation.

If the neutrinos propagate through matter, these expressions must be modified. The propagation of neutrinos through matter is described by the evolution equation

$$i\frac{d\nu_\alpha}{dt} = \sum_\beta \left[\left(\sum_j U_{\alpha j} U_{\beta j}^* \frac{m_j^2}{2E_\nu} \right) + \frac{A}{2E_\nu} \delta_{\alpha e} \delta_{\beta e} \right] \nu_\beta, \tag{35}$$

where $A/(2E_\nu)$ is the amplitude for coherent forward charged-current scattering of ν_e on electrons,

$$A = 2\sqrt{2}G_F N_e E_\nu = 1.52 \times 10^{-4} \text{ eV}^2 Y_e \rho (\text{g/cm}^3) E (\text{GeV}) \tag{36}$$

(for $\bar{\nu}_e$ A is replaced with $-A$). Here Y_e is the electron fraction and $\rho(t)$ is the matter density. Density profiles through the earth can be calculated using the Earth Model [25], and are shown in Fig. 12. For neutrino trajectories through the earth's crust, the density is typically of order 3 gm/cm^3 , and $Y_e \simeq 0.5$. For very long baselines a constant density approximation is not sufficient and oscillation calculations must explicitly take account of $\rho(t)$. However the constant density approximation is very useful to understand the physics of neutrinos propagating through the earth since the variation of the earth's density is not large.

The propagation Eq. (35) can be re-expressed in terms of mass-squared differences:

$$i\frac{d\nu_\alpha}{dt} = \sum_\beta \frac{1}{2E_\nu} \left[\delta m_{31}^2 U_{\alpha 3} U_{\beta 3}^* + \delta m_{21}^2 U_{\alpha 2} U_{\beta 2}^* + A \delta_{\alpha e} \delta_{\beta e} \right] \nu_\beta. \tag{37}$$

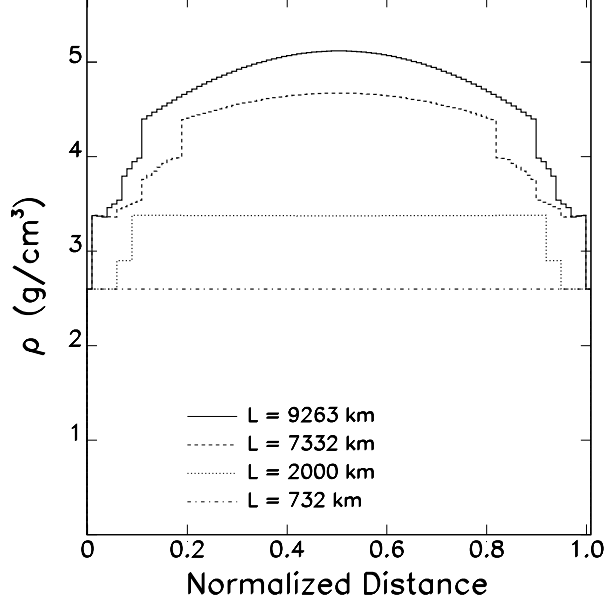


Figure 12: Density profiles for trajectories through the Earth. Calculation from Ref. 16.

This evolution equation can be solved numerically for given input values of the δm^2 and mixing matrix elements.

In the approximation where we neglect oscillations driven by the small δm^2 scale, the evolution equations are:

$$i \frac{d}{dt} \begin{pmatrix} \nu_e \\ \nu_\mu \\ \nu_\tau \end{pmatrix} = \frac{\delta m^2}{2E} \begin{pmatrix} \frac{A}{\delta m^2} + |U_{e3}|^2 & U_{e3}U_{\mu 3}^* & U_{e3}U_{\tau 3}^* \\ U_{e3}^*U_{\mu 3} & |U_{\mu 3}|^2 & U_{\mu 3}U_{\tau 3}^* \\ U_{e3}^*U_{\tau 3} & U_{\mu 3}^*U_{\tau 3} & |U_{\tau 3}|^2 \end{pmatrix} \begin{pmatrix} \nu_e \\ \nu_\mu \\ \nu_\tau \end{pmatrix}. \quad (38)$$

For propagation through matter of constant density, the flavor eigenstates are related to the mass eigenstates ν_j^m by

$$\nu_\alpha = \sum U_{\alpha j}^m |\nu_j^m\rangle, \quad (39)$$

where

$$U^m = \begin{pmatrix} 0 & c_{13}^m & s_{13}^m \\ -c_{23} & -s_{13}^m s_{23} & c_{13}^m s_{23} \\ s_{23} & -s_{13}^m c_{23} & c_{13}^m c_{23} \end{pmatrix} \quad (40)$$

and θ_{13}^m is related to θ_{13} by

$$\tan 2\theta_{13}^m = \sin 2\theta_{13} / \left(\cos 2\theta_{13} - \frac{A}{\delta m^2} \right). \quad (41)$$

We note that U^m has the form of the vacuum U with the substitutions

$$\theta_{13} \rightarrow \theta_{13}^m, \quad \theta_{23} \rightarrow \theta_{23}, \quad \theta_{12} \rightarrow \pi/2, \quad \delta = 0. \quad (42)$$

Equation (41) implies that

$$\sin^2 2\theta_{13}^m = \sin^2 2\theta_{13} / \left(\left(\frac{A}{\delta m^2} - \cos 2\theta_{13} \right)^2 + \sin^2 2\theta_{13} \right). \quad (43)$$

Thus there is a resonant enhancement for

$$A = \delta m^2 \cos 2\theta_{13} \quad (44)$$

or equivalently

$$E_\nu \approx 15 \text{ GeV} \left(\frac{\delta m^2}{3.5 \times 10^{-3} \text{ eV}^2} \right) \left(\frac{1.5 \text{ g/cm}^3}{\rho Y_e} \right) \cos 2\theta_{13}. \quad (45)$$

The resonance occurs only for positive δm^2 for neutrinos and only for negative δm^2 for anti-neutrinos.¹ For negative δm^2 the oscillation amplitude in Eq. (43) is smaller than the vacuum oscillation amplitude. Thus the matter effects give us a way in principle to determine the sign of δm^2 .

It is instructive to look at the dependence of the oscillation probabilities on the neutrino energy as a function of the oscillation parameters and the baseline. Some examples from Ref. [26] are shown in Fig. 13 for $\nu_e \rightarrow \nu_\mu$ oscillations. Note that for parameters corresponding to the large mixing angle MSW solar solution, maximal CP violation results in a small but visible effect. Matter effects, which have been computed using the density profile from the Earth Model, can have substantial effects, and are very sensitive to $\sin^2 2\theta_{13}$.

3.1.3 Three Active Flavor Oscillation Scenarios

We now define some representative three-flavor neutrino oscillation parameter sets that can be used to establish how well experiments at a neutrino factory could determine the oscillation parameters. We begin by considering constraints from existing experiments.

If we assume CPT invariance then the oscillation probability for $\bar{\nu}_e \rightarrow \bar{\nu}_e$ is equal to that for $\nu_e \rightarrow \nu_e$. The CHOOZ results [27] imply:

$$\sin^2 2\theta_{\text{reac}} \equiv 4|U_{e3}|^2(1 - |U_{e3}|^2) = \sin^2 2\theta_{13} \leq 0.1 \quad (46)$$

for the range $\delta M^2 \gtrsim 10^{-3} \text{ eV}^2$. On the other hand, for the solar neutrino experiments, with $|U_{e3}|^2 \ll 1$, one finds

$$\sin^2 2\theta_{\text{solar}} \equiv 4|U_{e1}|^2|U_{e2}|^2 = \sin^2 2\theta_{12} \cos^4 \theta_{13} \sim \sin^2 2\theta_{12} \quad (47)$$

¹If the LSND effect is due to neutrino oscillations then $\delta m^2 \gg \text{O}(10^{-3}) \text{ eV}^2$ and the resonance occurs at energies much higher than those of interest at the currently envisioned neutrino factory.

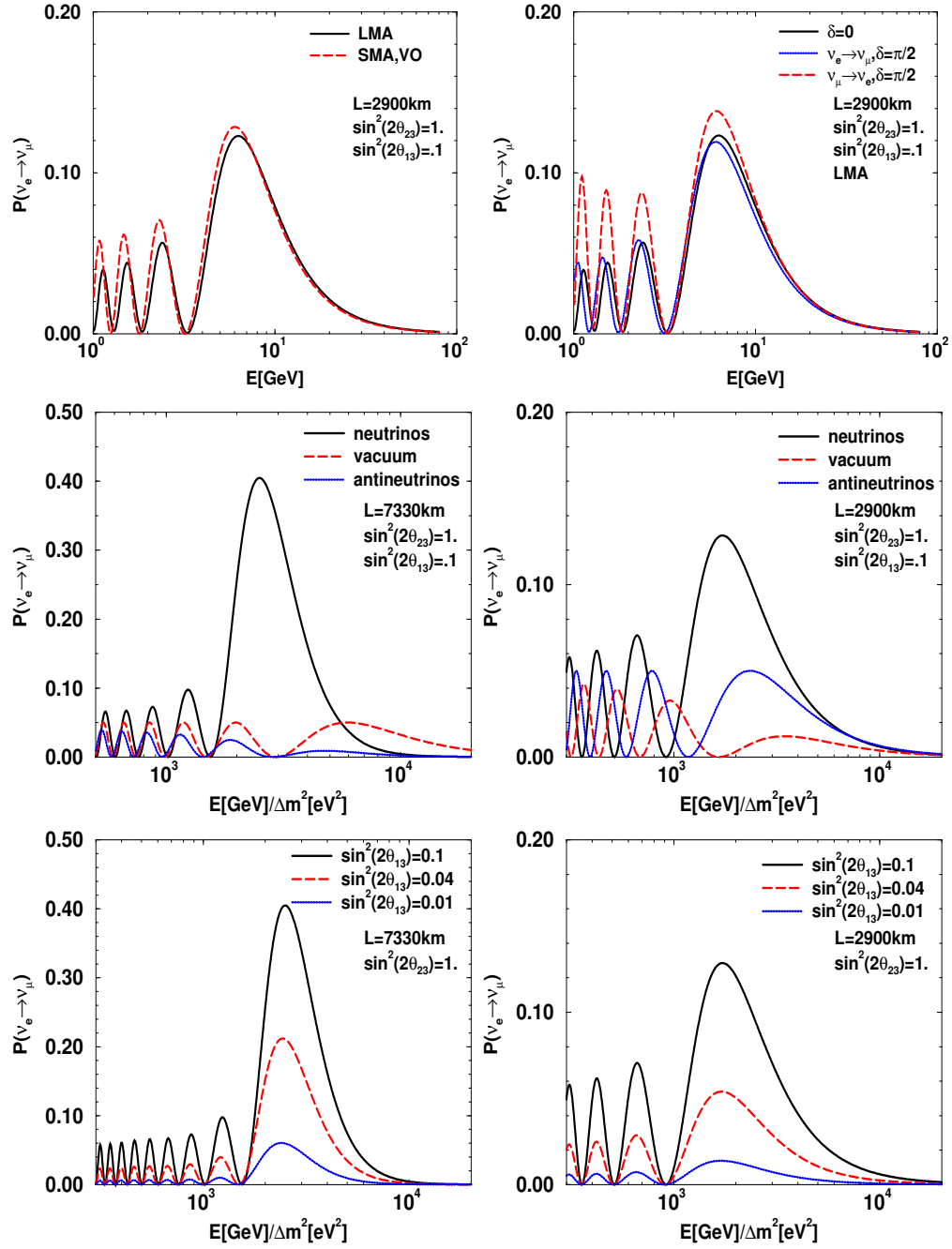


Figure 13: Dependence of $\nu_e \rightarrow \nu_\mu$ oscillation probability on neutrino energy for some representative oscillation parameters. Plots are from Ref. 26 and show the effects of varying δ (top plots), matter effects (middle plots), and $\sin^2 2\theta_{13}$ dependence (bottom plots).

with $\sin^2 2\theta_{12} \sim 0.006$ in the case of the small angle MSW solution with $\delta m_{21}^2 \sim 6 \times 10^{-6} \text{ eV}^2$ or $\sin^2 2\theta_{12} \sim 1.0$ in the case of the large angle MSW solution with $\delta m_{21}^2 \sim 5 \times 10^{-5} \text{ eV}^2$, the LOW solution with $\delta m_{21}^2 \sim 10^{-7} \text{ eV}^2$, or the vacuum solutions with $\delta m_{21}^2 \sim 4 \times 10^{-10} \text{ eV}^2$ or $\delta m_{21}^2 \sim 8 \times 10^{-11} \text{ eV}^2$.

The atmospheric neutrino oscillation experiments favor $\nu_\mu \rightarrow \nu_\tau$ [28], and in the one-mass-scale-dominant approximation the best fit from the SuperK experiment [29] yields

$$\sin^2 2\theta_{atm} \equiv 4|U_{\mu 3}|^2|U_{\tau 3}|^2 = \sin^2 2\theta_{23} \cos^4 \theta_{13} = 1.0 \quad (48)$$

with $\delta m_{atm}^2 = 3.5 \times 10^{-3} \text{ eV}^2$. Unpublished analyses of a substantially enlarged data set by the SuperK experiment have yielded the same central value for $\sin^2 2\theta_{atm}$ and essentially the same value of δm_{atm}^2 , 2.5×10^{-3} [29]; we shall use the published fits in the following.

Based on these considerations we define the representative three-flavor parameter sets shown in Table 3. The first three scenarios do not attempt to fit the LSND anomaly. These scenarios have the Atmospheric anomaly explained by $\nu_\mu \rightarrow \nu_\tau$ oscillation with maximal mixing and the Solar Anomaly explained by one of the MSW Solar solutions:

Scenario IA1 - Large Angle MSW

Scenario IA2 - Small Angle MSW

Scenario IA3 - LOW MSW.

Alternatively we can keep the LSND anomaly, and either drop the solar neutrino deficit, or attempt to find a “fit” (necessarily with a poor χ^2) that explains all three neutrino anomalies [30]:

Scenario IB1 - Atmospheric and LSND

Scenario IC1 - Atmospheric, Solar and LSND

For scenario IC1 the Atmospheric anomaly is a mixture of $\nu_\mu \rightarrow \nu_\tau$ and $\nu_\mu \rightarrow \nu_e$ and the solar electron neutrino flux is reduced by a factor two independent of energy. There are large contributions to the χ^2 for this scenario coming from the Atmospheric Neutrino Anomaly as well as the Homestake (Chlorine) Solar neutrino experiment.

Note that the Jarlskog J-factor is small for all scenarios. It is clear that CP violation will be very difficult to observe.

Table 3: Parameters for the three-flavor oscillation scenarios defined for the study.

parameter	IA1	IA2	IA3	1B1	1C1
δm_{32}^2 (eV ²)	3.5×10^{-3}	3.5×10^{-3}	3.5×10^{-3}	3.5×10^{-3}	0.3
δm_{21}^2 (eV ²)	5×10^{-5}	6×10^{-6}	1×10^{-7}	0.3	7×10^{-4}
$\sin^2 2\theta_{23}$	1.0	1.0	1.0	1.0	0.53
$\sin^2 2\theta_{13}$	0.04	0.04	0.04	0.015	0.036
$\sin^2 2\theta_{12}$	0.8	0.006	0.9	0.015	0.89
δ	$0, \pm\pi/2$	$0, \pm\pi/2$	$0, \pm\pi/2$	$0, \pm\pi/2$	$0, \pm\pi/2$
$\sin^2 2\theta_{atm}$	0.98	0.98	0.98	0.99	-
$\sin^2 2\theta_{reac}$	0.04	0.04	0.04	0.03	-
$\sin^2 2\theta_{solar}$	0.78	0.006	0.88	-	-
$\sin^2 2\theta_{LSND}$	-	-	-	0.03	0.036
J	0.02	0.002	0.02	0.002	0.015

3.1.4 Three Active and One Sterile Neutrinos

In order to incorporate the observed $\nu_\mu \rightarrow \nu_e$ and $\bar{\nu}_\mu \rightarrow \bar{\nu}_e$ LSND appearance results [9] and achieve an acceptable χ^2 in the fit, it is necessary to introduce at least one light sterile neutrino. As discussed earlier, the theoretical case for sterile neutrinos is unclear, and various neutrino mass schemes predict anything from $n_s = 0$ to many. To admit just one must be regarded as a rather unnatural choice. We consider this case because it allows us to explain the Atmospheric, Solar and LSND anomalies with the fewest number of new parameters.

Scenarios with three nearly degenerate neutrinos (for example $m_1 \leq m_2 \leq m_3 \ll m_4$ or $m_1 \ll m_2 \leq m_3 \leq m_4$) are essentially ruled out by a Schwarz inequality on the leptonic mixing elements [31]: $|U_{\mu 4} U_{e 4}^*|^2 \leq |U_{\mu 4}|^2 |U_{e 4}|^2 \leq 0.008$ which fails to be satisfied in the allowed LSND region. Of the two scenarios with $m_1 < m_2 \ll m_3 < m_4$, the one with $\delta m_{21}^2 \sim \delta m_{solar}^2$, $\delta m_{43}^2 \sim \delta m_{atm}^2$ is preferred over the other arrangement which is on the verge of being ruled out by the Heidelberg-Moscow $\beta\beta_{0\nu}$ decay experiment [32] giving $\langle m \rangle \leq 0.2$ eV.

With the three relevant mass scales given by

$$\delta m_{sol}^2 = \delta m_{21}^2 \ll \delta m_{atm}^2 = \delta m_{43}^2 \ll \delta m_{LSND}^2 = \delta m_{32}^2$$

and the flavors ordered according to $\{s, e, \mu, \tau\}$, the 4×4 neutrino mixing matrix depends on six angles and three phases and is conveniently chosen to be [33]

$$\begin{aligned}
U &= \begin{pmatrix} U_{s1} & U_{s2} & U_{s3} & U_{s4} \\ U_{e1} & U_{e2} & U_{e3} & U_{e4} \\ U_{\mu1} & U_{\mu2} & U_{\mu3} & U_{\mu4} \\ U_{\tau1} & U_{\tau2} & U_{\tau3} & U_{\tau4} \end{pmatrix} \\
&= R_{14}(\theta_{14}, 0) R_{13}(\theta_{13}, 0) R_{24}(\theta_{24}, 0) R_{23}(\theta_{23}, \delta_3) R_{34}(\theta_{34}, \delta_2) R_{12}(\theta_{12}, \delta_1)
\end{aligned} \tag{49}$$

where, for example,

$$R_{23}(\theta_{23}, \delta_3) = \begin{pmatrix} 1 & 0 & 0 & 0 \\ 0 & c_{23} & s_{23}e^{-i\delta_3} & 0 \\ 0 & -s_{23}e^{i\delta_3} & c_{23} & 0 \\ 0 & 0 & 0 & 1 \end{pmatrix}.$$

In the limit where the $m_1 - m_2$ and $m_3 - m_4$ pairs are considered degenerate, $R_{12}(\theta_{12}, \delta_1) = R_{34}(\theta_{34}, \delta_3) = I$, and only four angles and one phase appear in the mixing matrix

$$U = \begin{pmatrix} c_{14}c_{13} & -c_{14}s_{13}s_{23}e^{i\delta_3} - s_{14}s_{24}c_{23} & c_{14}s_{13}c_{23} - s_{14}s_{24}s_{23}e^{-i\delta_3} & s_{14}c_{24} \\ 0 & c_{24}c_{23} & c_{24}s_{23}e^{-i\delta_3} & s_{24} \\ -s_{13} & -c_{13}s_{23}e^{i\delta_3} & c_{23}c_{13} & 0 \\ -s_{14}c_{13} & s_{14}s_{13}s_{23}e^{i\delta_3} - c_{14}s_{24}c_{23} & -s_{14}s_{13}c_{23} - c_{14}s_{24}s_{23}e^{-i\delta_3} & c_{14}c_{24} \end{pmatrix} \tag{50}$$

with the same angle and phase rotation convention adopted as before.

In this one-mass-scale-dominant approximation with the large mass gap labeled $\delta M^2 = \delta m_{L\text{SND}}^2$, the oscillations are again CP-conserving, and a short baseline experiment is needed to determine the extra relevant mixing angles and phase. The oscillation probabilities of interest are:

$$\begin{aligned}
P(\nu_e \rightarrow \nu_e) &= 1 - 4c_{24}^2c_{23}^2(s_{24}^2 + s_{23}^2c_{24}^2)\sin^2\left(\frac{\delta M^2 L}{4E}\right), \\
P(\nu_e \rightarrow \nu_\mu) &= P(\nu_\mu \rightarrow \nu_e) = 4c_{13}^2c_{24}^2c_{23}^2s_{23}^2\sin^2\left(\frac{\delta M^2 L}{4E}\right), \\
P(\nu_e \rightarrow \nu_\tau) &= 4c_{23}^2c_{24}^2[(s_{13}^2s_{14}^2s_{23}^2 + c_{14}^2c_{23}^2s_{24}^2) \\
&\quad - 2c_{14}s_{14}c_{23}s_{23}s_{13}s_{24}\cos\delta_3]\sin^2\left(\frac{\delta M^2 L}{4E}\right), \\
P(\nu_\mu \rightarrow \nu_\mu) &= 1 - 4c_{13}^2c_{23}^2(s_{23}^2 + s_{13}^2c_{23}^2)\sin^2\left(\frac{\delta M^2 L}{4E}\right), \\
P(\nu_\mu \rightarrow \nu_\tau) &= 4c_{13}^2c_{23}^2[(s_{13}^2s_{14}^2c_{23}^2 + c_{14}^2s_{23}^2s_{24}^2) \\
&\quad + 2c_{14}s_{14}c_{23}s_{23}s_{13}s_{24}\cos\delta_3]\sin^2\left(\frac{\delta M^2 L}{4E}\right).
\end{aligned} \tag{51}$$

If the neutrinos propagate through matter, these expressions must be modified. Matter effects for the three active and one sterile neutrino scenario are similar in nature to those for the three active neutrino case, Eq. (35). However in Eq. (35) a flavor diagonal term that only contributes to an overall phase has

been discarded. This term comes from the coherent forward scattering amplitude for the active flavors scattering from the electrons, protons and neutrons in matter via the exchange of a virtual Z-boson. Since the sterile neutrino does not interact with the Z-boson this term must be added to the diagonal terms for the active neutrinos (or equivalently subtracted from the diagonal part for the sterile neutrino). That is in Eq. (35)

$$\frac{A}{2E_\nu}\delta_{\alpha e}\delta_{\beta e} \rightarrow \frac{A}{2E_\nu}\delta_{\alpha e}\delta_{\beta e} - \frac{A'}{2E_\nu}\delta_{\alpha s}\delta_{\beta s} \quad (52)$$

where A' is given by Eq. (36) with Y_e replaced by $-\frac{1}{2}(1 - Y_e)$ for electrically neutral matter.

In order to search for CP violation, at least two mass scales must be relevant. For simplicity consider

$$\begin{aligned} \delta m_{21}^2 &= 0, & \delta m_{43}^2 &= \delta m^2, \\ \delta m_{32}^2 &= \delta m_{31}^2 = \delta M^2, \\ \delta m_{42}^2 &= \delta m_{41}^2 = \delta M^2 + \delta m^2 \end{aligned} \quad (53)$$

with five angles and two phases present, since $U_{12}(\theta_{12}, \delta_1) = I$. The CP-odd parts of the relevant probabilities are:

$$\begin{aligned} P_{\text{CP-odd}}(\nu_e \rightarrow \nu_\mu) &= 8c_{13}^2 c_{23}^2 c_{24} c_{34} s_{24} s_{34} \sin(\delta_2 + \delta_3) \left(\frac{\delta m^2 L}{4E}\right) \sin^2\left(\frac{\delta M^2 L}{4E}\right) \\ P_{\text{CP-odd}}(\nu_e \rightarrow \nu_\tau) &= 4c_{23} c_{24} \{ 2c_{14} s_{14} c_{23} s_{23} s_{13} s_{24} (s_{13}^2 s_{14}^2 - c_{14}^2) \sin(\delta_2 + \delta_3) \\ &\quad + c_{14} c_{34} s_{13} s_{14} s_{34} [(s_{23}^2 - s_{24}^2) \sin \delta_2 + s_{23}^2 s_{24}^2 \sin(\delta_2 + 2\delta_3)] \\ &\quad + c_{14} c_{24} s_{13} s_{14} s_{23} s_{24} (c_{34}^2 - s_{34}^2) \sin \delta_3 \} \\ &\quad \times \left(\frac{\delta m^2 L}{4E}\right) \sin^2\left(\frac{\delta M^2 L}{4E}\right) \\ P_{\text{CP-odd}}(\nu_\mu \rightarrow \nu_\tau) &= 8c_{13}^2 c_{23}^2 c_{24} c_{34} s_{34} [c_{14} c_{23} s_{13} s_{14} \sin \delta_2 + c_{14}^2 s_{23} s_{24} \sin(\delta_2 + \delta_3)] \\ &\quad \times \left(\frac{\delta m^2 L}{4E}\right) \sin^2\left(\frac{\delta M^2 L}{4E}\right) \end{aligned} \quad (54)$$

where only the leading order term in δm^2 has been kept. The CP-even expressions also have such additional small corrections.

The present atmospheric neutrino data favors the $\nu_\mu \rightarrow \nu_\tau$ oscillation over the $\nu_\mu \rightarrow \nu_s$ oscillation. On the other hand, if a solar neutrino oscillates significantly into a sterile neutrino, only the small angle MSW solution is viable since the large angle solutions fail to provide enough $\nu + e^- \rightarrow \nu + e^-$ elastic scattering to be consistent with SuperK measurements [29]. Hence if it turns out that one of the large angle mixing solutions is the correct solution to the solar anomaly then something other than a single light sterile neutrino will be needed to explaining the solar, atmospheric and LSND results.

Table 4: Parameters for the four-flavor oscillation scenarios defined for the study. Note that for these parameter sets $\delta m_{41}^2 \sim \delta m_{31}^2 \sim \delta m_{42}^2 \sim \delta m_{32}^2 \equiv \delta M^2$, and $\sin^2 2\theta_{14} = \sin^2 2\theta_{13} = \sin^2 2\theta_{24} = \sin^2 2\theta_{23}$

parameter	IIA1	IIB1
δm_{43}^2 (eV ²)	3.5×10^{-3}	3.5×10^{-3}
δm_{21}^2 (eV ²)	6×10^{-6}	6×10^{-6}
δM^2 (eV ²)	0.3	1.0
$\sin^2 2\theta_{34}$	1.0	1.0
$\sin^2 2\theta_{12}$	0.006	0.006
$\sin^2 2\theta_{14}$	0.03	0.003
δ_1	0	0
δ_2	$0, \pm\pi/2$	$0, \pm\pi/2$
δ_3	0	0

3.1.5 Scenarios with Three Active plus One Sterile Neutrino

We now consider some representative four-flavor neutrino oscillation parameter sets that can be used to establish how well experiments at a neutrino factory could determine the oscillation parameters. As was noted earlier, the only viable solutions with one sterile and three active neutrinos require that there be two sets of almost degenerate neutrinos separated by the largest δm^2 . We begin by considering the constraints from CHOOZ and LSND. Note that the effective two-component atmospheric and solar mixing angles are:

$$\begin{aligned}\sin^2 2\theta_{atm} &= 4|U_{\mu 3}|^2|U_{\mu 4}|^2 = c_{23}^4 c_{13}^4 \sin^2 2\theta_{34} \\ \sin^2 2\theta_{sol} &= 4|U_{e 1}|^2|U_{e 2}|^2 = c_{24}^4 c_{23}^4 \sin^2 2\theta_{12}\end{aligned}\tag{55}$$

The CHOOZ constraint [27] from $P(\bar{\nu}_e \rightarrow \bar{\nu}_e)$ is:

$$c_{23}^2 \sin^2 2\theta_{24} + c_{24}^4 \sin^2 2\theta_{23} \leq 0.2\tag{56}$$

while the LSND constraint [9] from $P(\nu_\mu \rightarrow \nu_e)$ is:

$$10^{-3} \leq c_{13}^2 c_{24}^2 \sin^2 2\theta_{23} \leq 10^{-2}.\tag{57}$$

With this in mind, the parameter sets we have defined are summarized in Table 4. They are:

Scenario IIA1 - Low Mass LSND

Scenario IIB1 - High Mass LSND

3.2 Where will we be in 5-10 years ?

In this section, we briefly discuss the prospects for currently operating, planned, or proposed experiments exploring neutrino oscillations. The discussion will be broken down according to the various oscillation modes. The current limits and the expected reach of some of the future experiments are summarized in Fig. 14, and Tables 5 and 6.

3.2.1 $\nu_\mu \rightarrow \nu_\tau, \nu_s$

The evidence for ν_μ disappearance in atmospheric neutrinos at SuperK is convincing [34]. The preferred region of parameter space is given [35] by $10^{-3} < \delta m^2 < 10^{-2} \text{ eV}^2$ at near maximal mixing ($\sin^2 2\theta \sim 1$). The $\nu_\mu \leftrightarrow \nu_e$ interpretation of the atmospheric neutrino deficit is disfavored by the SuperK data and is ruled out by the CHOOZ [36] and PaloVerde [37] experiments. The two immediate issues are (1) the precise determination of δm^2 and $\sin^2 2\theta$, and (2) discrimination between $\nu_\mu \rightarrow \nu_\tau$ and $\nu_\mu \rightarrow \nu_s$.

Future SuperK data will probably not shrink the currently preferred region of parameter space by very much. The precision with which δm^2 can be extracted from the observed event distributions depends on the precisions with which the event-by-event values of L and E are determined. The greatest sensitivity to δm^2 comes from the sample of events with values of L/E corresponding to the region of the first oscillation maximum, which in practice are those events from neutrinos coming from approximately the horizontal direction. However, for these events the L precision is limited by the angular resolution of the detector.

SuperK can discriminate between $\nu_\mu \rightarrow \nu_s$ and $\nu_\mu \rightarrow \nu_\tau$ by looking for matter effects and by measuring the number of NC interactions. The lack of evidence for matter effects in up-going muons (in both partially-contained events and in the NC-enriched multi-ring event sample) already disfavors $\nu_\mu \rightarrow \nu_s$ at the 99% confidence level. This result is expected to become firmer in the future. In addition, if there is a significant fraction of incident sterile neutrinos, there will be fewer NC events detected. The cleanest sample of NC events is the sample of events with a single detected π^0 . By comparing the ratio of π^0 (“two-electron”) events to ν_e CC (single-electron) events, SuperK already has a statistically significant handle on the NC/CC ratio ($\pm 6\%$ for 848.3 days livetime). However, the measurement is currently limited by large uncertainties on the NC single π^0 cross section (23–25% total systematic). K2K will measure this cross section in its near detector, and over the next few years this new information may produce the most dramatic improvement in ν_τ/ν_s discrimination [28].

The next generation of long-baseline experiments have been designed to be sensitive to oscillations with parameters that correspond to the SuperK favored region. The currently running K2K experiment [39] will cover $\delta m^2 > 2 \times 10^{-3} \text{ eV}^2$ after 3–5 years of running, and MINOS [15] will cover $\delta m^2 > 0.6 \times 10^{-3} \text{ eV}^2$ (both at 90% CL and for maximal mixing). These experiments are expected to

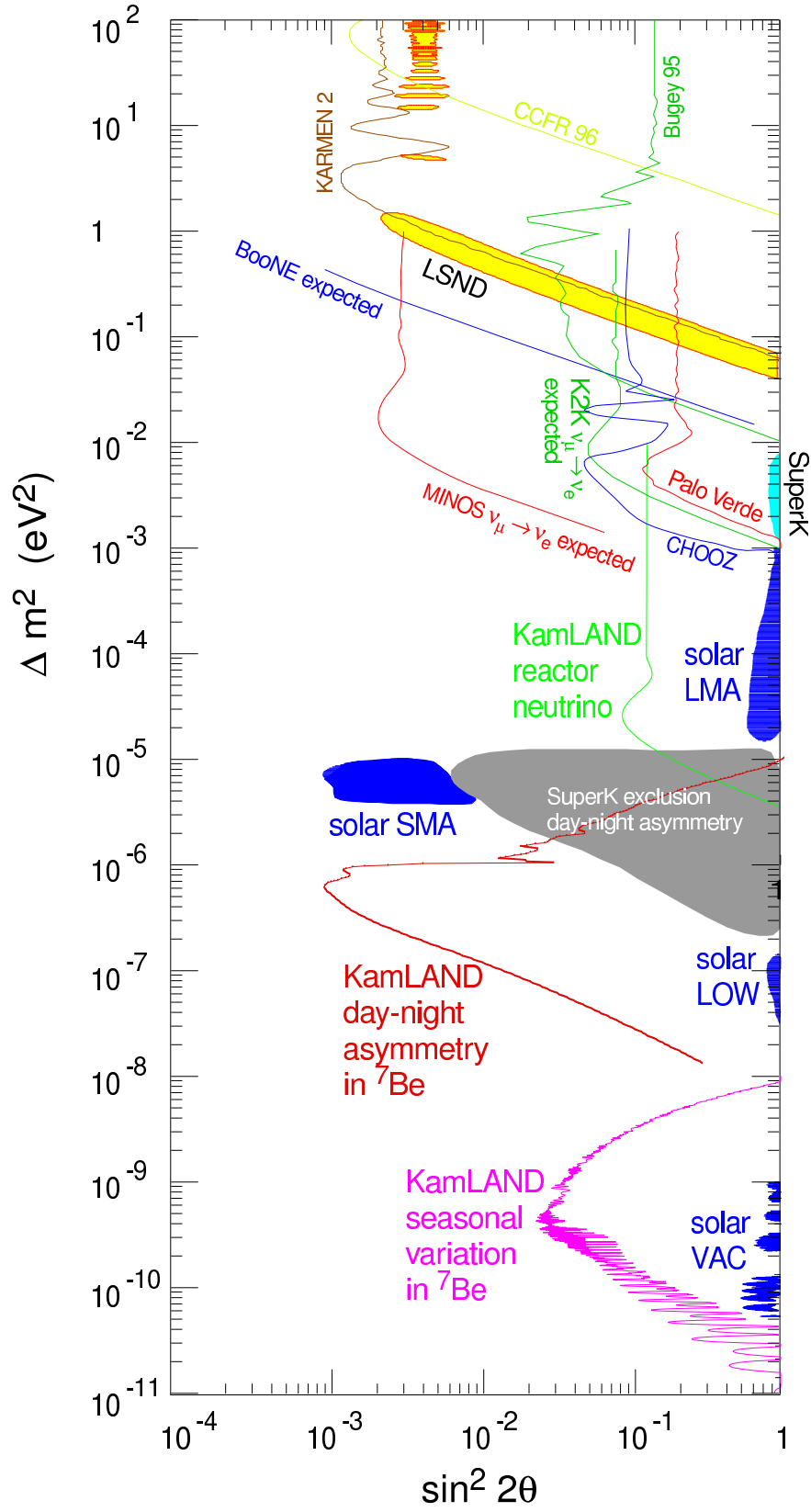


Figure 14: The current and expected limits at some of the future neutrino oscillation experiments. Note that different oscillation modes are shown together.

confirm the neutrino oscillation interpretation of the atmospheric neutrino data by about 2005. In addition to searching for ν_μ disappearance, K2K can also look for a distortion in the neutrino energy spectrum using quasi-elastic events, and MINOS can study NC/CC event energy distributions. In 2005 two experiments, OPERA [40] and ICANOE [41], are expected to begin taking data at the CNGS beam. Both OPERA and ICANOE aim primarily at τ -appearance and will cover $\delta m^2 > 2 \times 10^{-3} \text{ eV}^2$ after about 5 years of running.

Unless $\delta m^2 < 2 \times 10^{-3} \text{ eV}^2$ (allowed at 99% CL at SuperK), we expect to have a complete accelerator based experimental confirmation of atmospheric neutrino oscillations by 2010, and measurements of δm^2 and $\sin^2 2\theta$ at the O(10%) level (see Table 6). If $\delta m^2 < 2 \times 10^{-3} \text{ eV}^2$ some additional experiments will be necessary, such as MONOLITH (30 kt calorimeter) [42] or AQUARICH (novel 1 Mt Water Cerenkov) [43]. These experiments may study atmospheric neutrinos and exploit good angular resolution to search for dips in the zenith angle (or L/E) distribution.

3.2.2 $\nu_\mu \leftrightarrow \nu_e$

For large $\delta m^2 \sim 1 \text{ eV}^2$ suggested by the LSND experiment [9], Mini-BooNE [44] is expected to cover the entire preferred region of LSND parameter space with a wide safety margin. In the event of a positive signal, they plan to build another detector (BooNE) that will be able to measure the parameters with a precision O(10%) (see Table 6). Independent confirmation from ICANOE would also be expected. Should all of the experimental indications for oscillations (LSND, atmospheric, and solar) be confirmed we may be seeing evidence for the existence of sterile neutrinos. This would be a very exciting discovery, would raise many questions, and would require a new round of experiments.

For $\delta m^2 \sim 10^{-3}$ – 10^{-2} eV^2 we expect some $\nu_\mu \leftrightarrow \nu_e$ mixing if the heavier of the two mass eigenstates involved in the atmospheric neutrino oscillation contains any admixture of ν_e (*i.e.*, if $U_{e3} \neq 0$). Current limits from CHOOZ [36] and Palo Verde [37] require $|U_{e3}| < 0.1$. SuperK by itself is unlikely to improve on this sensitivity. K2K can look for ν_e appearance and improve the sensitivity to a finite $|U_{e3}|$ in some δm^2 range. MINOS and ICANOE are expected to be sensitive to $\sin^2 2\theta_{13} > \mathcal{O}(10^{-2})$ in the δm^2 region of interest by searching for ν_e appearance in their predominantly ν_μ beams. At this time it is not clear what is the interesting range for $\sin^2 2\theta_{13}$. If this mixing angle is not too small then K2K/MINOS/ICANOE can make a first measurement. The baselines for these experiments are too short, and statistics will be too limited, to observe matter effects. For very small mixing angles, comparable with the Small Mixing Angle MSW solution for the solar neutrino deficit (see [45]), an order of magnitude improvement in sensitivity beyond these experiments is required to make a first observation of $\nu_\mu \rightarrow \nu_e$ oscillations.

3.2.3 $\nu_e \rightarrow \nu_\mu, \nu_\tau, \nu_s$

Reactor and solar neutrino experiments can only look for these oscillations in the $\bar{\nu}_e$ disappearance mode.

The SNO [46] detector should discriminate between $\nu_e \rightarrow \nu_{\mu,\tau}$ and $\nu_e \rightarrow \nu_s$ solutions to the solar neutrino deficit by studying the distortion in the ν_e energy spectrum and by measuring the NC/CC ratio. The spectral distortion should occur for the SMA solution and for some regions of the VAC solution. Borexino [47] (or possibly KamLAND) will study ^7Be solar neutrinos, and should see day/night effects for the LOW scenario and seasonal effects for the VAC solution. The absence of the ^7Be electron neutrino flux would strongly suggest the SMA solution. There are additional experiments proposed to study lower energy neutrinos (esp. pp): HELLAZ, HERON, LENS, etc (see [48] for a recent overview). KamLAND [49] will look for the disappearance of $\bar{\nu}_e$ from reactors with sensitivity down to $\delta m^2 > 10^{-5} \text{ eV}^2$ for large mixing angles. With all of this data in the next 5-10 years we should have convincingly tested whether or not any of the current neutrino oscillation solutions to the solar neutrino problem are correct.

None of the solar neutrino experiments, however, discriminate between $\nu_e \rightarrow \nu_\mu$ and $\nu_e \rightarrow \nu_\tau$. MINOS, OPERA, and ICANOE can look for τ appearance but cannot separate $\nu_e \rightarrow \nu_\tau$ from $\nu_\mu \rightarrow \nu_\tau$.

3.2.4 Summary

To summarize, in 5–10 years:

- (i) $\nu_\mu \rightarrow \nu_\tau, \nu_s$. If the δm^2 associated with the atmospheric ν_μ deficit exceeds $\sim 2 \times 10^{-3} \text{ eV}^2$ accelerator experiments will measure δm^2 and $\sin^2 2\theta$ with precisions O(10%). If δm^2 is less than $\sim 2 \times 10^{-3} \text{ eV}^2$ new experiments will be required to accomplish this in the 2010 era.
- (ii) $\nu_\mu \leftrightarrow \nu_e$. If the LSND oscillations are confirmed BooNE would measure the associated δm^2 and $\sin^2 2\theta$ with precisions O(10%). However the oscillation framework (sterile neutrinos ?) might be complicated. If LSND is not confirmed and if $\sin^2 2\theta_{13} > 10^{-2}$, the first evidence for a finite value of $\sin^2 2\theta_{13}$ would be expected at long baseline accelerator experiments. If $\sin^2 2\theta_{13} < 10^{-2}$ then $\nu_\mu \rightarrow \nu_e$ will not be observed in the accelerator experiments and new experiments with at least an order of magnitude improved sensitivity will be needed.
- (iii) $\nu_e \rightarrow \nu_\mu, \nu_\tau, \nu_s$. Either one or none of the current solar neutrino deficit solutions will be remaining. If one survives, we will know whether the solar neutrino deficit is due to $\nu_e \rightarrow \nu_s$. If the $\nu_e \rightarrow \nu_\mu, \nu_\tau$ mode is favored we will not be able to distinguish between $\nu_e \rightarrow \nu_\mu$ or $\nu_e \rightarrow \nu_\tau$. In addition, $\nu_e \rightarrow \nu_\tau$ will not have been observed at long baseline accelerator experiments.

- (iv) Sterile neutrinos. If the LSND, atmospheric, and solar neutrino oscillation results are all confirmed we may be seeing evidence for the existence of sterile neutrinos. This would be a very exciting discovery ! Many new questions will arise requiring new experimental input.

Finally, it is worthwhile considering the possibility that a conventional neutrino beam and the corresponding detectors undergo significant upgrades within the coming decade. For example, a Fermilab proton driver upgrade might enable the acceleration of up to about a factor of four more beam in the Main Injector, resulting in a corresponding increase of the NUMI beam intensity. With an additional factor of 2 - 3 increase in detector mass, the event samples might be increased by an order of magnitude. However, systematic uncertainties must also be considered. For example, there will be limiting systematic uncertainties on the measurements of δm_{32}^2 and $\sin^2 2\theta_{23}$ with a MINOS-type experiment that arise from the uncertainties on the near/far detector CC reconstruction efficiencies, backgrounds to CC events from NC interactions, and an assumed 2% flux uncertainty from the near/far detector extrapolation. These uncertainties would prevent the precise determination of the oscillation parameters, even in the limit of infinite statistics. The ultimate (infinite statistics) precision that could be achieved with a MINOS-type experiment is shown in Fig. 15. A very-long-baseline neutrino factory experiment would be able to make very significant improvements to the precision with which δm_{32}^2 and $\sin^2 2\theta_{23}$ are determined.

Table 5: Experimental neutrino oscillation observations expected in the next 5–10 years at accelerator based experiments.

Scenario	Experiment	ν_μ Disap.	$\nu_\mu \rightarrow \nu_e$	$\nu_\mu \rightarrow \nu_\tau$	ν_e Disap.	$\nu_e \rightarrow \nu_\mu$	$\nu_e \rightarrow \nu_\tau$
IA1	K2K	Y	n	n	n	n	n
	MINOS	Y	n	Y	n	n	n
	ICANOE	Y	Y	Y	n	n	n
	OPERA	n	n	Y	n	n	n
	BooNE	n	n	n	n	n	n
IA2	K2K	Y	n	n	n	n	n
	MINOS	Y	n	Y	n	n	n
	ICANOE	Y	Y	Y	n	n	n
	OPERA	n	n	Y	n	n	n
	BooNE	n	n	n	n	n	n
IA3	K2K	Y	n	n	n	n	n
	MINOS	Y	Y	Y	n	n	n
	ICANOE	Y	Y	Y	n	n	n
	OPERA	n	n	Y	n	n	n
	BooNE	n	n	n	n	n	n
IB1	K2K	Y	n	n	n	n	n
	MINOS	Y	Y	Y	n	n	n
	ICANOE	Y	Y	Y	n	n	n
	OPERA	n	n	Y	n	n	n
	BooNE	n	Y	n	n	n	n
IC1	K2K	Y	n	n	n	n	n
	MINOS	Y	Y	Y	n	n	n
	ICANOE	Y	Y	Y	n	n	n
	OPERA	n	n	Y	n	n	n
	BooNE	Y	Y	n	n	n	n
IIA1	K2K	Y	n	n	n	n	n
	MINOS	Y	Y	Y	n	n	n
	ICANOE	Y	Y	Y	n	n	n
	OPERA	n	Y	Y	n	n	n
	BooNE	n	Y	n	n	n	n
IIB1	K2K	Y	n	n	n	n	n
	MINOS	Y	n	Y	n	n	n
	ICANOE	Y	Y	Y	n	n	n
	OPERA	n	n	Y	n	n	n
	BooNE	n	Y	n	n	n	n

Table 6: Neutrino oscillation mixing angle and leading δm^2 measurements expected in the next 5–10 years at accelerator based experiments.

Scenario	Experiment	Parameter			
		$\sin^2 2\theta_{12}$	$\sin^2 2\theta_{23}$	$\sin^2 2\theta_{13}$	δ
IA1	K2K		30%		50%
	MINOS		10% [†]		10% [†]
	ICANOE		13%	60%	11%
	OPERA		20%		14%
	BooNE				
IA2	K2K		30%		50%
	MINOS		10% [†]		10% [†]
	ICANOE		13%	60%	11%
	OPERA		20%		14%
	BooNE				
IA3	K2K		30%		50%
	MINOS		10% [†]		10% [†]
	ICANOE		13%	60%	11%
	OPERA		20%		14%
	BooNE				
IB1	K2K		30%		50%
	MINOS		10%		15%
	ICANOE		13%		11%
	OPERA		20%		14%
	BooNE	10%			10%
IC1	K2K		100%		100%
	MINOS		10%		15%
	ICANOE	25%	5%		7%
	OPERA		5%		7%
	BooNE		10%	15%	10%
		$\sin^2 2\theta_{23}$	$\sin^2 2\theta_{34}$	δm_{23}^2 (eV ²)	δm_{34}^2 (eV ²)
IIA1	K2K		30%		50%
	MINOS		10%		6%
	ICANOE	10%	13%	7%	11%
	OPERA	30%	20%	30%	14%
	BooNE	10%		10%	
IIB1	K2K		30%		50%
	MINOS		10%		6%
	ICANOE	50%	13%	50%	11%
	OPERA		20%		14%
	BooNE	10%		10%	

[†] With $\sin^2 2\theta_{23}$ constraint from SuperK.

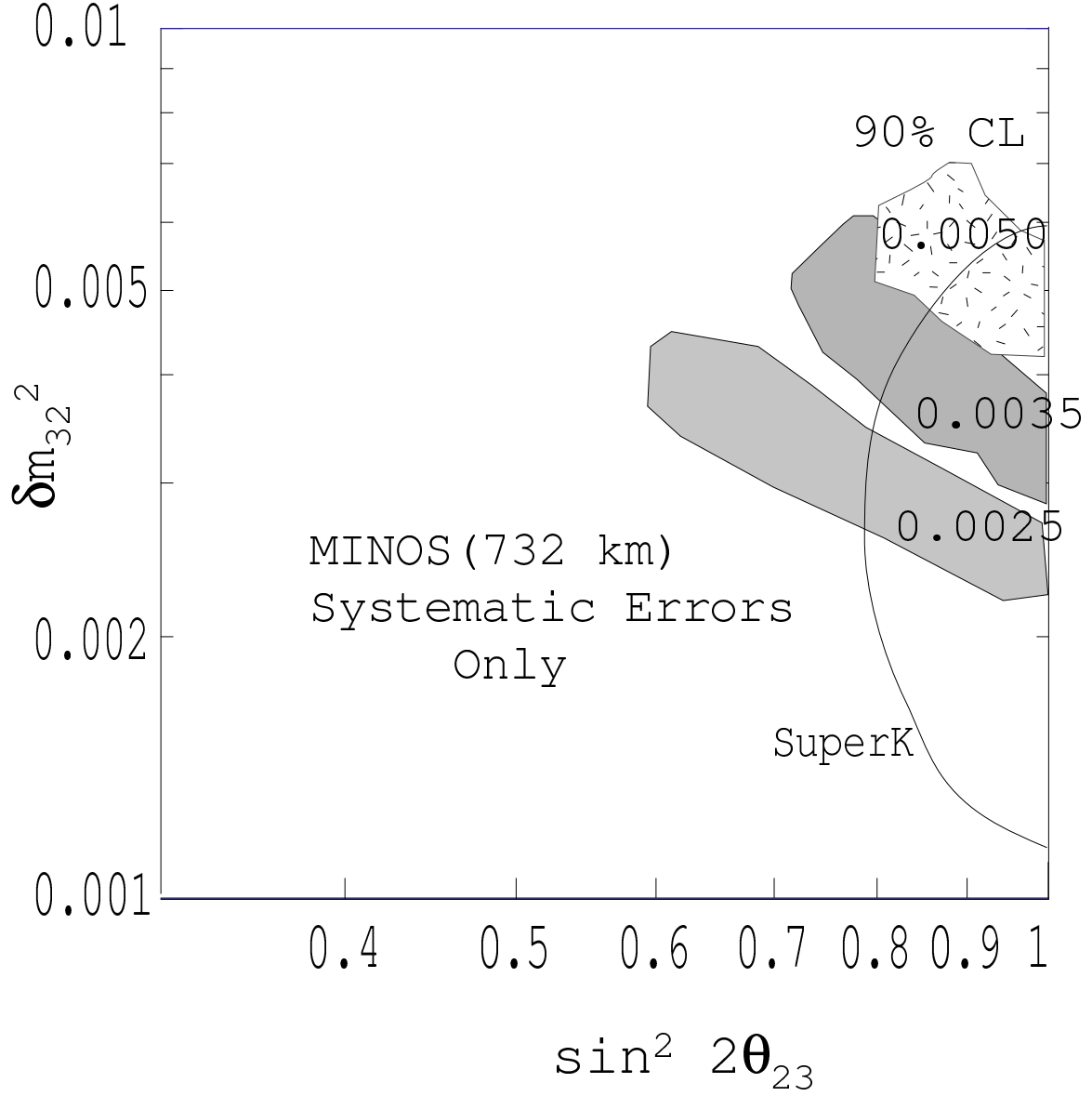


Figure 15: The expected precision that could be achieved by a MINOS-like experiment (low energy, baseline 732 km) in the limit of infinite statistics but with conservative estimates of systematic errors. The calculated sensitivities are based only on disappearance measurements. The oscillation parameters correspond to scenario IA1, and the regions of sensitivity shown are at 90% CL.

3.3 The neutrino factory oscillation physics program

We now consider the program of neutrino oscillation measurements at a neutrino factory in the era beyond the next generation of long baseline experiments. The main goals in this era are likely to be to precisely establish the oscillation framework, determine the pattern of neutrino masses, measure matter effects to confirm the MSW phenomenon, make precise measurements or place stringent limits on all of the mixing-matrix elements (and hence mixing-angles), and observe or place stringent limits on CP violation in the lepton sector. A neutrino factory can address each of these goals:

- (i) Establishing the oscillation framework. This requires measuring as a function of L/E , or putting stringent limits on, all of the oscillation probabilities $P(\nu_e \rightarrow \nu_x)$ and $P(\nu_\mu \rightarrow \nu_x)$. The oscillation framework can be established by summing the probabilities (a) $P(\nu_e \rightarrow \nu_e) + P(\nu_e \rightarrow \nu_\mu) + P(\nu_e \rightarrow \nu_\tau)$, and (b) $P(\nu_\mu \rightarrow \nu_e) + P(\nu_\mu \rightarrow \nu_\mu) + P(\nu_\mu \rightarrow \nu_\tau)$. In a three-flavor mixing framework, both sums should be unity for all L/E . If there are sterile neutrinos participating in the oscillations one or both of the sums will be less than unity. Part (b) of the test will almost certainly be made with conventional neutrino beams, although with a precision that will be limited by the $\nu_\mu \rightarrow \nu_\tau$ statistics and by the uncertainty on the $P(\nu_\mu \rightarrow \nu_e)$ measurement arising from the $O(1\%)$ ν_e contamination in the beam. Part (a) of the test, which includes the first observation of (or stringent limits on) $\nu_e \rightarrow \nu_\tau$ oscillations, can only be made with an energetic ($E_\nu > 10$ GeV) ν_e (or $\bar{\nu}_e$) beam, and will therefore be a unique part of the neutrino factory physics program.
- (ii) Determining the pattern of neutrino masses. The present experimental data suggests that, within a three-flavor mixing framework, there are two neutrino mass eigenstates separated by a small mass difference, and a third state separated from the pair by a “large” mass difference δM^2 . What is unknown is whether there is one low state plus two high states, or two low states plus one high state. This can be determined by measuring the sign of δM^2 . The only way we know of making this measurement is to exploit matter effects which, in a very long baseline experiment, alter the probabilities for oscillations that involve electron neutrinos; the modification being dependent on the sign of δM^2 . In principle the measurement could be made using a conventional neutrino beam and measuring $\nu_\mu \rightarrow \nu_e$ and $\bar{\nu}_\mu \rightarrow \bar{\nu}_e$ transitions over a baseline of several thousand km. However, the $O(1\%)$ ν_e ($\bar{\nu}_e$) contamination in the beam will introduce an irreducible background that is comparable to, or larger than, the ν_e signal. In contrast, at a neutrino factory it appears that the measurement can be done with great precision. Hence, determining the sign of δM^2 and the pattern of neutrino masses would be a key measurement at a neutrino factory.

- (iii) Measuring matter effects to confirm the MSW phenomenon. The same technique used to determine the sign of δm_{32}^2 can, with sufficient statistics, provide a precise quantitative confirmation of the MSW effect for neutrinos passing through the Earth. The modification to $P(\nu_e \rightarrow \nu_\mu)$, for example, depends upon the matter parameter A (Eq. (36)). Global fits to appearance and disappearance spectra that are used to determine the oscillation parameters can include A as a free parameter. The quantitative MSW test would be to recover the expected value for A . This measurement exploits the clean $\nu_e \rightarrow \nu_\mu$ signal at a neutrino factory, and would be a unique part of the neutrino factory physics program.
- (iv) Making precise measurements or placing stringent limits on all of the mixing-matrix elements. In practice the measured oscillation probability amplitudes are used to determine the mixing angles. If any of the angles are unmeasured or poorly constrained the relevant entries in the mixing matrix will also be poorly determined. At present there is only an upper limit on θ_{13} , the angle that essentially determines the $\nu_e \rightarrow \nu_\mu$ oscillation amplitude. A neutrino factory would provide a precise measurement of, or stringent limit on, this difficult angle. In fact, because all of the $\nu_\mu \rightarrow \nu_x$ and $\nu_e \rightarrow \nu_x$ oscillation amplitudes can be measured at a neutrino factory, global fits can be made to the measured spectra to provide a very precise determination of the mixing angles. This exploits the ν_e component in the beam. Finally, it should be noted that it is important to test the overall consistency of the oscillation framework by determining the mixing angles in more than one way, i.e. by using more than one independent set of measurements. Clearly the ν_e beam is an asset for this check.
- (v) Placing stringent limits on, or observing, CP violation in the lepton sector. Most of the oscillation scenarios defined for the study predict very small CP violating amplitudes. An important test of these scenarios would be to place stringent experimental limits on CP violation in the lepton sector. The LMA scenario IA1 might result in sufficiently large CP violating effects to be observable at a neutrino factory. The CP test involves comparing $\nu_e \rightarrow \nu_\mu$ with $\bar{\nu}_e \rightarrow \bar{\nu}_\mu$ oscillation rates, possible at a neutrino factory because backgrounds are very small. A search for CP violation in the lepton sector with the required precision cannot be done with a conventional neutrino beam, and is therefore a unique part of the neutrino factory physics program.

Note that it is the ν_e ($\bar{\nu}_e$) component in the neutrino factory beam that drives the oscillation physics program. A ν_e beam would (a) enable a basic test of the oscillation framework that cannot be made with a ν_μ beam, (b) enable the first observation of (or stringent limits on) $\nu_e \rightarrow \nu_\tau$ oscillations, (c) make a convincing determination of the pattern of neutrino masses that would be difficult or impossible with a conventional neutrino beam, (d) make a quantitative check of the MSW effect only possible with a neutrino factory beam,

(e) enable measurements or stringent limits on all of the (three-flavor) mixing angles with a precision that requires both ν_e and ν_μ beams, and (f) measure or put meaningful limits on CP violation in the lepton sector, which requires a signal purity only available at a neutrino factory.

A neutrino factory operating in the next decade, after the next generation of long baseline experiments, would appear to be the right tool at the right time. However, before we can quantitatively assess how well a neutrino factory might realize the physics program we have listed, we must first understand the capabilities of neutrino detectors in the neutrino factory era.

3.4 Detector considerations

We would like to measure the oscillation probabilities $P(\nu_\alpha \rightarrow \nu_\beta)$ as a function of the baseline L and neutrino energy E (and hence L/E) for all possible initial and final flavors α and β . This requires a beam with a well known initial flavor content, and a detector that can identify the flavor of the interacting neutrino. The neutrinos interact in the detector via charged current (CC) and neutral current (NC) interactions to produce a lepton accompanied by a hadronic shower arising from the remnants of the struck nucleon. In CC interactions the final state lepton tags the flavor (β) of the interacting neutrino.

At a neutrino factory in which, for example, positive muons are stored, the initial beam consists of 50% ν_e and 50% $\bar{\nu}_\mu$. In the absence of oscillations, the ν_e CC interactions produce electrons and the $\bar{\nu}_\mu$ CC interactions produce positive muons. Note that the charge of the final state lepton tags the flavor (α) of the initial neutrino or antineutrino. In the presence of $\nu_e \rightarrow \nu_\mu$ oscillations the ν_μ CC interactions produce negative muons (i.e. wrong-sign muons). Similarly, $\bar{\nu}_\mu \rightarrow \bar{\nu}_e$ oscillations produce wrong-sign electrons, $\bar{\nu}_\mu \rightarrow \bar{\nu}_\tau$ oscillations produce events tagged by a τ^+ and $\nu_e \rightarrow \nu_\tau$ oscillations produce events tagged by a τ^- . Hence, there is a variety of information that can be used to measure or constrain neutrino oscillations at a neutrino factory, namely the rates and energy distributions of events tagged by (a) right-sign muons, (b) wrong-sign muons, (c) electrons or positrons (their charge is difficult to determine in a massive detector), (d) positive τ -leptons, (e) negative τ -leptons, and (f) no charged lepton. If these measurements are made when there are alternately positive and negative muons decaying in the storage ring, there are a total of 12 spectra that can be used to extract information about the oscillations. Some examples of the predicted measured spectra are shown as a function of the oscillation parameters in Figs. 16 and 17 for a 10 kt detector sited 7400 km downstream of a 30 GeV neutrino factory. Clearly, the high intensity ν_e , $\bar{\nu}_e$, ν_μ , and $\bar{\nu}_\mu$ beams at a neutrino factory would provide a wealth of precision oscillation data.

The detectors required at a neutrino factory will have many similarities to the detectors that have been designed for the next generation of experiments at conventional neutrino beams. However, there are some important differences. First, we can anticipate more massive detectors. The sensitivity of a neutrino

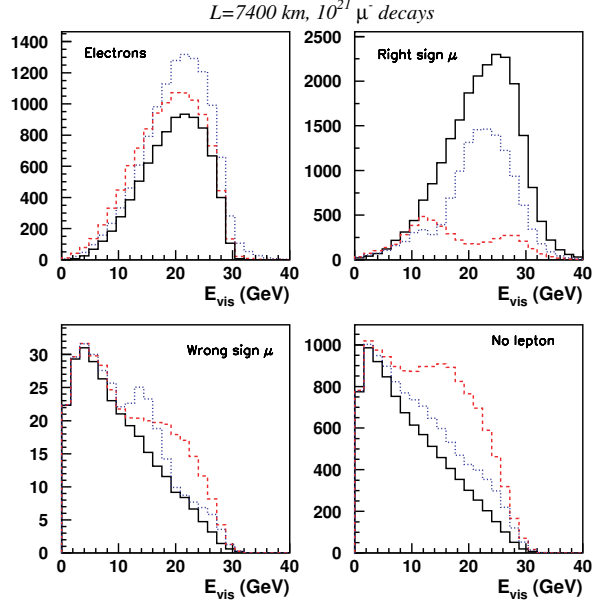


Figure 16: Visible energy spectra for four event classes when $10^{21} \mu^-$ decay in a 30 GeV neutrino factory at $L = 7400 \text{ km}$. Black histogram: no oscillations. Blue dotted histogram: $\delta m_{32}^2 = 3.5 \times 10^{-3} \text{ eV}^2/c^4$, $\sin^2 \theta_{23} = 1$. Red dashed histogram: $\delta m_{32}^2 = 7 \times 10^{-3} \text{ eV}^2/c^4$, $\sin^2 \theta_{23} = 1$. The distributions in this figure and the following figure are for an ICANOE-type detector, and are from Ref. 50.

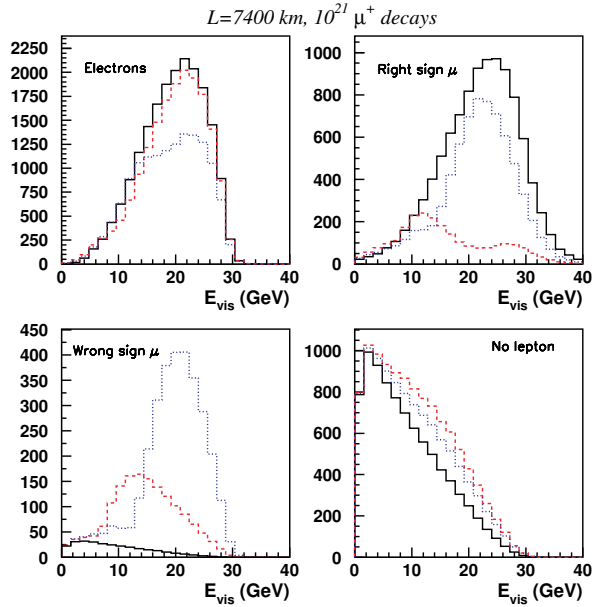


Figure 17: Same as previous figure, but with positive muons circulating in the storage ring. The difference between the two figures is due to the different cross section for neutrinos and antineutrinos, and to matter effects.

factory oscillation experiment is proportional to the product of the detector mass and beam intensity. It is likely that the cost of increasing the MINOS detector fiducial mass (for example) by a factor of a few is smaller than the cost of increasing the neutrino factory beam intensity by a factor of a few. Therefore, we believe that it is reasonable to assume that detectors at a neutrino factory would be a factor of a few to a factor of 10 more massive than the generation of neutrino detectors presently under construction. Second, the presence of both neutrinos and antineutrinos in the same beam at a neutrino factory places a premium on measuring the sign of the charge of the lepton produced in CC interactions. Charge–sign determination may not be practical for electrons, but is mandatory for muons and highly desirable for τ -leptons. Finally, a relatively low energy threshold for the detection and measurement of wrong–sign muons is very desirable. This is because high muon detection thresholds require high energy interacting neutrinos, and hence a high energy neutrino factory. Since the muon acceleration system at a neutrino factory is likely to be expensive, low energies are preferable.

In the following sections we begin by considering general detector issues for the measurement of final state muons and τ -leptons, and then consider some specific candidate detectors for a neutrino factory. Some of these detector types are quite new and are just beginning to be studied; for the more mature detectors the “neutrino” energy resolution, the signal efficiency, background rejection, and fiducial mass are discussed.

3.4.1 Muon identification and measurement

The detection and measurement of muons (especially those of opposite sign to the muons in the storage ring) is crucial for many of the key oscillation physics measurements at a neutrino factory. Before considering some specific neutrino factory detectors it is useful to consider more generally muon backgrounds and related issues. Background muons can be produced in NC and CC interactions by:

- (i) Pions or kaons from the hadronic shower that decay to produce a muon.
- (ii) Non-interacting pions which fake a muon signature (punch-through).
- (iii) Charm meson production and muonic decay.

A background muon event can be produced when a background “muon” of the appropriate sign is recorded in (a) a NC event or (b) a CC event in which the primary lepton has been lost. If the background muon has the same charge sign as that in the storage ring the resulting event will be a background for disappearance measurements, but more importantly, if it has the opposite sign then the event will be a background for wrong–sign muon appearance measurements.

The integrated wrong-sign background fraction from the hadronic shower is shown in Fig. 18 as a function of the minimum muon energy accepted for

Steel/Scintillator and water detectors downstream of 20 GeV and 50 GeV neutrino factories. The charm background comes from ν_μ CC events where the primary muon was less than 2 GeV. The peak at low muon energies is from the hadron shower itself and from punch through, while the long tail is from shower particles decaying to muons.

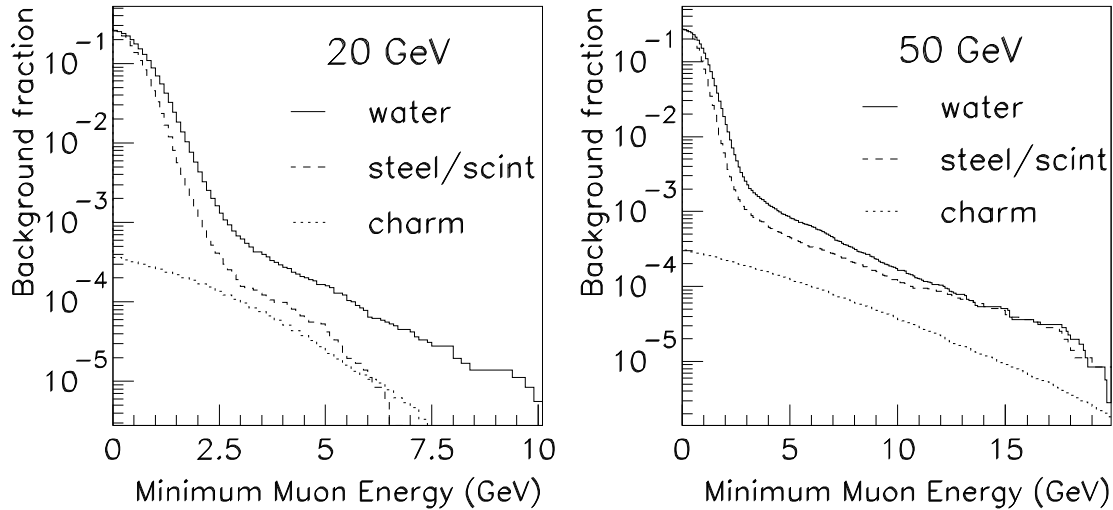


Figure 18: Background levels from punch through, pion/kaon decay, and charm backgrounds for 20 GeV (left) and 50 GeV (right) neutrino factories. The fraction of neutrino interactions that produce a wrong-sign muon background event is shown as a function of the minimum muon energy accepted.

In general there are two different standards for background levels which are relevant: that of a disappearance experiment and that of an appearance experiment. Background estimates are not trivial, but if the backgrounds for a disappearance measurement are at the one per cent level, then the uncertainties on those backgrounds can be expected to be small compared to the flux uncertainty. On the other hand, wrong-sign muon appearance measurement uncertainties are expected to be dominated by the statistics. An extremely aggressive background level requirement would be to have less than of the order of one background event. If there are several thousand CC events expected, then this would require a minimum background rejection factor of 10^4 .

Backgrounds can be suppressed by imposing a minimum energy requirement on the measured muon. Figure 19 shows the effect of several different minimum muon energy cuts on a simulated oscillation signal observed in a steel-scintillator type detector at a 20 GeV muon storage ring, at a baseline length of 2800km [51]. A muon threshold energy of 4 GeV for example depletes the low energy part of observed measured “neutrino energy” distribution, degrading but not completely removing the information about the neutrino oscillation parameters

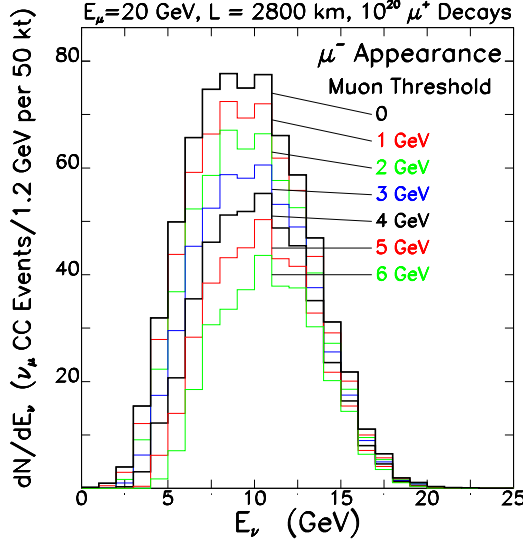


Figure 19: Reconstructed neutrino energy distribution for several different minimum muon energy cuts for a 20 GeV ring. Result is from Ref. 51.

that is encoded in the shape of the distribution. A 4 GeV threshold at a 20 GeV neutrino factory is probably tolerable. If higher thresholds are needed to reject backgrounds, then a higher energy neutrino factory is desirable. If a lower energy neutrino factory is to be viable, then lower muon thresholds are desirable.

As is shown in Fig. 18, to get to a background level of 10^{-4} one would need a 5 (6.5) GeV muon momentum cut in Steel/scintillator (Water) for a 20 GeV muon storage ring, and a 10 (12) GeV muon momentum cut in Steel/Scintillator (Water) for a 50 GeV muon storage ring. Clearly more background rejection is desirable. Fortunately muons from hadron decay in the hadronic shower are likely to be more aligned with the shower direction than muons from the leptonic vertex of the CC interaction. This provides another handle on the background. A useful variable to cut on is the momentum of the muon in the direction transverse to the hadronic shower (p_t). Figure 20 shows the generated p_t^2 distribution for background and signal events, with no cut on the final state muon momentum. Note that requiring $p_t^2 > 1$ the background is extremely low, while the signal efficiency is high. The resolution with which p_t^2 is determined is detector dependent, and for detectors with reasonable transverse and longitudinal segmentation is dominated by the hadronic energy resolution.

3.4.2 τ -lepton identification and measurement

The detection and measurement of τ -leptons is crucial for $\nu_\mu \rightarrow \nu_\tau$ and $\nu_e \rightarrow \nu_\tau$ measurements at a neutrino factory. Note that $\nu_e \rightarrow \nu_\tau$ oscillations will be of special interest since they will not have been previously observed. The $\nu_e \rightarrow \nu_\tau$

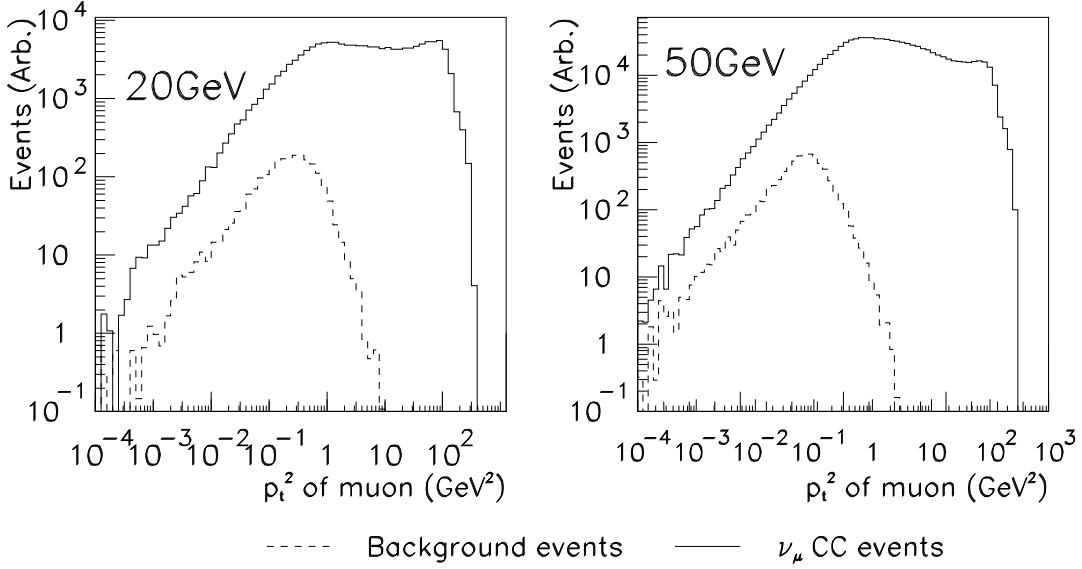


Figure 20: Distributions of the square of the muon momentum component transverse to the hadronic shower direction for ν_μ charged current events compared to background muons for a 20 and 50 GeV muon storage ring.

signal can be separated from $\nu_\mu \rightarrow \nu_\tau$ “background” if the sign of the τ -lepton charge is measured. The majority of τ -lepton decays produce either one charged track (electron, muon, or hadron) or three charged tracks (hadrons). There are two general techniques that can be used to identify τ -leptons. The first technique exploits the one-prong and three-prong topologies, and uses kinematic cuts to suppress backgrounds. The second technique uses a detector with a high spatial resolution to look for the displaced vertex or kink resulting from τ -lepton decay.

The advantage of the displaced vertex or kink detection τ -lepton technique is that the detailed τ -lepton decay is measured and background suppression is therefore large. The disadvantage is that detectors that have sufficient spatial resolution are necessarily less massive than coarse-grained detectors.

The advantage of the kinematic technique is that a very massive detector can be used. If the τ -leptons decay muonically ($\text{BR} = 17\%$) a measurement of the muon charge-sign determines the sign of the τ charge. However, there are substantial backgrounds that must be reduced. In the case of muonic τ decays, the backgrounds are from (a) ν_μ (or $\bar{\nu}_\mu$) CC interactions which typically produce muons at high momentum and high p_t^2 , and (b) meson decays (discussed earlier) which are at low momentum and low p_t^2 . For $\tau \rightarrow e$ decays, the main background comes from ν_e and $\bar{\nu}_e$ CC interactions. Fortunately the undetected neutrinos from τ decays result in a larger missing transverse momentum than expected for background events. Exploiting these kinematic characteristics the backgrounds can be reduced by a large factor. For example, for an ICANOE-type detector a background rejection factor of 200 has been estimated, with a corresponding signal efficiency of 30%. In the electron channel background can also come

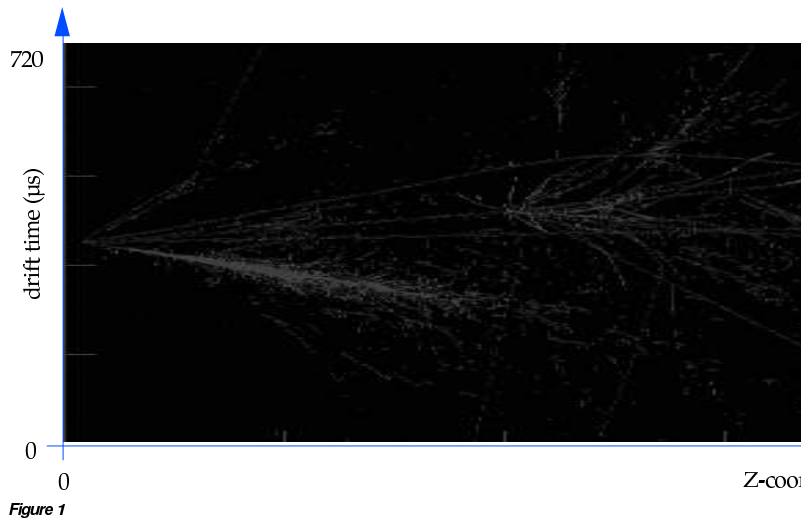


Figure 21: Example of a ν_e Charged current event from the full simulation of the ICANOE detector.

from NC interactions which produce photon conversions or Dalitz π^0 decays. These backgrounds can be suppressed in detectors with good pattern recognition allowing conversions, for example, to be identified and rejected. The analysis of hadronic τ decays requires the identification of the τ decay product inside a jet. This can only be done with a detector having good pattern recognition. It has been demonstrated that with an ICANOE-type detector a background rejection factor of 200 can be expected for $\tau \rightarrow 1$ prong, $\tau \rightarrow \rho$, and $\tau \rightarrow 3\pi$ decays, with a signal efficiency of 8%.

3.4.3 A Liquid Argon neutrino detector

We have studied the performance of a large Liquid Argon neutrino detector at a neutrino factory using the ICANOE monte carlo program. One ICANOE detector unit consists of a liquid argon TPC followed by a magnetic spectrometer.

The Liquid Argon TPC has extremely fine granularity, producing bubble chamber like event images. Figure 21 shows an example of an electron neutrino charged current event—note the separation between the electromagnetic shower and the hadronic shower of the nucleon remnant. The TPC is instrumented with 3 mm pitch wires which allow tracking, dE/dx measurements, electromagnetic, and hadronic calorimetry. Electrons and photons can be identified and their energies are measured with a resolution given by $\sigma_E/E = 0.03/\sqrt{E} \oplus 0.01$. The hadron energy resolution is given by $\sigma_E/E = 0.2/\sqrt{E} \oplus 0.05$. The magnetic spectrometer is primarily needed to measure muon energy and charge, but it is assumed that it will also be instrumented as a calorimeter to allow the hadron energy of showers which leak into the spectrometer to be correctly measured (albeit with worse resolution). The muon momentum resolution is expected to

be 20%.

In the design we have simulated, the liquid Argon module is 18 m deep with a cross section of $11.3m \times 11.3m$. The active (total) mass of one Liquid Argon module is 1.4 kt (1.9 kt). The magnetized calorimeter module is 2.6 m deep with a cross section of $9m \times 9m$, and has a mass of 0.8 kt. It consists of 2 m of steel, corresponding to $7.4 \lambda_{int}$ and $59 X_0$, interleaved with tracking chambers. Four Super-Modules are assumed, yielding a total detector length of 82.5 m and a total active mass of 9.3 kt that is fully instrumented.

ICANOE can reconstruct neutrino (and antineutrino) events of all active flavors, and with an energy ranging from tens of MeV to tens of GeV, for the relevant physics analyses. The unique imaging capabilities of the liquid argon TPC allow one to cleanly determine whether a given event is a ν_μ CC event, a ν_e CC event, or a NC event.

For our studies the ICANOE fast simulation was used. Neutrino interaction events are generated, with a proper treatment of quasi-elastic interactions, resonance and deep-inelastic processes. The 4-vectors for all the particles generated are smeared, according to the resolutions derived from the full simulation. Muonic decays of pions and kaons are also considered, for a proper wrong- and right-sign muon background treatment. Once a 2-GeV cut is placed on the outgoing muon momentum, the background levels tend to be about 10^{-5} times the actual charged current event rate, and are dominated by meson decay in the hadronic shower.

Examples of simulated oscillation signals in an ICANOE-type detector at a neutrino factory are shown in Figs. 16 and 17. More detailed results from a study of the sensitivity that might be achieved using an ICANOE-type detector are discussed in the oscillation measurements section of this report.

3.4.4 A magnetized Steel/Scintillator neutrino detector

Steel/Scintillator calorimeters have been used extensively in past neutrino experiments. Their performance is well understood and well simulated. Typically a magnetized Steel/Scintillator (MINOS-like) neutrino detector consists of iron plates interspersed with scintillator planes. To obtain transverse position information the scintillator can be segmented transversely, or a separate detector system (e.g. drift chambers) used. Penetrating charged particles (muon candidates) can then be reconstructed. With a reasonable transverse segmentation, the transverse position resolution is dominated by multiple coulomb scattering. The detector performance depends primarily on its longitudinal segmentation. The segmentation needs to be fine enough to determine whether a charged track has penetrated beyond the region of the accompanying hadronic shower. If it has, then the penetrating track is a muon candidate. The muon momentum resolution is determined by the magnetic field and the thickness of the steel plates.

Neutrino CC and NC interactions have well defined signatures. In a MINOS-like detector NC interactions produce a hadronic shower reconstructed as a large energy deposition in a small number of scintillator units. A ν_μ or $\bar{\nu}_\mu$ CC interaction will produce a muon in the final state, characterized by a long track in addition to the hadronic shower. These events can be identified provided the muon penetrates well beyond the hadronic shower. This imposes a minimum track-length, and hence minimum energy, requirement on muons that can be identified. If the muon is not identified the CC interaction will look like a NC event. A ν_e or $\bar{\nu}_e$ CC interaction, will produce an electron in the final state which cannot be resolved, so these events look similar to NC interactions. A ν_τ or $\bar{\nu}_\tau$ CC interaction will also look like a NC interaction unless the τ -lepton decays muonically.

To study the performance of a magnetized Steel/Scintillator detector at a neutrino factory we have considered a detector geometry similar to the CCFR/NuTeV calorimeter [52], but with the addition of a toroidal magnetic field of 1T. The detector is constructed from $3 \times 3 \times 0.3 \text{ m}^3$ modules (see Fig. 22). The 0.7 kt CCFR detector consists of 42 modules. A neutrino factory detector with a mass of 50 kt ($10 \times$ the MINOS detector) would require 3000 of these modules. The ultimate transverse size (and hence module mass) that is practical is probably determined by the largest size over which a large magnetic field can be generated.

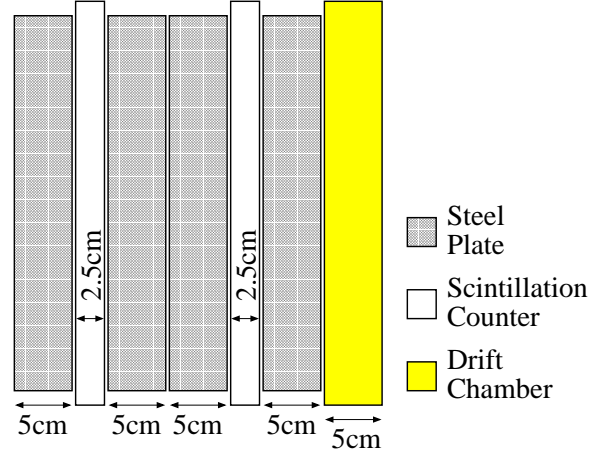


Figure 22: Schematic of a CCFR/NuTeV calorimeter module.

In the following we consider how well a magnetized Steel/Scintillator detector can identify and measure wrong-sign muon events at a neutrino factory. For our simulations, we used the parameterized Monte Carlo developed by the NuTeV collaboration, modified to include particle tracking in the magnetic field. The hadron energy resolution of this detector is described in detail in [52], and is approximately given by $\sigma_E/E = 0.85/\sqrt{E}$. The muon momentum resolution depends on the track length in the steel, and whether the muon is contained

within the detector. For muons which range out in the detector the effective momentum resolution is $\sigma_P/P = 0.05$, while for tracks which leave the fiducial volume of the detector the resolution is described by $\sigma_P/P \sim \theta_{MCS}\theta_{BdL}$, where the angles θ_{MCS} and θ_{BdL} describe respectively the change in direction due to multiple scattering and curvature in the magnetic field.

The simulation includes a detailed parameterization of the hadron-shower development, with the inclusion of charm production and π , K decays (the data set on which the decay probability parameterization was tuned contained only muons with momentum higher than 4 GeV/c). Note that π punchthrough was not included in the parameterization, but is expected to make only a small contribution to background muons above 4 GeV.

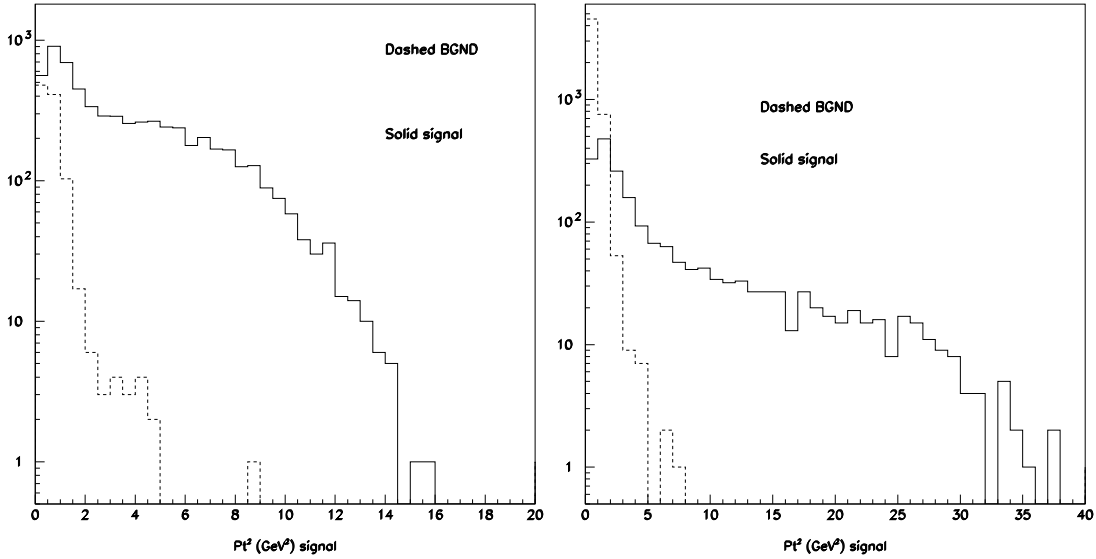


Figure 23: Reconstructed $\mu^- P_t^2$ with respect to the shower direction for 20 GeV and 50 GeV μ^+ decaying in a neutrino factory. The muons are required to have energies exceeding 4 GeV.

To be conservative, and reduce the dependence of our study on low energy processes that may not be adequately described by the Monte Carlo program, in our analysis all muons with generated energy below 4 GeV are considered lost. Muons with track length in steel less than 50 cm past the hadronic shower are also considered lost. All other muons are assumed to be identified with 100% efficiency, and measured sufficiently well to determine their charge sign. For the background events we considered (i) all the π , K decay events producing “wrong-sign” muons in NC interactions, and (ii) all the charm production and π , K decay events producing “wrong-sign” muons in CC events where the primary muon was considered lost. To reduce the backgrounds, we cut on P_t^2 . The reconstructed P_t^2 distribution is shown in Fig. 23 for signal and background muons in a 10 kt detector 2800 km downstream of 20 GeV and 50 GeV neutrino factories which provide 10^{20} μ^+ decays. The oscillation parameters corresponding to the LMA scenario IA1. As expected, background wrong-sign muons, tend to have smaller

P_t^2 than genuine wrong-sign muons from the leptonic vertex. The reconstructed wrong-sign muon spectrum is shown in Fig. 24 for a 20 GeV storage ring before (top plot) and after (bottom plot) muon energy, track length and $P_t^2 > 2 \text{ GeV}^2$ cut were applied. Signal and background rates are summarized in Table 7. After the cuts the signal/background ratio is above 10 to 1 in scenario IA1 for a detector 2800 km away, while 40–50% of the $\nu_e \rightarrow \nu_\mu$ signal events are retained.

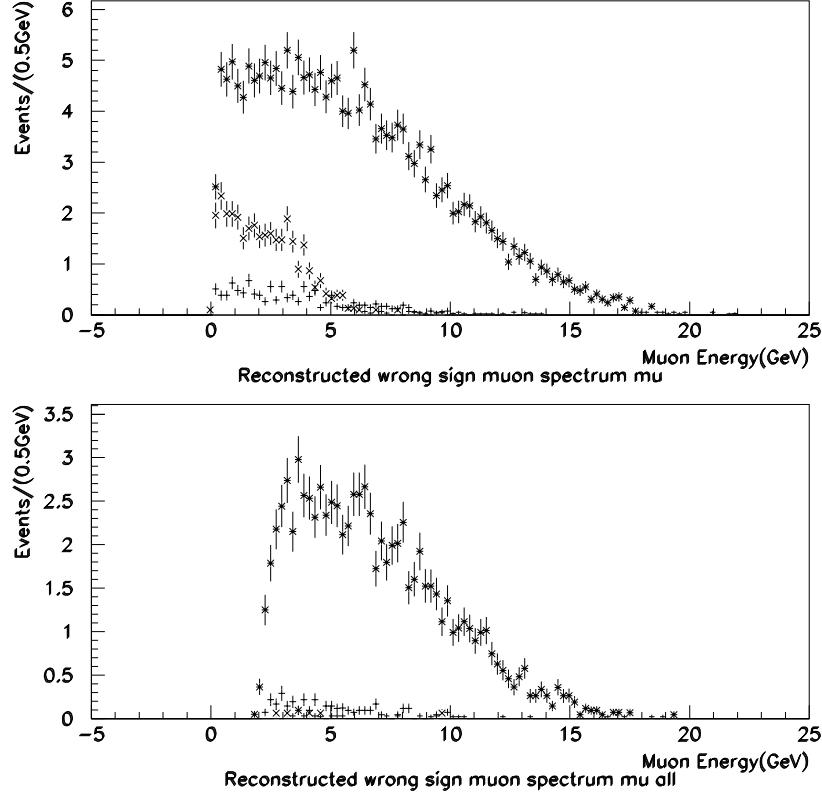


Figure 24: Reconstructed wrong-sign muons as a function of the muon energy for a $\mu+$ 20 GeV ring. Top plot accepted events for the signal ($\nu_e \rightarrow \nu_\mu$ -stars- and $\nu_e \rightarrow \nu_\tau \rightarrow \mu + X$ -crosses) and the potential backgrounds (x). The bottom plot shows the signal and the background after cuts.

3.4.5 A Water Cerenkov detector

Preliminary studies have explored the possibility of using a large water Cerenkov detector as a distant target for a neutrino factory beam. Traditionally this type of detector has been used for measuring much lower energy neutrinos than expected at a muon storage ring, but to date water Cerenkov neutrino detectors are the only existing neutrino detectors with masses already in the 50 kt range. Water is of course the lightest target material under consideration in this report, but

Table 7: Wrong-sign muon rates after all cuts for a 10 kt steel-scintillator detector downstream of a neutrino factory providing 10^{20} muon decays. The oscillation parameters correspond to scenario IA1. The loss of signal acceptance and the background rejection are due solely to the kinematic and reconstruction cuts.

μ Ring		$\nu_e \rightarrow \nu_\mu$	$\nu_e \rightarrow \nu_\tau$			
Energy	Charge	events	$\rightarrow \mu + X$	background	signal	background/CC
GeV		accepted	events	events	acceptance	rate
50	+	268.5	15.4	21.6	0.50 ± 0.02	4.5×10^{-4}
50	-	55.2	4.7	3.5	0.48 ± 0.02	4.0×10^{-5}
20	+	85.7	3.5	0.7	0.41 ± 0.02	2.0×10^{-4}

this type of detector has several advantages when extrapolating to large masses, namely (i) low cost target material, (ii) only the surface of a very large volume needs to be instrumented, and (iii) good calorimetry. A large volume guarantees containment of hadronic and electromagnetic showers (as well as muons up to a certain energy). The low density of the target and good angular resolution from the Cerenkov cone might yield an overall hadron angle resolution that is as good as or better than the corresponding resolution obtained with steel-scintillator calorimeters.

Water Cerenkov devices as large as 50 kt (SuperK) are already in operation and is expected to continue data-taking for ten years or more. Therefore, the response of the existing SuperK detector at a baseline distance of 9100 km has been studied as a test case. Next generation detectors, up to 1 Mton in mass, are technically feasible and are currently under consideration for proton decay and neutrino measurements, sited perhaps at the Kamioka mine or elsewhere.

For this initial study, the primary question is the suitability of a water Cerenkov detector for the higher energy neutrino beam produced by a 10-50 GeV muon storage ring. At these energies, the multiplicity of hadrons is greater than for typical atmospheric neutrino interactions, and event topologies are correspondingly more complex. Figure 25 shows the Cerenkov light produced in a typical neutrino event from a 50 GeV muon storage ring at the SuperK detector: the circles in the display are estimates of the outgoing angles of different charged particles produced in the hadronic shower. Some particle identification is possible from the pulse-height information. Reconstruction software from the SuperK experiment must be further optimized to study the detector response to neutrinos from 10 GeV and 50 GeV muon storage rings. It is worth noting that neutrinos produced by a 50 GeV muon beam induce a large number of events in the material (rock) surrounding any detector (producing an entering muon), and for a SuperK sized device these events outnumber the those produced in the detector's water volume. Both contained and entering events have therefore been studied.

The response of a detector the size of SuperK changes drastically as a func-

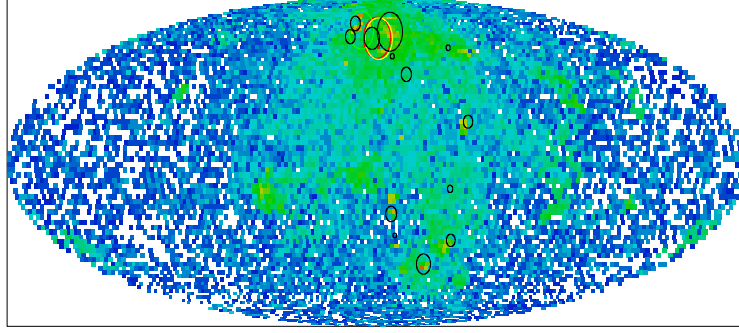


Figure 25: Simulated neutrino event from a 50 GeV muon storage ring in the SuperKamiokande detector. The rings indicate where the reconstruction software found charged particles in the hadronic shower, as well as the exiting muon.

tion of beam energy. At a 10 GeV neutrino factory, 57% of the muon CC events are fully contained in the inner water volume, whereas only 11% are fully contained at a 50 GeV neutrino factory. This large difference only exists for events containing penetrating muons; at 10 GeV (50 GeV) both $\bar{\nu}_e$ and NC events are contained greater than 98% (90%) of the time. The existing μ -like particle identification algorithm works to produce a reasonably pure (89%) ν_μ -CC sample for fully contained events in the 10 GeV beam, but e -like events are a mixture of $\bar{\nu}_e$ -CC, NC and ν_μ -CC contamination. Exiting and entering events are pure samples of ν_μ -CC simply because of their penetrating nature. The muon angular resolution (3°) is much less than the muon-neutrino angular correlation (15°). With 2×10^{20} decays at a 50 GeV neutrino factory and a baseline of 9100 km, approximately 200,000 ν_μ CC events would be observed entering or exiting the current SuperK detector. Combined with muon charge identification this sample should be able to provide good oscillation measurements.

Implementing charge identification in a water Cerenkov detector is not trivial. Two possibilities have been proposed: (i) several large water targets, each one followed by a thin external muon spectrometer, and (ii) a magnetic field introduced into the water volume itself. Although the first design would have lower geometrical acceptance and a higher muon energy threshold, it would pose much less of a problem for the phototubes since the magnetic field would presumably be well-contained in the spectrometer. The second proposal could in principle have good low energy muon momentum acceptance, but the resolution on the muon and hadron shower angles might be compromised.

For a magnetic field internal to the target, 0.5-1 kG is sufficient to visually determine the charge of a several meter-long (> 1 GeV) muon, but no automated algorithms have yet been developed. A number of conceptual magnet designs have been studied: solenoidal, toroidal, and concentric current loops in the center or at the ends of the detector. A detailed study of one particular design has shown that one can immerse the central volume of a SuperK sized detector in a 0.5 kG

magnetic field while leaving only a 0.5 G fringe field (which may be acceptable with shielding and/or local compensation) in the region of the PMTs. Many of the difficulties inherent in placing a field inside a water detector would be avoided if an alternative light collector (insensitive to the field) were used. Work on magnet design and alternative light collection is ongoing, but the internal magnetic field option must be considered speculative at this point.

The results we will describe in the remainder of this section are for a water Cerenkov detector with an external magnetic field, because neutrino event reconstruction is more straightforward to simulate and the spectrometer technology is well-understood. Although the studies of this detector are very preliminary, they look promising and warrant further investigation. We have used a LUND/GEANT Monte Carlo program which uses as its geometry a $40 \times 40 \times 100$ m³ box of water, followed by a 1 m long muon spectrometer. This simulation can be used to study acceptance issues and background contamination for a range of geometries and storage ring energies.

Figure 3.4.5 shows the geometrical acceptance for the box-like water Cerenkov detector as a function of distance of the neutrino interaction vertex from the spectrometer, for CC ν_μ events from 20 and 50 GeV storage rings. The loss in acceptance close to the spectrometer is due to rejection of events where there is more than one muon which traverses the spectrometer (where the extra muon comes from background processes). It is clear that for a 20 GeV muon storage ring one would want a muon spectrometer much more frequently than once every 100 m. Of course, noting that steel has a density of 8 times that of water, the smaller the ratio of water thickness to steel thickness the more it approximates a magnetized steel/scintillator target interspersed with water volumes with fine granularity.

Clearly more work is needed to optimize the design for this kind of detector, but it might be an inexpensive compromise between a coarse-grained sampling calorimeter and a very fine-grained liquid argon TPC.

3.4.6 Specialized τ -lepton detectors

The measurement of τ -lepton appearance in large mass neutrino detectors is challenging. There are several ideas that might lead to viable new τ -appearance detectors within the next 5–10 years, and that might be suitable for use at a neutrino factory. We briefly describe three examples in the following: (i) a perfluorohexane Cerenkov detector, (ii) a hybrid emulsion detector, and (iii) a very fine-grained micro-strip gas chamber target.

Consider first a Cerenkov detector filled with perfluorohexane (C_6F_{14}), which has a density 1.7 times that of water. This has been proposed [53] for use in the CERN to Gran Sasso beamline. The detector geometry consists of several target volumes followed by short muon spectrometer modules. A 1 Ton perfluorohexane detector (with a very different geometry) exists at DELPHI. The τ -lepton signature in this type of detector consists of a sparsely populated Cerenkov ring

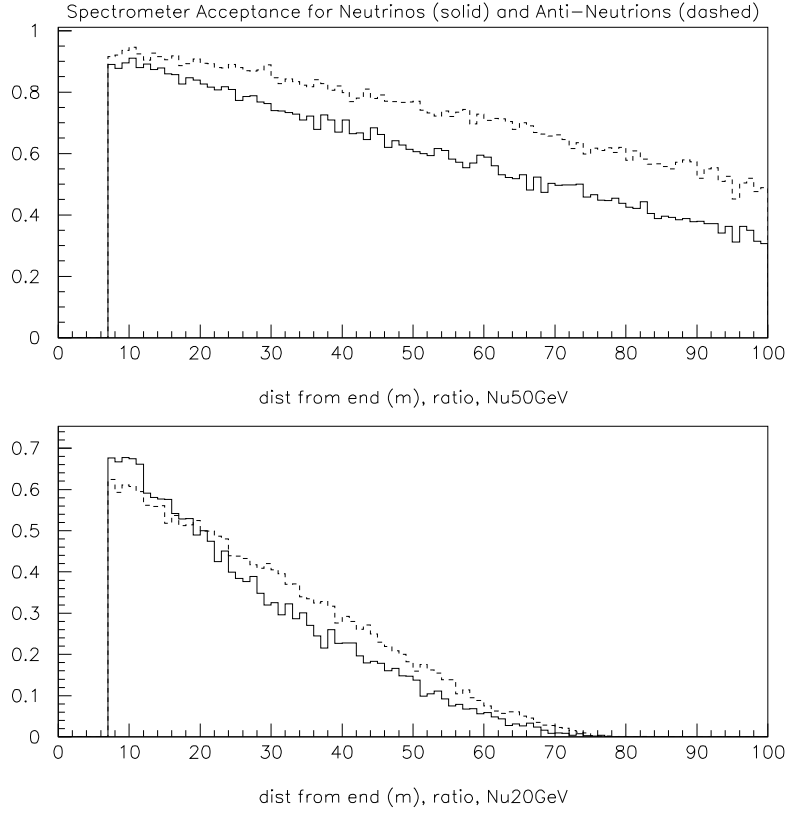


Figure 26: Acceptance in a water target for charged current ν_μ (solid) and $\bar{\nu}_\mu$ (dashed) events in a 20 and 50 GeV storage ring, as a function of distance of the neutrino interaction vertex from the muon spectrometer.

from the τ before it decays, together with a more densely populated ring from the daughter muon. The two rings would have offset centers. Figure 27 shows a simulated quasi-elastic ν_τ event (no hadron energy) from this kind of detector. This technique would probably not work for events with high energy hadron showers because of the large number of charged particles that would result in overlapping rings near the initial τ -lepton ring.

Next consider a hybrid emulsion detector consisting of, for example, thin ($\sim 100\mu\text{m}$) sheets of emulsion combined with low-density ($\sim 300\mu\text{m}$) spacers. The signature for a τ -lepton 1-prong decay would be a change in direction of the track measured before and after the spacer [54]. For charge identification the detector could be within a large magnetic field volume. With an emulsion track angular resolution of 2 mrad, a 5σ charge-sign determination of a 10 GeV/c charged particle could be achieved with a 2 T field and a 1.2 mm thick spacer [55]. An ~ 20 kt hybrid emulsion detector of this type might consist of 20 kt of steel segmented into 1 mm thick sheets, and an equal volume of thin emulsion layers plus low density spacers. The resulting detector would fit into the ATLAS

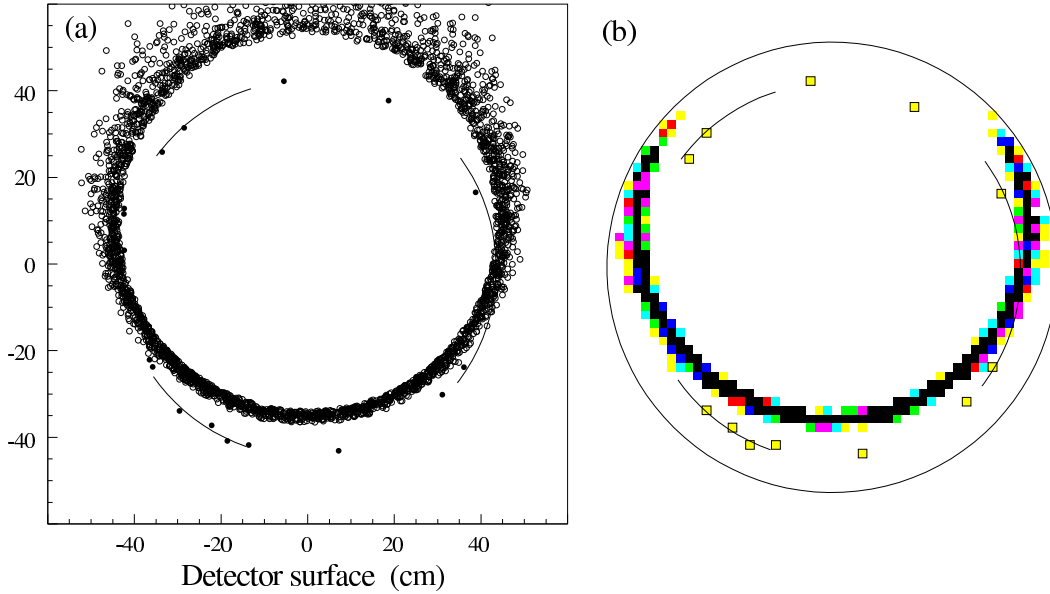


Figure 27: Quasi-elastic ν_τ event in a perfluoroHexane Cerenkov detector: the ring described by about eight hits on the left is from the tau before it decays.

barrel toroid magnet, which has a magnetic field ranging from 2 to 5 Tesla [56]. A hybrid emulsion detector with an external downstream muon spectrometer will be used by the OPERA experiment, which is to be put in the CERN to Gran Sasso beam. The muon spectrometer will determine the charge sign for $\tau \rightarrow \mu$ decays provided the muon reaches the spectrometer. According to the OPERA studies [57], with an average neutrino energy of 20 GeV the total efficiency for seeing the τ decays is 29% (including the branching ratios). The efficiency is largely geometric and should not be compromised by the addition of a magnetic field, provided the bend in the spacer due to the magnetic field is much less than the "apparent bend" due to the τ -lepton decay.

Finally, consider a target consisting of a tracking chamber constructed from micro-strip gas chambers (MSGCs) and a low Z material (for example, nylon) in a large magnetic field volume. This would be a NOMAD [58]-like detector with a much larger O(1 kt) fiducial mass and an improved spatial resolution. Because of the low Z of the material electrons can travel a long distance in the detector before showering, and with a high enough field their charge can therefore be measured. Although a kink is not seen, the tau decay could be distinguished kinematically. For example, nylon has a radiation length of 37 cm. With a B field of 1 Tesla and MSGC's every 10 cm one would have an 8σ measurement of a 50 GeV electron's charge. This idea is worthy of further consideration, particularly if the LSND signal is confirmed and lower-mass tau detectors are warranted.

3.4.7 Detector summary

In our initial studies we have simulated the performance of steel/scintillator and liquid Argon detectors at a neutrino factory. Results are encouraging. These technologies could provide detectors with masses of order 10 kt (liquid Argon) to a few $\times 10$ kt (steel/scintillator) that yield good wrong-sign muon identification and adequate background rejection. Our simulations of the capabilities of water Cerenkov detectors at a neutrino factory are less advanced, but initial results are encouraging, and this detector technology might permit very large detector masses to be realized. Some relevant characteristics of steel/scintillator, liquid Argon, and water Cerenkov detectors are listed in Table 8. It is premature to choose between detector types at this early stage. However, some general points are worth noting:

- (i) We believe that a cost optimization of detector mass (cost) versus neutrino factory beam intensity (cost) will probably favor detectors that are at least a factor of a few to a factor of 10 more massive than, for example, ICANOE or MINOS. A detector mass in the range 10 kt to 50 kt does not seem unreasonable.
- (ii) The minimum energy a muon must have for good identification and measurement may well determine the minimum viable muon storage ring energy. This threshold is a few GeV, and is detector technology dependent. With a steel/scintillator detector and a threshold of 4 GeV, for example, the minimum acceptable neutrino factory energy appears to be in the neighborhood of 20 GeV.

In this initial study we have not comprehensively considered to what extent massive detectors at a neutrino factory need to be deep underground. It seems very likely that detectors with low detection thresholds (water Cerenkov and liquid argon) will need to be well protected from cosmic ray backgrounds, regardless of the neutrino factory energy. For the steel/scintillator detector, the cosmic ray backgrounds for charged current events with muons in them are likely to be small for a detector at the surface of the earth, but there will be substantial background to neutral current or ν_e charged current interactions. Finally, we note that the development of a new generation of very massive detectors capable of identifying and measuring the charge-sign of muons and τ -leptons, would be of great benefit to a neutrino factory. There is a possible area of mutual interest with the nucleon decay community in developing the technology for a really massive 1 Mton scale water Cerenkov detector. This possibility deserves further investigation.

Table 8: Comparison of detector parameters for candidate detectors at a neutrino factory.

Characteristic	Steel/Scint	Detector Technology	
		Liquid Argon TPC	Water Cerenkov
Resolutions of:			
Electron Energy	$50\%/\sqrt{E}$	$3\%/\sqrt{E} \oplus 1\%$	$0.6 \oplus 2.6\%/\sqrt{E}$
Hadron Energy	$85\%/\sqrt{E}$	$20\%/\sqrt{E} \oplus 5\%$	20-30%
Muon Energy	5%	20%	20% [†]
Hadron Shower Angle		$.13/\sqrt{p}$ rad (each hadron)	
Muon Angle	5% for 50cm track	$.02 \oplus .21/\sqrt{p}$	3°
Maximum mass	50 kton	30 kton	1Mton?
What limits size?		safety, tunnel	tunnel
Required Overburden**	0 m	50 m	50-100m
Analysis Cuts	$P_\mu > 4 \text{ GeV}$ $P_t^2 > 2 \text{ GeV}^2$	$P_\mu > 2 \text{ GeV}$	
Background level	10^{-4}	2×10^{-5}	

** The overburden required for all technologies depends on the neutrino factory duty factor. The overburden required for a steel-scintillator calorimeter also depends on the energy of the muon storage ring; but in the past this type of detector has been used at ground level with minimal contamination in the ν_μ charged current sample above a neutrino energy of 5 GeV.[†] The muon momentum resolution would be comparable to that of an ICANOE detector if the muon spectrometer were separated from the water tank volume.

3.5 Oscillation measurements

Using the oscillation scenarios described in section 3.1 as examples, we can now assess how well the neutrino oscillation physics program outlined in section 3.3 can be pursued at a neutrino factory with the detectors described in section 3.4. In the following sub-sections the oscillation measurements that can be made at a neutrino factory are discussed as a function of baseline, muon beam energy, and muon beam intensity. In particular we consider:

- (i) The first observation of $\nu_e \rightarrow \nu_\mu$ oscillations, the measurement of the sign of δm^2 and hence the pattern of neutrino masses (section 3.5.1).
- (ii) The first observation of $\nu_e \rightarrow \nu_\tau$ oscillations (section 3.5.2).
- (iii) The measurement of $\nu_\mu \rightarrow \nu_\tau$ oscillations (section 3.5.3).
- (iv) Precision measurements of the oscillation parameters (section 3.5.4).
- (v) The search for CP violation in the lepton sector (section 3.5.5).

The results are based on the calculations described in more detail in Refs. [59, 51, 60, 50]. The calculations from Ref. [50] are for an ICANOE type detector, and include realistic resolution functions, analysis cuts, and background modeling, but use a constant average matter density to compute matter effects. The calculations from Refs. [60, 51, 59] all use resolution functions typical of steel/scintillator detectors and, unless explicitly stated, reasonable thresholds on the detected muon energies. The calculation from Ref. [51] does not include backgrounds but covers a broad range of scenarios, and uses the explicit trans-Earth density profile to compute matter effects. In contrast, the calculations from Refs. [60, 59] have been used to look at only a few oscillation scenarios, but include backgrounds and use respectively the average Earth density and the explicit density profile in computing matter effects. It should be noted that although there are significant differences in the details implemented in the calculations, in general all the four groups arrive at similar assessments for the measurement sensitivity at a neutrino factory as a function of energy, intensity, and baseline.

3.5.1 Observation of $\nu_e \rightarrow \nu_\mu$ oscillations and the pattern of neutrino masses

At a neutrino factory $\nu_e \rightarrow \nu_\mu$ oscillations would be signaled by the appearance of CC interactions tagged by a wrong-sign muon [2]. Within the framework of three-flavor oscillations the $\nu_e \rightarrow \nu_\mu$ oscillation amplitude is approximately proportional to $\sin^2 2\theta_{13}$. At the present time only an upper limit exists on $\sin^2 2\theta_{13}$. The next generation long-baseline oscillation experiments are expected to be able to improve the sensitivity to $\sin^2 \theta_{13} \approx 10^{-2}$, i.e. about one order of

magnitude below the present bound. If $\sin^2 2\theta_{13}$ is in this range we would expect to observe $\nu_e \rightarrow \nu_\mu$ oscillations at a relatively low intensity neutrino factory, measure matter effects, and determine the pattern of neutrino masses [63]. This is discussed further in the remainder of this sub-section.

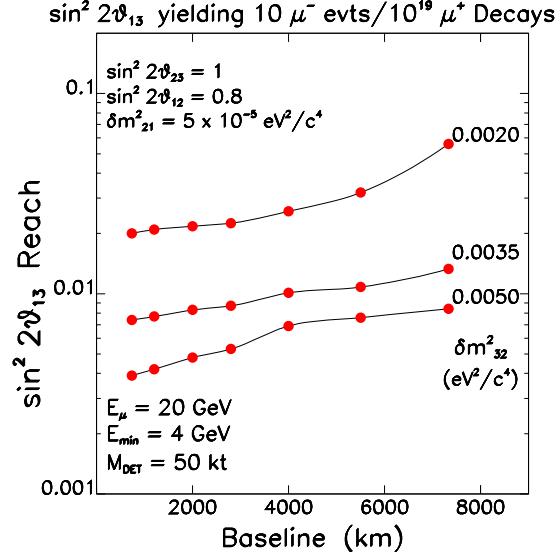


Figure 28: Reach in $\sin^2 2\theta_{13}$ for the observation of 10 μ^- events from $\nu_e \rightarrow \nu_\mu$ oscillations, shown versus baseline for three δm^2_{32} spanning the favored SuperK range. The other oscillation parameters correspond to the LMA scenario IA1. The curves correspond to $10^{19} \mu^+$ decays in a 20 GeV neutrino factory with a 50 kt detector, and a minimum muon detection threshold of 4 GeV. Results are from Ref. 51.

It is useful to define [51] the $\sin^2 2\theta_{13}$ “reach” for an experiment as the value of $\sin^2 2\theta_{13}$ for which a given physics goal would be met. We take as our initial goal the observation of 10 $\nu_e \rightarrow \nu_\mu$ events tagged by a wrong-sign muon. Consider first the $\sin^2 2\theta_{13}$ reach for a 50 kt detector sited a distance L from a 20 GeV neutrino factory in which there are $10^{19} \mu^+$ decays in the beam-forming straight section. The baseline-dependent $\sin^2 2\theta_{13}$ reach is shown in Fig. 28 for a three-flavor oscillation scenario in which δm^2_{21} , $\sin^2 2\theta_{12}$, and $\sin^2 2\theta_{23}$ correspond to the LMA scenario IA1, and the value of δm^2_{32} is varied over the favored SuperK range. Backgrounds are expected to be less than one event for $L \geq 2800 \text{ km}$ (Table 9), and are not included in the calculation shown in the figure. If δm^2_{32} is in the center of the SuperK range, the $\sin^2 2\theta_{13}$ reach is about an order of magnitude below the currently excluded region, improving slowly with decreasing L . However, at short baselines ($L < 2800 \text{ km}$) backgrounds may degrade the $\sin^2 2\theta_{13}$ reach. The reach improves (degrades) by a about a factor of 2 (3) if δm^2_{32} is at the upper (lower) end of the current SuperK range. If the oscillation parameters correspond to the LMA scenario IA1 ($\sin^2 2\theta_{13} = 0.04$), then only 2×10^{18} muon decays are required at a 20 GeV neutrino factory to observe 10 signal events

in a 50 kt detector at $L = 2800$ km. The calculation [51] assumes that CC events producing muons with energy less than (greater than) 4 GeV are detected with an efficiency of 0 (1). The number of muon decays needed to observe 10 $\nu_e \rightarrow \nu_\mu$ events is shown in Fig. 29 as a function of E_μ for the LMA scenario IA1, the SMA scenario IA2, and the LOW scenario IA3. The required muon beam intensities decrease with increasing E_μ , and are approximately proportional to $E_\mu^{-1.5}$. Compared with the SMA and LOW scenarios, slightly less intensity is needed for the LMA scenario, showing the small but finite contribution to the signal rate from the sub-leading δm^2 scale. In all three scenarios (LMA, SMA, LOW) a 20 GeV neutrino factory providing 10^{19} decays in the beam-forming straight section would enable the first observation of $\nu_e \rightarrow \nu_\mu$ oscillations in a 50 kt detector provided $\sin^2 2\theta_{13} > 0.01$. It should be noted that although $\sin^2 2\theta_{13}$ could be very small, there are models [61] that predict $\sin^2 2\theta_{13} \simeq 0.01$.

Having established $\nu_e \rightarrow \nu_\mu$ oscillations, further data taking would facilitate the measurement of matter effects and the determination of the sign of δm^2 , and hence the pattern of neutrino masses. To illustrate the effect of matter on the $\nu_e \rightarrow \nu_\mu$ oscillation probability, the predicted measured energy distributions 2800 km downstream of a 30 GeV neutrino factory are shown in Figs. 30 and 31 for respectively $\nu_e \rightarrow \nu_\mu$ and $\bar{\nu}_e \rightarrow \bar{\nu}_\mu$ wrong-sign muon events. The distributions are shown for a range of positive and negative values of δm_{32}^2 . Note that for a given $|\delta m_{32}^2|$, if $\delta m_{32}^2 < 0$ we would expect to observe a lower wrong-sign muon event rate and a harder associated spectrum when positive muons are stored in the neutrino factory than when negative muons are stored. On the other hand, if $\delta m_{32}^2 > 0$ we would expect to observe a higher wrong-sign muon event rate and a softer associated spectrum when positive muons are stored in the neutrino factory than when negative muons are stored. Hence, measuring the differential spectra when positive and negative muons are alternately stored in the neutrino factory can enable the sign of δm_{32}^2 to be unambiguously determined [63].

The expected number of wrong-sign muon events are listed in Table 9 for the LMA scenario IA1, and a 50 kt detector downstream of a neutrino factory providing $10^{19}\mu^+$ decays and the same number of μ^- decays. The event rates are shown for both signs of δm_{32}^2 , and for various storage ring energies and baselines. Even at a 20 GeV neutrino factory the signal rates at $L = 7332$ and 2800 km are large enough to permit the sign of δm_{32}^2 to be determined with a few years of data taking.

We conclude that for the LMA, SMA, and LOW three-flavor mixing scenarios we have considered, a 20 GeV neutrino factory providing 10^{19} decays in the beam-forming straight section would be a viable entry-level facility. In particular, with a 50 kt detector and a few years of data taking either $\nu_e \rightarrow \nu_\mu$ oscillations would be observed and the sign of δm_{32}^2 determined or a very stringent upper limit on $\sin^2 2\theta_{13}$ will have been obtained (discussed later). Long baselines (> 2000 km) are preferred. The longest baseline we have considered (7332 km) has the advantage of lower total event rates and hence lower background rates.

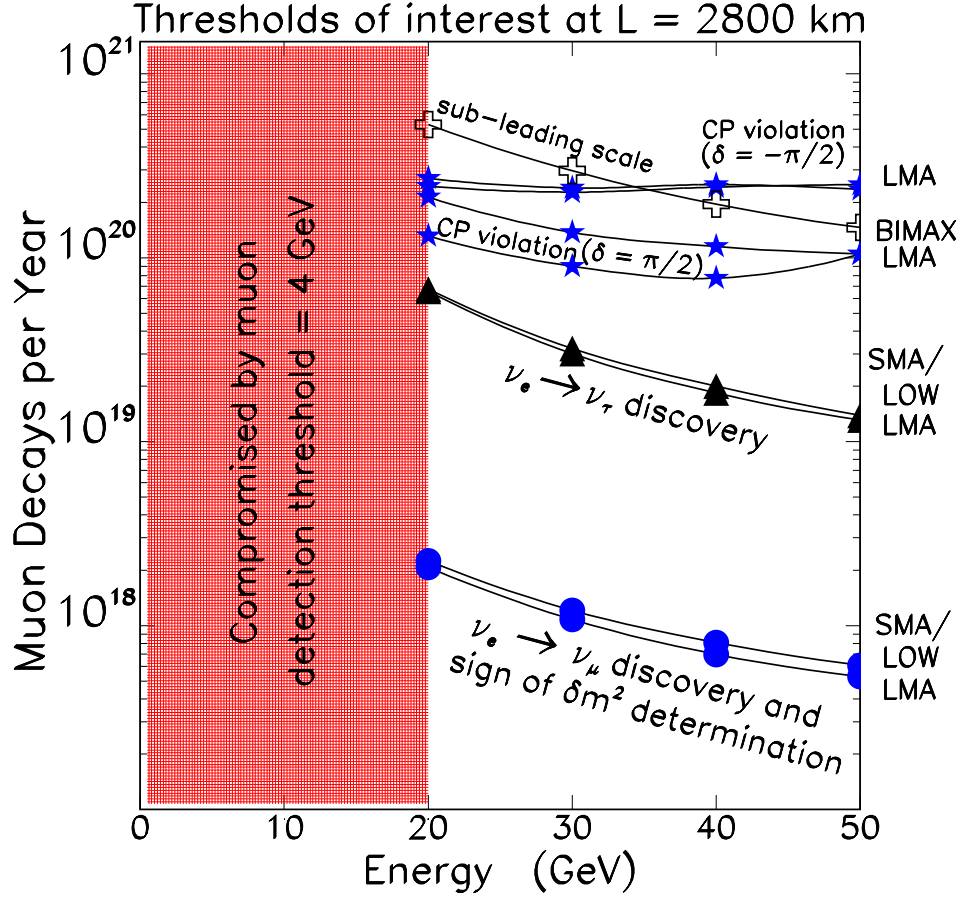


Figure 29: The required number of muon decays needed in the beam-forming straight section of a neutrino factory to achieve the physics goals described in the text, shown as a function of storage ring energy for the LMA scenario IA1, SMA scenario IA2, LOW scenario IA3, and a bimaximal mixing scenario BIMAX. The baseline is taken to be 2800 km, and the detector is assumed to be a 50 kt wrong-sign muon appearance device with a muon detection threshold of 4 GeV or, for $\nu_e \rightarrow \nu_\tau$ appearance, a 5 kt detector. Results are from Ref. 51.

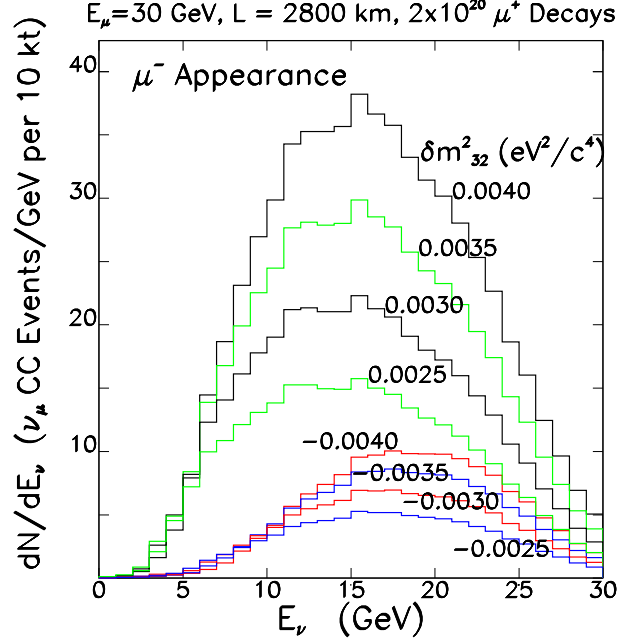


Figure 30: Predicted measured energy distributions for CC events tagged by a wrong-sign (negative) muon from $\nu_e \rightarrow \nu_\mu$ oscillations (no cuts or backgrounds), shown for various δm_{32}^2 , as labeled. The predictions correspond to 2×10^{20} decays, $E_\mu = 30$ GeV, $L = 2800$ km, with the values for δm_{12}^2 , $\sin^2 2\theta_{13}$, $\sin^2 2\theta_{23}$, $\sin^2 2\theta_{12}$, and δ corresponding to the LMA scenario IA1. Results are from Ref. 63.

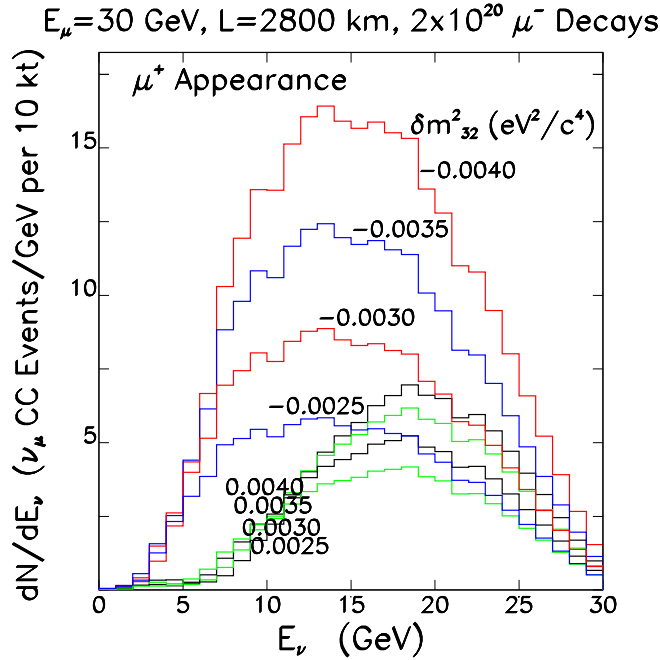


Figure 31: Same as previous figure, for CC events tagged by a wrong-sign (positive) muon from $\bar{\nu}_e \rightarrow \bar{\nu}_\mu$ oscillations.

Table 9: Wrong-sign muon rates for a 50 kt detector (with a muon threshold of 4 GeV) a distance L downstream of a neutrino factory (energy E_μ) providing 10^{19} muon decays. Rates are shown for LMA scenario IA1 with both signs of δm_{32}^2 considered separately. The background rates listed correspond to an assumed background level of 10^{-4} times the total CC rates (see section 3.4) with no energy dependence. Energy dependent cuts might suppress backgrounds further. Results are from Ref. 63.

E_μ GeV	L km	μ^+ stored			μ^- stored		
		$\delta m_{32}^2 > 0$	$\delta m_{32}^2 < 0$	Backg	$\delta m_{32}^2 > 0$	$\delta m_{32}^2 < 0$	Backg
20	732	52.	36.	7.3	32.	26.	6.5
	2800	46.	9.2	0.43	7.1	26.	0.36
	7332	33.	0.97	0.063	0.55	19.	0.05
30	732	100.	72.	25.	58.	45.	24.
	2800	90.	26.	1.6	19.	43.	1.4
	7332	43.	3.3	0.19	2.1	33.	0.17
40	732	150.	110.	60.	83.	65.	58.
	2800	140.	48.	4.0	36.	64.	3.8
	7332	54.	5.6	0.49	3.1	28.	0.43
50	732	200.	140.	120.	110.	84.	120.
	2800	180.	71.	7.9	53.	82.	7.7
	7332	56.	8.0	1.1	5.0	34.	1.0

3.5.2 Observation of $\nu_e \rightarrow \nu_\tau$ oscillations

We begin by considering the LMA scenario IA1, and ask: What beam intensity is needed to make the first observation of $\nu_e \rightarrow \nu_\tau$ oscillations in a detector that is 2800 km downstream of a 20 GeV neutrino factory? The $\nu_e \rightarrow \nu_\tau$ and the accompanying $\bar{\nu}_\mu \rightarrow \bar{\nu}_\tau$ event rates are shown in Fig. 32 as a function of the oscillation parameters $\sin^2 2\theta_{13}$ and δm_{32}^2 . The $\nu_e \rightarrow \nu_\tau$ signal rate is sensitive to both of these parameters, and hence provides an important consistency check for three-flavor mixing: the observation or non-observation of a $\nu_e \rightarrow \nu_\tau$ signal must be consistent with the oscillation parameters measured from, for example, $\nu_e \rightarrow \nu_\mu$, $\nu_\mu \rightarrow \nu_\tau$, and ν_μ disappearance measurements. For the LMA scenario IA1 the observation of 10 signal events in a 5 kt detector (with 30% τ -lepton efficiency) would require 3 years with $7 \times 10^{19} \mu^+$ decays per year in the beam forming straight section. Very similar beam intensities are required for the SMA and LOW scenarios (IA2 and IA3). Note that, over the $\sin^2 2\theta_{13}$ range shown in Fig. 32, the $\bar{\nu}_\mu \rightarrow \bar{\nu}_\tau$ rates are one to two orders of magnitude higher than the $\nu_e \rightarrow \nu_\tau$ rates. Hence, we will need a detector that can determine the sign of the tau-lepton charge at the $2\sigma - 3\sigma$ level, or better.

Let us define the $\sin^2 2\theta_{13}$ “reach” for an experiment as the value of $\sin^2 2\theta_{13}$ for which we would observe 10 $\nu_e \rightarrow \nu_\tau$ events when there are 10^{20} muon decays in the beam-forming straight section of a neutrino factory. The $\sin^2 2\theta_{13}$ reach

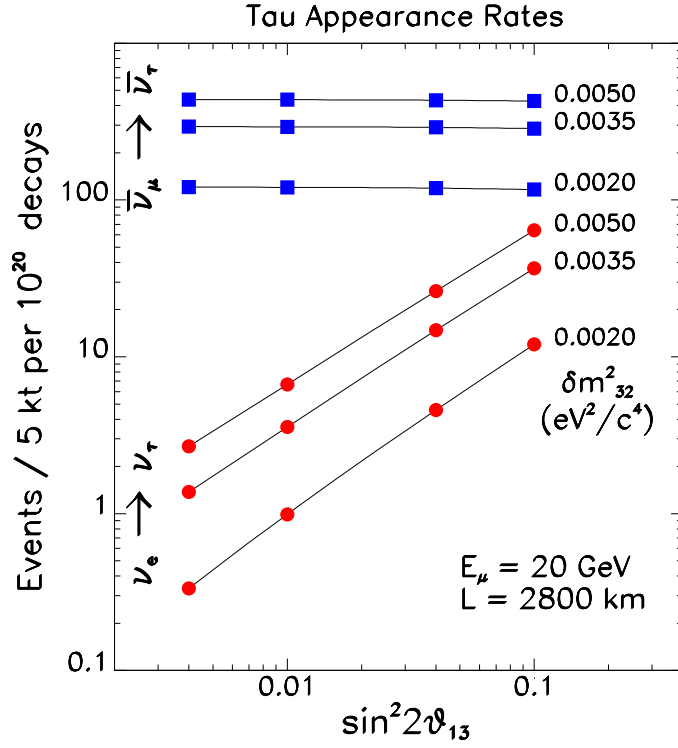


Figure 32: ν_τ CC appearance rates in a 5 kt detector 2800 km downstream of a 20 GeV neutrino factory in which there are $10^{20}\mu^+$ decays in the beam-forming straight section. The rates are shown as a function of $\sin^2 2\theta_{13}$ and δm_{32}^2 with the other oscillation parameters corresponding to the LMA scenario IA1. The top 3 curves are the predictions for $\bar{\nu}_\mu \rightarrow \bar{\nu}_\tau$ events and the lower curves are for $\nu_e \rightarrow \nu_\tau$ events. Results are from Ref. 51.

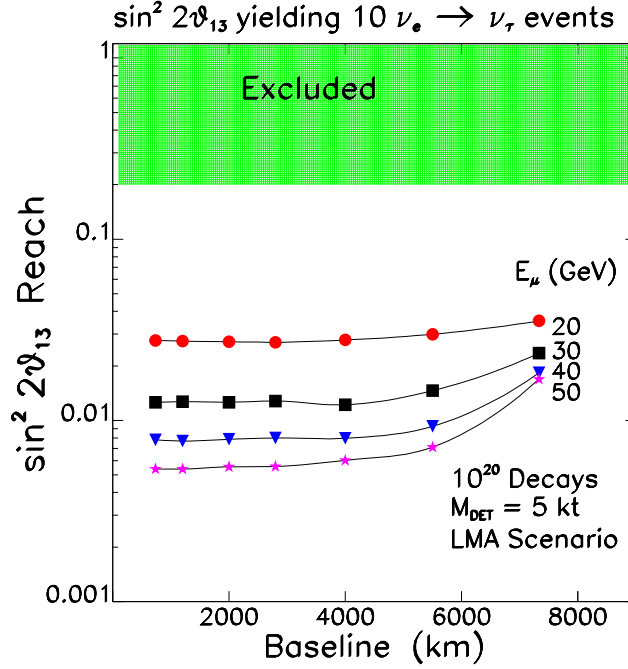


Figure 33: Reach in $\sin^2 2\theta_{13}$ for the observation of 10 $\nu_e \rightarrow \nu_\tau$ oscillation events, shown as a function of baseline for four storage ring energies. The oscillation parameters correspond to the LMA scenario IA1. The curves correspond to 10^{20} μ^+ decays in a 20 GeV neutrino factory with a 5 kt detector. Results are from Ref. 51.

is shown as a function of the baseline and storage ring energy in Fig. 33 for a 5 kt detector and an oscillation scenario in which all of the parameters except $\sin^2 2\theta_{13}$ correspond to scenario IA1. The reach improves with energy (approximately $\sim E^{-1.5}$ [51]) and is almost independent of baseline except for the highest energies and baselines considered. However, backgrounds to a $\nu_e \rightarrow \nu_\tau$ oscillation search have not been studied in detail, and are not included in the calculation. Background considerations will favor longer baselines. The number of muon decays needed to observe 10 $\nu_e \rightarrow \nu_\tau$ events is shown as a function of muon beam energy in Fig. 29 for the LMA scenario IA1, the SMA scenario IA2, and the LOW scenario IA3. We conclude that within these three-flavor mixing scenarios, a 20 GeV storage ring in which there are $O(10^{20})$ muon decays per year would begin to permit an observation of, or meaningful limits on, $\nu_e \rightarrow \nu_\tau$ oscillations provided a multi-kt detector with good tau-lepton identification and charge discrimination is practical.

Next, consider the oscillation scenarios IB1 (atmospheric + LSND scales) and IC1 (three-flavor with atmospheric, solar, and LSND data stretched). In these cases the leading δm^2 is large ($0.3 \text{ eV}^2/c^4$) and medium baseline experiments ($L = 10\text{-}100 \text{ km}$) become interesting. As an example, consider a medium baseline experiment a few $\times 10 \text{ km}$ downstream of a 20 GeV neutrino factory in which there are $10^{20} \mu^+$ decays. The $\nu_e \rightarrow \nu_\tau$ and accompanying $\bar{\nu}_\mu \rightarrow \bar{\nu}_\tau$ event rates

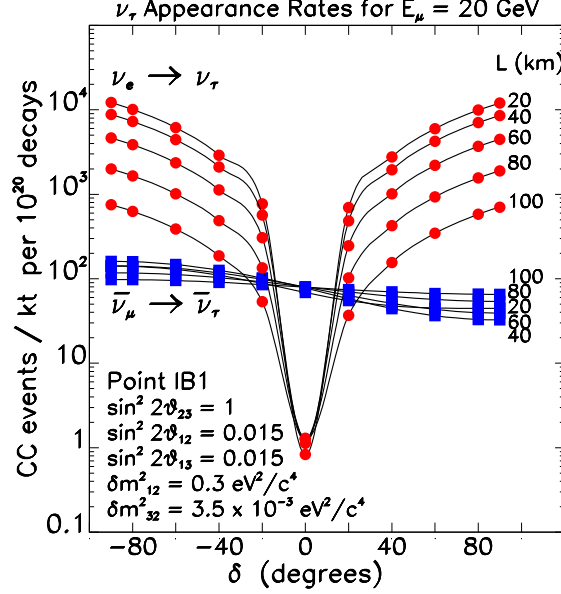


Figure 34: ν_τ CC appearance rates in a 1 kt detector downstream of a 20 GeV neutrino factory in which there are $10^{20}\mu^+$ decays. Rates are shown as a function of the baseline L and phase δ , with the other oscillation parameters corresponding to the LSND + Atmospheric scenario IB1. Predictions for $\nu_e \rightarrow \nu_\tau$ and $\bar{\nu}_\mu \rightarrow \bar{\nu}_\tau$ are shown separately, as labeled. Results are from Ref. 62.

are shown in Fig. 34 as a function of the baseline and the phase δ with the other oscillation parameters corresponding to scenario IB1. In contrast to the $\bar{\nu}_\mu \rightarrow \bar{\nu}_\tau$ rates, the $\nu_e \rightarrow \nu_\tau$ rates are very sensitive to δ , and for $|\delta| > 20^\circ$ can be very large, yielding thousands of events per year in a 1 kt detector at $L = 60$ km, for example. Note that the corresponding $\bar{\nu}_\mu \rightarrow \bar{\nu}_\tau$ rate is of order 100 events. For small $|\delta|$ the $\bar{\nu}_\mu \rightarrow \bar{\nu}_\tau$ rate will dominate the τ appearance event sample. For larger $|\delta|$ the $\nu_e \rightarrow \nu_\tau$ rate dominates. Good τ charge determination will therefore be important to measure both $\nu_e \rightarrow \nu_\tau$ and $\bar{\nu}_\mu \rightarrow \bar{\nu}_\tau$ oscillations.

Now consider the τ appearance rates in scenario IC1. In this case the rates are not sensitive to δ and, for a 1 kt detector at $L = 60$ km, there are about 8000 $\nu_e \rightarrow \nu_\tau$ events and 93000 $\bar{\nu}_\mu \rightarrow \bar{\nu}_\tau$ events [62]. A detector with 3σ (or better) τ -lepton charge discrimination would enable these two rates to be separately measured.

We conclude that measurements of the $\nu_e \rightarrow \nu_\tau$ oscillation rate at a neutrino factory would provide an important test of the oscillation scenario. In LMA, SMA, and LOW three-flavor oscillation scenarios, a 20 GeV neutrino factory providing $O(10^{20})$ muon decays could permit an observation of, or meaningful limits on, $\nu_e \rightarrow \nu_\tau$ oscillations. In LSND-type scenarios where the leading δm^2 scale is large, a 20 GeV neutrino factory providing $O(10^{19})$ muon decays might already permit hundreds of $\nu_e \rightarrow \nu_\tau$ events to be measured. It should be noted that the feasibility of a multi-kt detector with good τ identification efficiency

(for example 30%) and good charge sign determination has not been explored in detail at this stage, and further work is required to identify the best detector technology for this, and determine the expected resolutions and efficiencies.

3.5.3 Measurement of $\nu_\mu \rightarrow \nu_\tau$ oscillations

The present SuperK data suggests that the atmospheric neutrino deficit is due to $\nu_\mu \rightarrow \nu_\tau$ oscillations. If this is correct the next generation of accelerator based long baseline experiments are expected to measure these oscillations. Nevertheless, for a fixed neutrino factory energy and baseline, it is important to measure or put stringent constraints on all of the appearance channels so that the sum of the appearance modes can be compared with the disappearance measurements. Hence, we briefly consider $\nu_\mu \rightarrow \nu_\tau$ rates at a neutrino factory. Note that at a 20 GeV neutrino factory the average interacting neutrino energy is of order 15 GeV, and for δm^2 within the favored SuperK range, the first oscillation maximum occurs at baselines of 7000 ± 3000 km. At shorter baselines the oscillation probabilities are lower and hence the signal/background ratio is lower, although the signal rate can be higher.

Consider first a 5 kt detector 2800 km downstream of a 20 GeV neutrino factory in which there are 10^{20} muon decays. The $\bar{\nu}_\mu \rightarrow \bar{\nu}_\tau$ event rates are shown in Fig. 32 as a function of $\sin^2 2\theta_{13}$ and δm_{32}^2 , with the other oscillation parameters corresponding to the LMA scenario IA1. If negative muons are stored in the neutrino factory, the resulting $\nu_\mu \rightarrow \nu_\tau$ event rates would be about a factor of two higher than the $\bar{\nu}_\mu \rightarrow \bar{\nu}_\tau$ rates shown in the figure. A neutrino factory providing $O(10^{20})$ muon decays would enable $\nu_\mu \rightarrow \nu_\tau$ appearance data samples of a few hundred to a few thousand events to be obtained. Similar rates are expected in SMA and LOW three-flavor mixing scenarios.

Next consider a longer baseline example in which a 10 kt ICANOE-type detector is 7400 km downstream of a 30 GeV neutrino factory which provides 10^{20} muon decays in the beam forming straight section [50]. The main advantage of a longer baseline is that the total interaction rate, and hence the τ -lepton background, is reduced. The energy distribution for events in which there is no charged lepton can directly reflect the presence of a ν_τ signal (see Fig. 16). The non- τ events in this event sample can be suppressed using topology-dependent kinematic cuts. It is desirable that the τ charge-sign also be determined which, with an external muon spectrometer, will be possible for the $\tau \rightarrow \mu$ subsample. We conclude that the measurement of $\nu_\mu \rightarrow \nu_\tau$ oscillations with high statistical precision will be possible at a neutrino factory in long and very long baseline experiments. A more complete study is warranted.

3.5.4 Determination of $\sin^2 2\theta_{13}$, $\sin^2 2\theta_{23}$, and δm_{32}^2

Consider first the determination of $\sin^2 2\theta_{13}$. The most sensitive way to measure $\sin^2 2\theta_{13}$ at a neutrino factory is to measure the $\nu_e \rightarrow \nu_\mu$ oscillation amplitude,

which is approximately proportional to $\sin^2 2\theta_{13}$. More explicitly, the value of $\sin^2 2\theta_{13}$ is extracted from a fit to the spectrum of CC interactions tagged by a wrong-sign muon. Background contributions from, for example, muonic decays of charged mesons must be kept small, which favors small total event samples and hence long baselines.

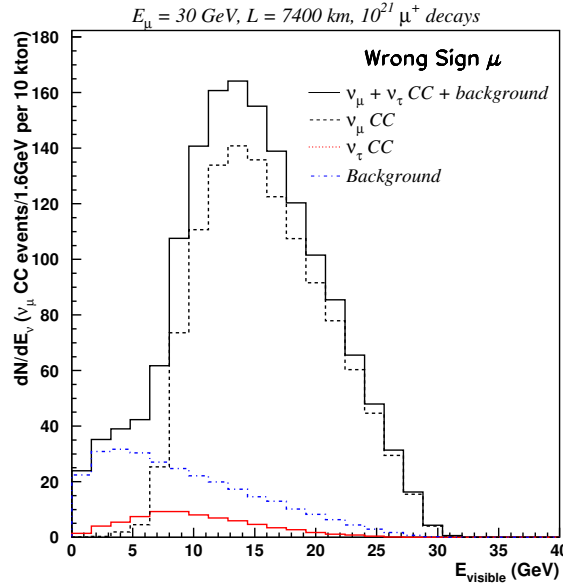


Figure 35: Visible energy spectrum for events tagged by wrong-sign muons in an ICANOE-type detector (full histogram). The oscillation parameters are $\delta m_{32}^2 = 3.5 \times 10^{-3} \text{ eV}^2/\text{c}^4$, $\sin^2 \theta_{23} = 1$, and $\sin^2 2\theta_{13} = 0.05$. Also shown are the contributions from $\nu_e \rightarrow \nu_\mu$ oscillations (black dashed curve), $\nu_e \rightarrow \nu_\tau$, with a subsequent muonic decay of the τ lepton (red curve), and background from muonic decays of pions or kaons in neutral current or charged current events (blue dot-dashed curve). Results are from Ref. 50.

As an example, consider a 10 kt ICANOE-like detector that is 7400 km downstream of a 30 GeV neutrino factory [50]. The simulated energy spectrum of wrong-sign muon events is shown in Fig. 35 for three-flavor oscillations with the parameters $\delta m_{32}^2 = 3.5 \times 10^{-3} \text{ eV}^2/\text{c}^4$, $\sin^2 2\theta_{23} = 1$, and $\sin^2 2\theta_{13} = 0.05$. Note that the backgrounds predominantly contribute to the low energy part of the spectrum. To fit the observed spectrum and extract $\sin^2 2\theta_{13}$ matter effects must be taken into account. The modification of the oscillation probability due to matter effects is a function of the profile of the matter density ρ between the neutrino source and the detector. The density profile is known from geophysical measurements, and this knowledge can either be used in the fit, or alternatively ρ can be left as a free parameter. It has been shown that both methods give consistent results [50], and that the uncertainties on the fitted values of ρ and $\sin^2 2\theta_{13}$ are not strongly correlated. However, the fitted value for $\sin^2 2\theta_{13}$ does depend on the assumed values for $\sin^2 \theta_{23}$ and δm_{32}^2 . The measured right-sign muon (ν_μ

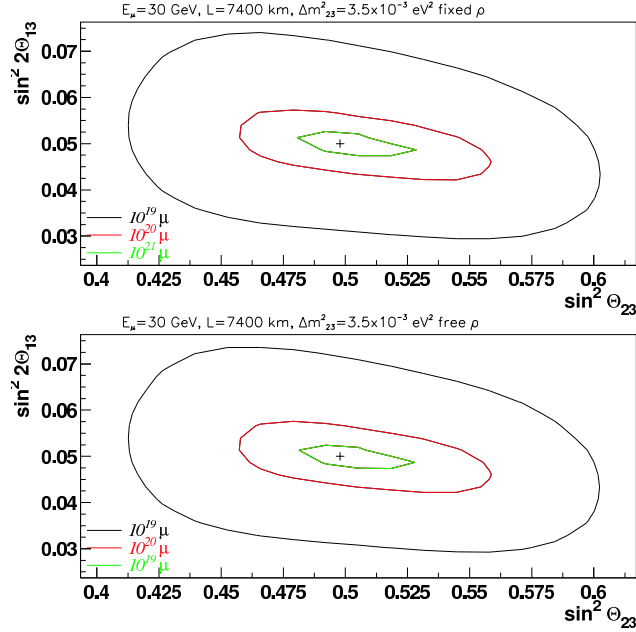


Figure 36: Results from a global fit to the visible energy distributions for various event classes recorded in a 10 kt ICANOE-type detector 7400 km downstream of a 30 GeV neutrino factory. The 68% CL contours correspond to experiments in which there are 10^{19} , 10^{20} , and $10^{21} \mu^+$ decays in the neutrino factory (as labeled) followed by the same number of μ^- decays. Upper plot: density fixed to its true value. Lower plot: density is a free parameter of the fit. Results are from Ref. 50.

disappearance) distribution, together with the distributions of events tagged by electrons, τ -leptons, or the absence of a lepton, can be used to constrain these additional oscillation parameters. Hence, the best way to extract $\sin^2 2\theta_{13}$ is from a global fit to all of the observed event distributions, with the oscillation parameters (and optionally ρ) left as free parameters. If the density profile is left as a free parameter, the fit determines its value with an uncertainty of about 10% [50, 59]. This provides a quantitative test of the MSW effect ! Examples of fit results in the $(\sin^2 2\theta_{13}, \sin^2 \theta_{23})$ -plane are shown in Fig. 36 for 10^{19} , 10^{20} , and 10^{21} muon decays in the neutrino factory. As the beam intensity increases the measurements become more precise. With $10^{19} \mu^+$ and μ^- decays $\sin^2 2\theta_{13}$ and $\sin^2 \theta_{23}$ are determined with precisions of 40% and 20% respectively. With 10^{21} decays these precisions have improved to $\sim 5\%$. If the baseline is decreased from 7400 km to 2900 km the oscillation parameters are determined with comparable (although slightly worse) precisions (Fig. 37). We conclude that within the framework of three-flavor mixing, provided $\sin^2 2\theta_{13}$ is not too small, a global fit to the observed oscillation distributions would enable $\sin^2 2\theta_{13}$, $\sin^2 \theta_{23}$, and δm_{32}^2 to be simultaneously determined, and the MSW effect to be measured.

Consider as a second example a 20 kt MINOS-type detector 2800 km downstream of a 30 GeV neutrino factory providing 10^{20} muon decays. Some prelim-

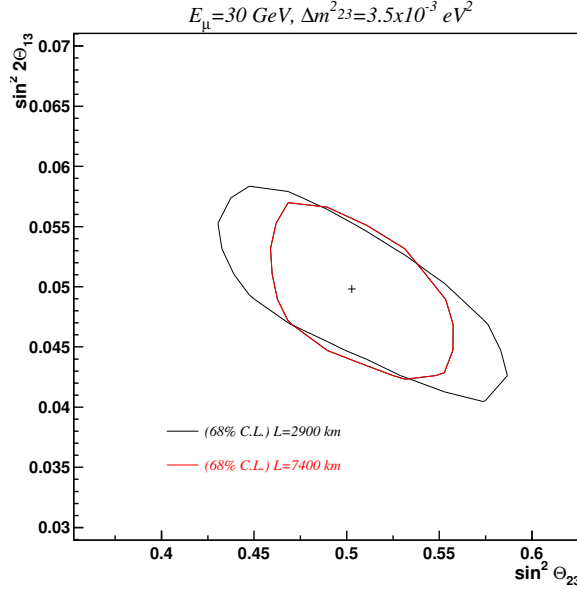


Figure 37: Results from a global fit to the visible energy distributions for various event classes recorded in a 10 kt ICANOE-type detector downstream of a 30 GeV neutrino factory in which there are $10^{20} \mu^+$ decays in the neutrino factory followed by the same number of μ^- decays. The 68% CL contours correspond to baselines of 7400 km and 2900 km, as labeled. Results are from Ref. 50.

inary fit results [60] for a LMA type scenario are shown in Fig. 43b. For this example the analysis required $p_\mu < 4$ GeV/c, but did not use the full set of cuts described in section 3.4, and therefore tolerated a background level a factor of a few greater than shown in Fig. 24 and Table 7. Nevertheless, the fits to the measured distribution of energies for events tagged by wrong-sign muons were able to determine $\sin^2 2\theta_{13}$ and δm_{32}^2 with precisions of 14% and 10% respectively for scenario IA1.

To illustrate the ultimate sensitivity to the oscillation parameters that might be achievable at a high intensity neutrino factory, consider next a 40 kt Fe-scintillator detector downstream of a 50 GeV neutrino factory in which there are $10^{21} \mu^+$ decays followed by $10^{21} \mu^-$ decays [59]. Fit results in the (matter density, $\sin^2 2\theta_{13}$)-plane are shown in Fig. 38 for three baselines. The precision on the $\sin^2 2\theta_{13}$ determination is a few percent. Note that the analysis described in Ref. [59] suggests that backgrounds can be suppressed to less than 10^{-5} of the total CC rate in the detector. This impressive level of background rejection deserves further study. At the shortest baselines (732 km) matter effects are too small to obtain a good determination of the matter density parameter.

Consider next the precision with which the oscillation parameters can be determined if $\sin^2 2\theta_{13}$ is very small, and hence no $\nu_e \rightarrow \nu_\mu$ oscillation signal is observed. The resulting limits on $\sin^2 2\theta_{13}$ are shown as a function of δm_{32}^2 in Fig. 39 for a 10 kt ICANOE type detector 7400 km downstream of a 30 GeV

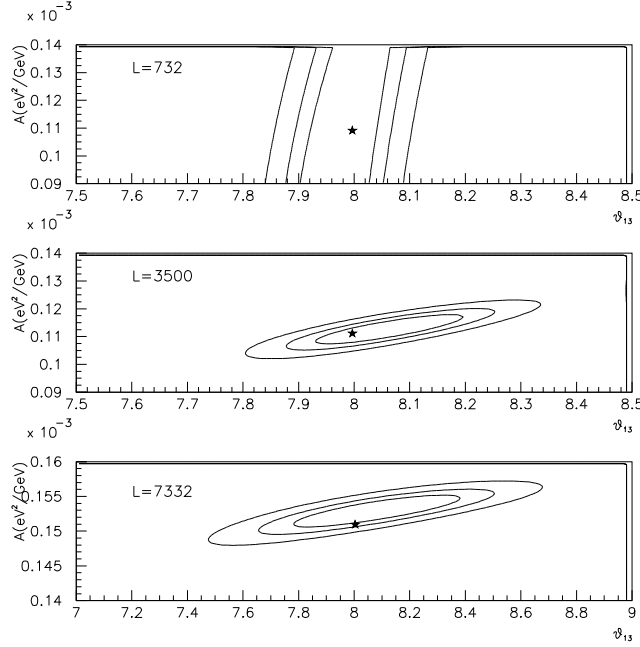


Figure 38: Fit results in the (A, θ_{13}) -plane for a simulated experiment in which a 40 kt Fe-scintillator detector is a distance L km downstream of a 50 GeV neutrino factory in which there are $10^{21}\mu$ decays. The density parameter A is defined in Eq. (36). The curves are 68.5, 90, and 99% CL contours. Results are from Ref. 59.

neutrino factory in which there are $10^{20}\mu^+$ decays followed by $10^{20}\mu^-$ decays [50]. The resulting upper limit on $\sin^2 2\theta_{13}$ would be $O(10^{-3}-10^{-4})$, about three orders of magnitude below the present experimental bound, and one to two orders of magnitude below the bound that would be expected at the next generation of long-baseline experiments.

The limit would become even more stringent at a higher intensity neutrino factory. As an example of the ultimate sensitivity that might be achievable, in Fig. 40 the limits on $\sin^2 2\theta_{13}$ are shown as a function of δm_{32}^2 and baseline for a 40 kt Fe-scintillator detector downstream of a 50 GeV neutrino factory in which there are $10^{21}\mu$ decays [59]. The non-observation of $\nu_e \rightarrow \nu_\mu$ oscillations could result in an upper limit on $\sin^2 2\theta_{13}$ below 10^{-5} ! With this level of sensitivity $\nu_e \rightarrow \nu_\mu$ oscillations driven by the sub-leading δm^2 scale might be observed [51]. For example, the number of muon decays required to produce 10 $\nu_e \rightarrow \nu_\mu$ events in a 50 kt detector 2800 km downstream of a neutrino factory is shown for a bimaximal mixing scenario ($\sin^2 2\theta_{13} = 0$) in Fig. 29 as a function of the stored muon energy. Approaching 10^{21} muon decays might be sufficient to observe oscillations driven by the sub-leading scale, but would require background levels of the order of 10^{-5} of the total CC rate, or better.

With a vanishing or very small $\sin^2 2\theta_{13}$ only the $\nu_\mu \rightarrow \nu_\tau$ oscillations will have a significant rate, and the oscillation parameters $\sin^2 2\theta_{23}$ and δm_{32}^2 can be

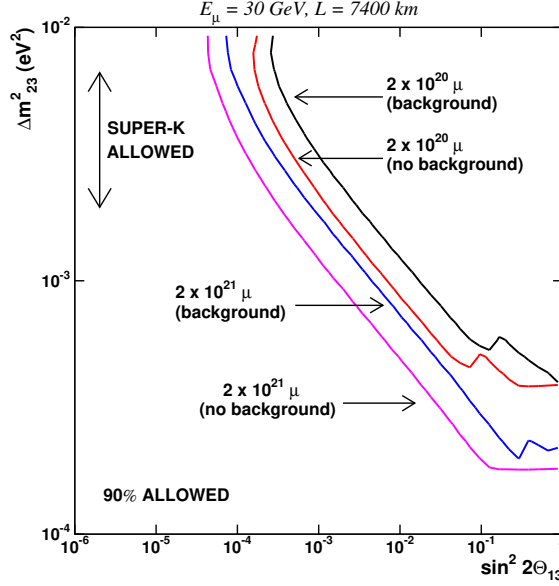


Figure 39: Allowed regions in oscillation parameter space calculated for a simulated experiment in which there are $N \mu^+$ decays followed by $N \mu^-$ decays in a 30 GeV neutrino factory that is 7400 km from a 10 kt ICANOE-type detector. The contours correspond to $N = 10^{20}$ and 10^{21} with and without backgrounds included in the calculation. Results are from Ref. 50.

determined by fitting the right-sign muon (ν_μ disappearance) spectrum. Good sensitivity can be obtained provided the baseline is chosen such that the first oscillation maximum occurs in the middle of the visible energy spectrum. As a first example, spectra of events tagged by right-sign muons are shown in Fig. 41 as a function of δm_{32}^2 for a 10 kt MINOS-type detector 2800 km downstream of a 30 GeV neutrino factory in which there are $2 \times 10^{20} \mu^-$ decays in the beam-forming straight section [51]. The position of the oscillation maximum (resulting in a dip in the observed distributions) is clearly sensitive to δm_{32}^2 . The depth of the observed dip is sensitive to the oscillation amplitude, and hence to $\sin^2 2\theta_{23}$. The visible energy spectrum of right-sign muon events can be fit to obtain $\sin^2 2\theta_{23}$ and δm_{32}^2 . We begin by considering the statistical precision that could be obtained with a perfect detector having MINOS-type resolution functions, no backgrounds, no selection requirements, and no systematic uncertainty on the neutrino flux. Fit results are shown in Fig. 42. For $\delta m_{32}^2 = 3.5 \times 10^{-3} \text{ eV}^2/c^4$ the fit yields statistical precisions of a few percent on the values of the oscillation parameters. If L is increased to 7332 km, the statistical precision improves to about 1%. With this level of precision it is likely that systematic uncertainties will be significant [60]. To illustrate this in Fig. 43a the 1σ contours are shown in the $(\delta m_{32}^2, \sin^2 2\theta_{23})$ from fits which include backgrounds together with 0% and 2% systematic uncertainties on the beam flux. With a 2% flux uncertainty the precision on δm_{32}^2 and $\sin^2 2\theta_{23}$ are respectively 11% and 14%.

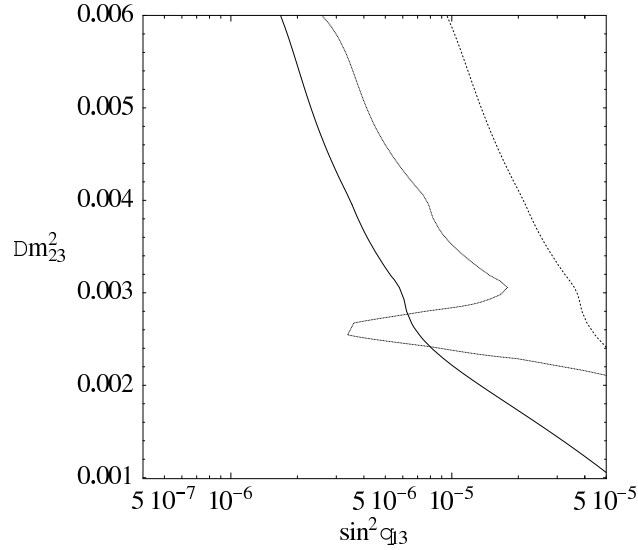


Figure 40: Allowed regions in oscillation parameter space calculated for a simulated experiment in which a 40 kt Fe-scintillator detector is a distance L km downstream of a 50 GeV neutrino factory in which there are $10^{21}\mu$ decays. The curves are 90% CL contours for $L = 732$ km (dashed), 3500 km (solid), and 7332 km (dotted). Results are from Ref. 59.

As a second example, consider a 10 kt ICANOE-type detector that is downstream of a 30 GeV neutrino factory in which there are $10^{20}\mu^+$ decays in the beam-forming straight section followed by $10^{20}\mu^-$ decays [50]. The sensitivity to the oscillation parameters has been studied by fitting simulated visible energy distributions for events tagged by a right-sign muon. The analysis includes a 2% bin-to-bin uncorrelated systematic error on the number of neutrino interactions which takes into account the uncorrelated uncertainties on neutrino flux, the cross section, and the selection efficiency. To reduce background from charged meson decays, the events entering the fit are those with muons having momenta > 2 GeV/c. Figures 44-47 show fit results in the $(\sin^2 2\theta_{23}, \delta m_{32}^2)$ -plane as a function of the oscillation parameters and baseline. Note that for the “short” baseline ($L = 732$ km) the first oscillation maximum for the reference value of $\delta m_{32}^2 = 3.5 \times 10^{-3}$ eV²/c⁴ occurs at a neutrino energy of about 2 GeV. This is too low to produce a clear dip in the visible energy spectrum, and as a result $\sin^2 2\theta_{23}$ and δm_{32}^2 can only be determined with relatively low precision (Fig. 44), and the fit results are sensitive to systematic uncertainties on the neutrino flux. At the longer baselines ($L = 2900$ km and 7400 km) the oscillation dip is visible, and the oscillation parameters can be measured with a precision that is mostly determined by the statistical uncertainty (Fig. 45). For a 30 GeV neutrino factory and $\delta m_{32}^2 = 3.5 \times 10^{-3}$ eV²/c⁴ the longer baseline (7400 km) yields the most precise result. Specifically, for $10^{20}\mu$ decays the statistical precisions on

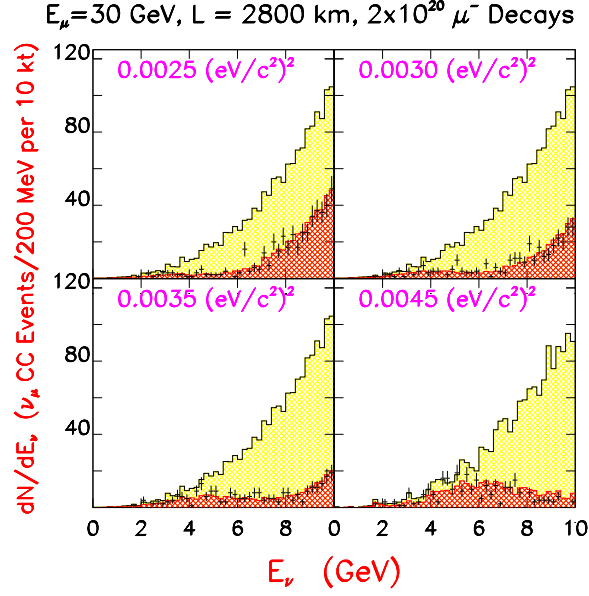


Figure 41: Visible energy distributions for events tagged by a right-sign muon in a MINOS-type detector 2800 km downstream of a 20 GeV neutrino factory in which there are $2 \times 10^{20} \mu^-$ decays. Predicted distributions are shown for four values of δm_{32}^2 , with the other parameters corresponding to the LMA scenario IA1. For each panel, the points with statistical error bars show an example of a simulated experiment. The light shaded histograms show the predicted distributions in the absence of oscillations. Results are from Ref. 51.

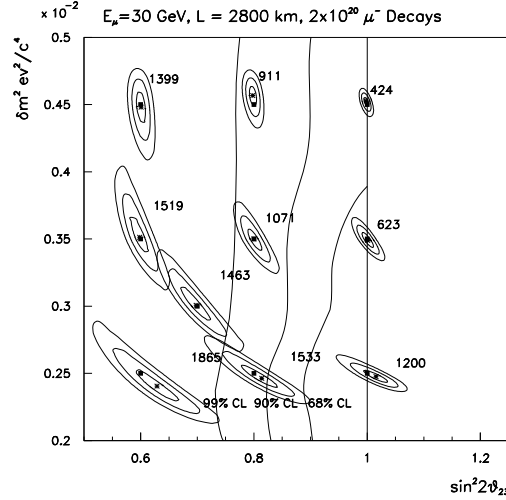


Figure 42: Fit results for simulated ν_μ disappearance measurements with a 10 kt MINOS-type detector 2800 km downstream of a 30 GeV neutrino factory in which there are $2 \times 10^{20} \mu^-$ decays. For each trial point the 1σ , 2σ , and 3σ contours are shown for a perfect detector (no backgrounds) and no systematic uncertainty on the beam flux. The 68%, 90% and 95% SuperK regions are indicated. Results are from Ref. 51.

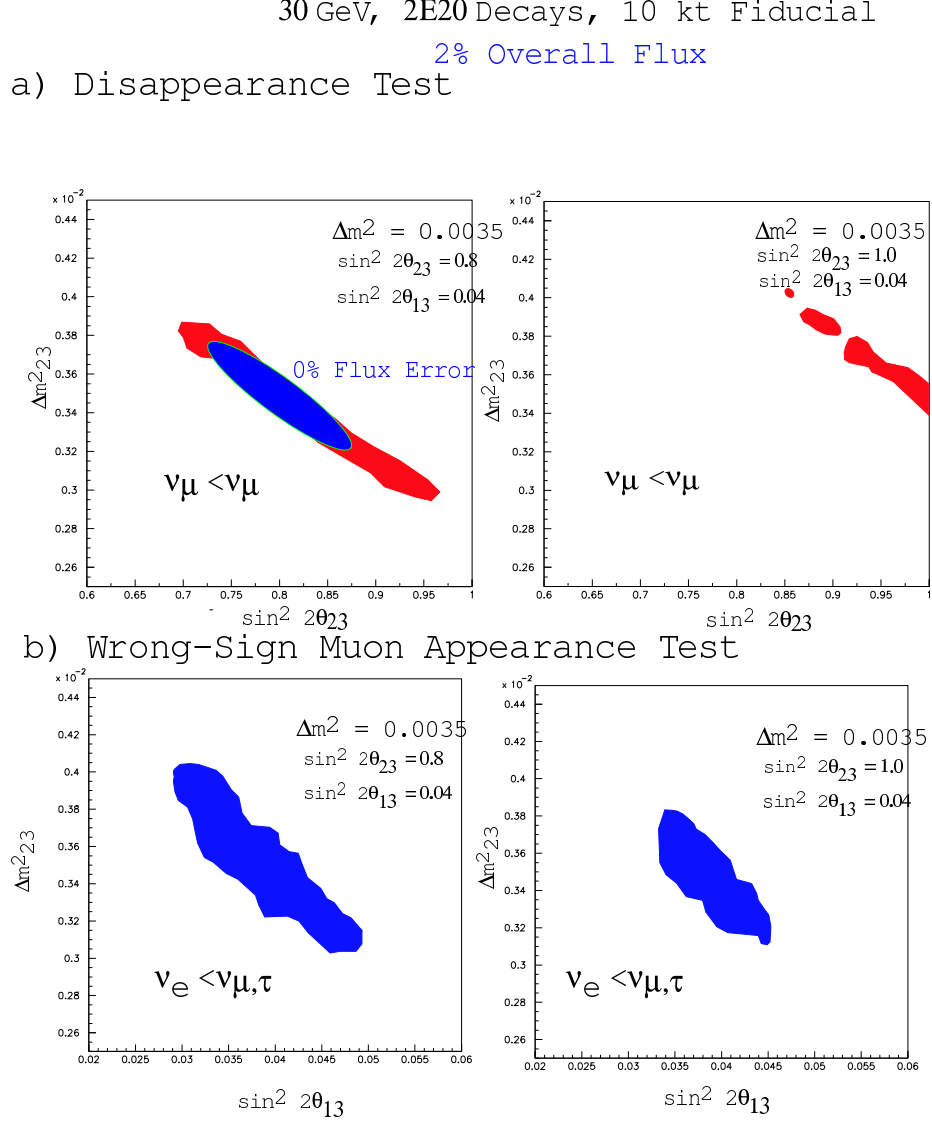


Figure 43: Fit results (1σ contours) for (a) simulated ν_μ disappearance measurements with a 10 kt MINOS-type detector 2800 km downstream of a 30 GeV neutrino factory in which there are $2 \times 10^{20} \mu^-$ decays, with and without an ad hoc 2% systematic uncertainty on the neutrino flux, and (b) wrong-sign muon appearance measurements including an ad hoc 2% systematic uncertainty on the flux. The acceptance for a muon is zero for $p_\mu < 4$ GeV and unity for $p_\mu \geq 4$ GeV. Backgrounds are included but no p_\perp^2 cut has been used. Results are from Ref. 60.

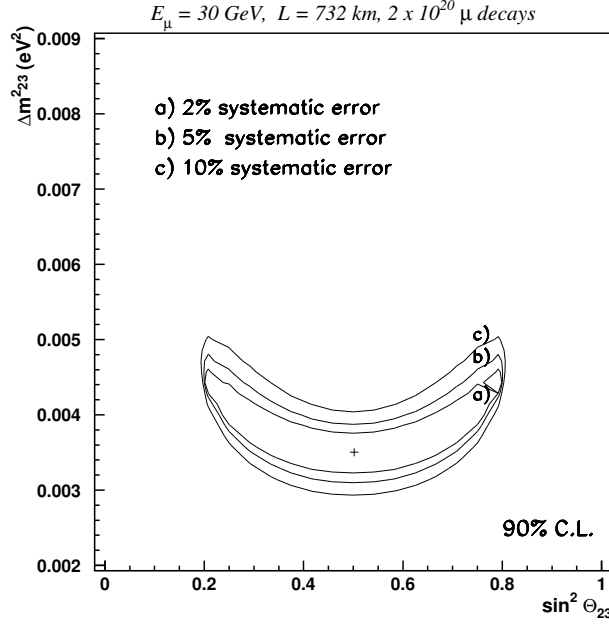


Figure 44: Fit results for simulated ν_μ disappearance measurements with a 10 kt ICANOE type detector 732 km downstream of a 30 GeV neutrino factory in which there are $10^{20}\mu$ decays. The effect of a systematic uncertainty on the neutrino flux is shown. Results are from Ref. 50.

$\sin^2 2\theta_{23}$ and δm_{32}^2 are respectively about 10% and 1%. With $10^{21}\mu$ decays the $\sin^2 2\theta_{23}$ precision improves by about a factor of 2. It should be noted that the best baseline choice depends on δm_{32}^2 (Figs. 46-47), or more specifically $\delta m_{32}^2/E$.

We conclude that, within the framework of three-flavor mixing, the oscillation parameters $\sin^2 2\theta_{13}$, $\sin^2 2\theta_{23}$, and δm_{32}^2 can be determined at a neutrino factory by fitting the observed visible energy distributions for various event types. A comprehensive study of the expected precisions of the measurements as a function of the oscillation parameters, baseline, and neutrino factory parameters has not yet been undertaken. However, detailed studies have been made for some examples in which there are $10^{20}\mu^+$ decays followed by $10^{20}\mu^-$ decays in a 30 GeV neutrino factory. For these examples we find that (i) if $\sin^2 2\theta_{13} > O(10^{-2})$ global fits can be used to determine its value, (ii) if $\sin^2 2\theta_{13}$ is too small to observe $\nu_e \rightarrow \nu_\mu$ oscillations then we would expect to place the very stringent upper limit on its value of 10^{-3} or better, and (iii) the values of $\sin^2 2\theta_{23}$, and δm_{32}^2 could be determined with precisions of respectively better than or of order 10% and of order 1%, provided the baseline is chosen so that the dip corresponding to the first oscillation maximum is in the middle of the visible energy distribution. At a high-intensity neutrino factory (for example with 10^{21} decays of 50 GeV muons) the mixing angles could be measured with a precision of a few percent, and if $\sin^2 2\theta_{13}$ is vanishingly small, the resulting upper limit could be at the $O(10^{-5})$ -level.

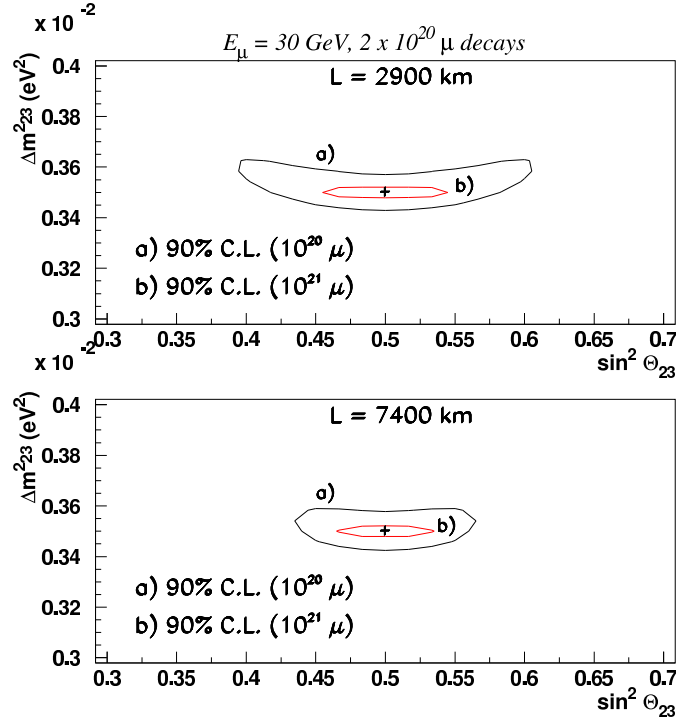


Figure 45: Fit results for simulated ν_μ disappearance measurements with a 10 kt ICANOE type detector 2900 km (top plot) and 7400 km (bottom plot) downstream of a 30 GeV neutrino factory in which there are (a) $10^{20} \mu$ decays and (b) $10^{21} \mu$ decays. Results are from Ref. 50.

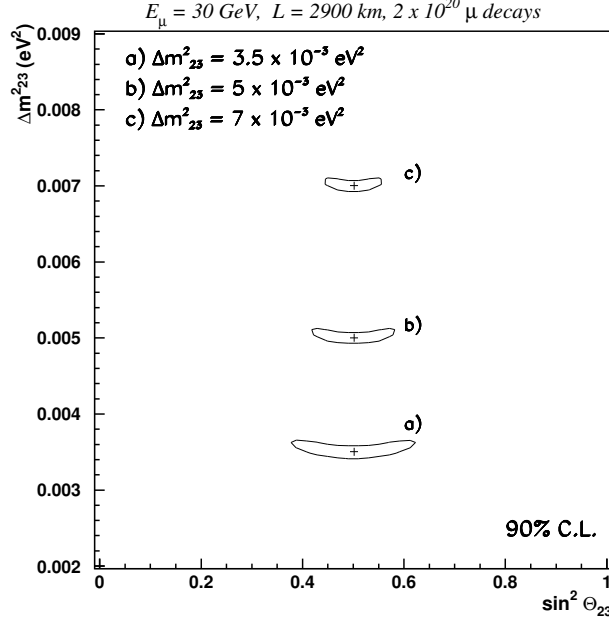


Figure 46: Fit results for simulated ν_μ disappearance measurements with a 10 kt ICANOE type detector 2900 km downstream of a 30 GeV neutrino factory in which there are $10^{20}\mu^-$ decays followed by $10^{20}\mu^+$ decays. Results are shown for 3 values of δm_{32}^2 , and are from Ref. 50.

3.5.5 Search for CP violation

In the majority of the three-flavor oscillation scenarios described in section 3.1 the CP violating amplitude is too small to produce an observable effect. Nevertheless, in these cases stringent limits on CP violation would provide an important check of the overall interpretation of the oscillation data. If however the LMA scenario provides the correct description of neutrino oscillations, CP violating effects might be sufficiently large to be observable at a high-intensity neutrino factory [59, 51]. This is illustrated in Fig. 48 which shows, as a function of baseline at a 20 GeV neutrino factory, the ratio R for $\delta = 0$ and $\pm\pi/2$, where R is defined as the $\bar{\nu}_e \rightarrow \bar{\nu}_\mu$ event rate divided by the $\nu_e \rightarrow \nu_\mu$ event rate. The upper group of curves is for $\delta m_{32}^2 < 0$, the lower group is for $\delta m_{32}^2 > 0$, and the statistical errors correspond to 10^{21} muon decays of each sign with a 50 kt detector. If L is a few thousand km a non-zero δ can produce a modification to R that is sufficiently large to be measured !

Since the $\nu_e \rightarrow \nu_\mu$ oscillation rates are to a good approximation proportional to $\sin^2 2\theta_{13}$, it is useful to define the $\sin^2 2\theta_{13}$ reach as that value of $\sin^2 2\theta_{13}$ that will produce a 3σ change in the predicted ratio R when δ is changed from 0 to $\pm\pi/2$. The $\sin^2 2\theta_{13}$ reach is shown as a function of baseline and stored muon energy in Fig. 49 for a 50 kt detector at a neutrino factory in which there are $10^{21}\mu^+$ decays followed by $10^{21}\mu^-$ decays. With an optimum baseline of about

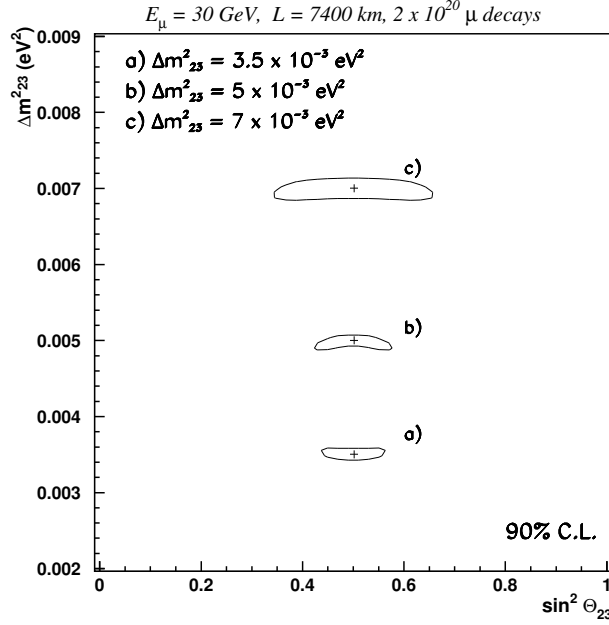


Figure 47: Fit results for simulated ν_μ disappearance measurements with a 10 kt ICANOE type detector 7400 km downstream of a 30 GeV neutrino factory in which there are $10^{20}\mu^+$ decays followed by $10^{20}\mu^+$ decays. Results are shown for 3 values of δm_{32}^2 , and are from Ref. 50.

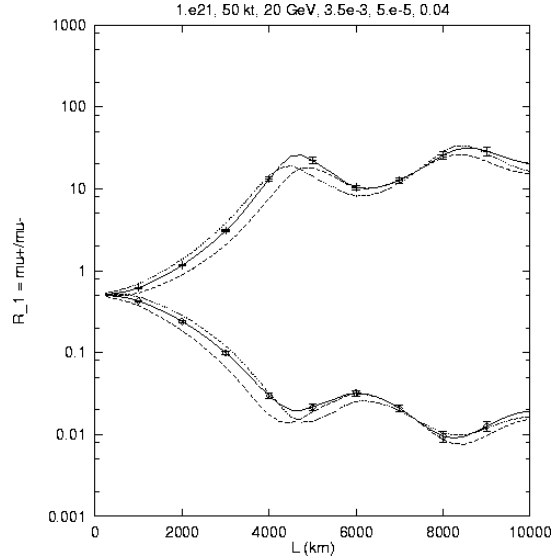


Figure 48: The ratio R of $\bar{\nu}_e \rightarrow \bar{\nu}_\mu$ to $\nu_e \rightarrow \nu_\mu$ event rates at a 20 GeV neutrino factory for $\delta = 0$ and $\pm\pi/2$. The upper group of curves is for $\delta m_{32}^2 < 0$, the lower group is for $\delta m_{32}^2 > 0$. The statistical errors correspond to 10^{21} muon decays of each sign and a 50 kt detector. The oscillation parameters correspond to the LMA scenario IA1. With no matter or CP effects $R \sim 0.5$ for all baselines. Results are from Ref. 51.

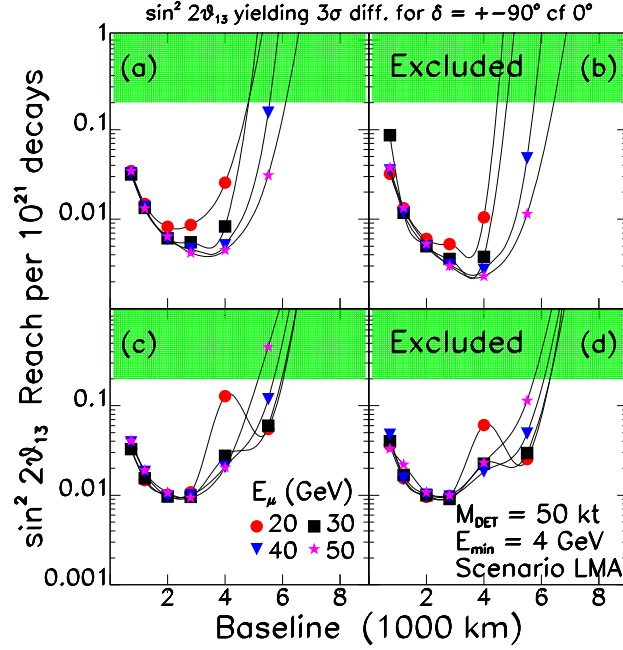


Figure 49: Reach in $\sin^2 2\theta_{13}$ that yields a 3σ discrimination between (a) $\delta = 0$ and $\pi/2$ with $\delta m_{32}^2 > 0$, (b) $\delta = 0$ and $\pi/2$ with $\delta m_{32}^2 < 0$, (c) $\delta = 0$ and $-\pi/2$ with $\delta m_{32}^2 > 0$, and (d) $\delta = 0$ and $-\pi/2$ with $\delta m_{32}^2 < 0$. The discrimination is based on a comparison of wrong-sign muon CC event rates in a 50 kt detector when 10^{21} positive and negative muons alternately decay in the neutrino factory. The reach is shown versus baseline for four storage ring energies. The oscillation parameters correspond to the LMA scenario IA1. Results are from Ref. 51.

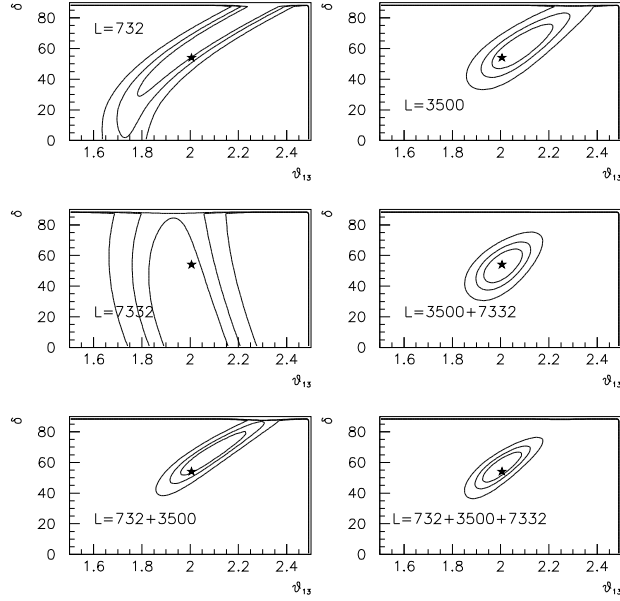


Figure 50: Fit results in the CP phase δ versus θ_{13} plane for a LMA scenario with $\delta m_{21}^2 = 1 \times 10^{-4} \text{ eV}^2/c^4$. The 68.5, 90, and 99% CL contours are shown for a 40 kt detector a distance L km downstream of a 50 GeV neutrino factory in which there are $10^{21}\mu^+$ and $10^{21}\mu^-$ decays. Results are from Ref. 59.

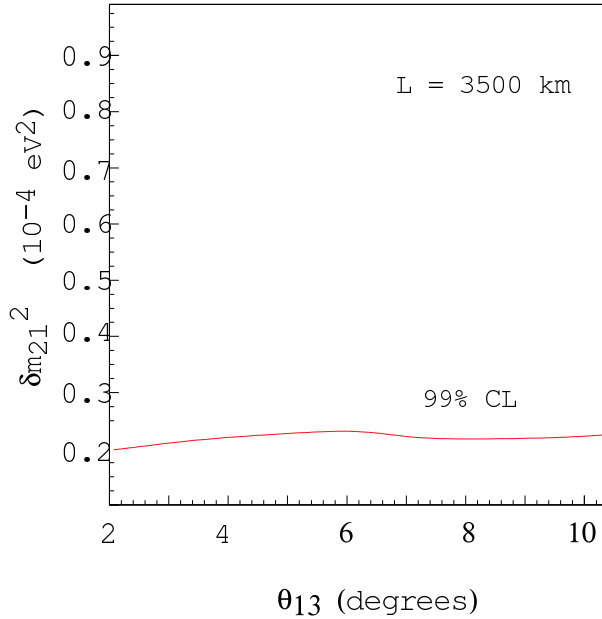


Figure 51: The lowest value of δm_{21}^2 , shown as a function of θ_{13} , for which the maximal CP phase $\delta = \pi/2$ can be distinguished from a vanishing phase in a LMA oscillation scenario. The curve corresponds to a 40 kt detector 3500 km downstream of a 50 GeV neutrino factory in which there are $10^{21}\mu^+$ and $10^{21}\mu^-$ decays. Results are from Ref. 59.

3000 km (for $\delta m_{32}^2 = 3.5 \times 10^{-3} \text{ eV}^2/\text{c}^4$) the $\sin^2 2\theta_{13}$ reach is approximately 10^{-2} , an order of magnitude below the current experimental bound. Thus, in a LMA scenario, CP violation in the lepton sector might be measurable at a neutrino factory providing $O(10^{21})$ muon decays.

As an example, consider a 40 kt Fe-scintillator detector downstream of a 50 GeV neutrino factory providing $10^{21}\mu^+$ decays followed by $10^{21}\mu^-$ decays in the beam-forming straight section [59]. The results of fits to the simulated wrong-sign muon event distributions, with δ and $\sin^2 2\theta_{13}$ left as free parameters, are shown in Fig. 50 for various baselines, with the sub-leading scale $\delta m_{21}^2 = 1 \times 10^{-4} \text{ eV}^2/\text{c}^4$. The analysis includes the detector resolutions, reasonable event selection criteria, and backgrounds. As might be expected from Fig. 48 at $L = 7332 \text{ km}$ there is little sensitivity to δ , and at the “short” baseline $L = 732 \text{ km}$ the fit has difficulty untangling δ from $\sin^2 2\theta_{13}$. However, at a baseline of $L = 3500 \text{ km}$ for the example shown δ and $\sin^2 2\theta_{13}$ can be determined with precisions of respectively about 15° and a few percent. Note that a combination of baselines can yield a modest improvement in the precision of the measurement. The sensitivity to CP violation decreases with decreasing δm_{21}^2 . Figure 51 shows as a function of $\sin^2 2\theta_{13}$ the lowest value of δm_{21}^2 for which the maximal CP phase $\delta = \pi/2$ can be distinguished from a vanishing phase at $L = 3500 \text{ km}$. This limiting δm_{21}^2 is below the current central value for the LMA parameter space suggested by solar neutrino deficit, and is about $2 \times 10^{-5} \text{ eV}^2/\text{c}^4$, independent of $\sin^2 2\theta_{13}$.

Finally we note that the sensitivity of short and medium baseline experiments to CP violation in a three-active plus one sterile neutrino scenario has been considered in Ref. [64]. They concluded that a 1 kt detector and a 100 km baseline could provide a clean test of CP violation, particularly in the $\tau - \text{lepton}$ appearance channel.

3.6 Summary

The oscillation physics that could be pursued at a neutrino factory is compelling. In particular, experiments at a neutrino factory would be able to simultaneously measure, or put stringent limits on, all of the appearance modes $\nu_e \rightarrow \nu_\tau$, $\nu_e \rightarrow \nu_\mu$, and $\nu_\mu \rightarrow \nu_\tau$. Comparing the sum of the appearance modes with the disappearance measurements would provide a unique basic check of candidate oscillation scenarios that cannot be made with a conventional neutrino beam. In addition, for all of the specific oscillation scenarios we have studied, the ν_e component in the beam can be exploited to enable crucial physics questions to be addressed. These include (i) the pattern of neutrino masses (sign of δm^2) and a quantitative test of the MSW effect, (ii) the precise determination of (or stringent limits on) all of the leading oscillation parameters, which in a three-flavor mixing scenario would be $\sin^2 2\theta_{13}$, $\sin^2 2\theta_{23}$, and δm_{32}^2 , and (iii) the observation of, or stringent limits on, CP violation in the lepton sector.

To be more quantitative in assessing the beam energy, intensity, and baseline

required to accomplish a given set of physics goals it is necessary to consider two very different experimental possibilities: (a) the LSND oscillation results are not confirmed by the MiniBooNE experiment, or (b) the LSND results are confirmed.

- (a) LSND not confirmed. Fairly extensive neutrino factory studies have been made within the framework of three-flavor oscillation scenarios in which there is one “large” δm^2 scale identified with the atmospheric neutrino deficit results, and one small δm^2 identified with the solar neutrino deficit results. A summary of the energy dependent beam intensities required to cross a variety of “thresholds of interest” is provided by Fig. 29. A 20 GeV neutrino factory providing 10^{19} muon decays per year is a good candidate “entry-level” facility which would enable either (i) the first observation of $\nu_e \rightarrow \nu_\mu$ oscillations, the first direct measurement of matter effects, and a determination of the sign of δm_{32}^2 and hence the pattern of neutrino masses, or (ii) a very stringent limit on $\sin^2 2\theta_{13}$ and a first comparison of the sum of all appearance modes with the disappearance measurements. The optimum baselines for this entry-level physics program appears to be of the order of 3000 km or greater, for which matter effects are substantial. Longer baselines also favor the precise determination of $\sin^2 2\theta_{13}$. A 20 GeV neutrino factory providing 10^{20} muon decays per year is a good candidate upgraded neutrino factory (or alternatively a higher energy facility providing a few $\times 10^{19}$ decays per year). This would enable the first observation of, or meaningful limits on, $\nu_e \rightarrow \nu_\tau$ oscillations, and precision measurements of the leading oscillation parameters. In the more distant future, a candidate for a second (third ?) generation neutrino factory might be a facility that provides $O(10^{21})$ decays per year and enables the measurement of, or stringent limits on, CP violation in the lepton sector.
- (b) LSND confirmed. Less extensive studies have been made for the class of scenarios that become of interest if the LSND oscillation results are confirmed. However, in the scenarios we have looked at (IB1 and IC1) we find that the $\nu_e \rightarrow \nu_\tau$ rate is sensitive to the oscillation parameters and can be substantial. With a large leading δm^2 scale medium baselines (for example a few $\times 10$ km) are of interest, and the neutrino factory intensity required to effectively exploit the ν_e beam component might be quite modest ($< 10^{19}$ decays per year).

The neutrino factory oscillation physics study we have pursued goes beyond previous studies. In particular we have explored the physics capabilities as a function of the muon beam energy and intensity, and the baseline. Based on the representative oscillation scenarios and parameter sets defined for the study, it would appear that a 20 GeV neutrino factory providing $O(10^{19})$ decays per year would be a viable entry-level facility for experiments at baselines of ~ 3000 km or greater. There are still some basic open questions that deserve further study: (1) We have sampled, but not fully explored, the beam energy and intensity required

to explore the scenarios that become relevant if the LSND oscillation results are confirmed. (2) Possible technologies for a very massive neutrino factory detector have been considered, but these considerations deserve to be pursued further. The chosen detector technology will determine whether it is necessary to go deep underground. (3) We have developed tools that can explore the utility of having polarized muon beams. The physics payoff with polarization is a detailed issue. It deserves to be studied in the coming months.

Based on our study, we believe that a neutrino factory in 5–10 years from now would be the right tool at the right time.

4 Non–Oscillation Physics

Due to the theoretically clean nature of weak interactions, conventional neutrino scattering experiments have always provided precise measurements of fundamental parameters. These include: a crucial role in the extraction of parton distribution functions, measurements of the Weinberg angle[65], and the strong coupling constant [66] α_s , which are competitive with any other methods. Perhaps because of this success, we forget how crude existing neutrino experiments are. The high statistics experiments such as CDHSW[67] and CCFR/NuTeV[66, 65], in order to obtain samples of more than 10^5 events, rely on coarsely segmented massive iron/scintillator calorimeters weighing close to 1000 tons. Measurements on proton targets and detailed studies of the final state have been confined to very low statistics bubble chamber experiments. As a result we have virtually no precise measurements of neutrino-proton scattering and no measurements on polarized targets which could offer new insights into the spin structure of the nucleon.

The advent of a neutrino factory, with neutrino fluxes of 10^{20} /year instead of the 10^{15-16} at existing facilities would open a new era in conventional neutrino physics. We would be able to use low mass targets and high resolution detection technologies and still achieve better statistical power than present-day experiments. For example a 50 GeV muon storage ring at the above rate would produce around 18 M neutrino charge-current interactions per year in a 10 kg hydrogen target. This is 5-10 times the statistics of the CCFR and NuTeV experiments with 600 ton detectors. Better understanding of neutrino fluxes from the decay of monochromatic muons will also reduce many of the dominant systematic errors.

In this study we have concentrated on measurements that are only possible with higher fluxes rather than repeating older measurements with thousands of times the statistics. As a result, the statistical errors shown are often not negligible, but without the high flux at a neutrino factory the measurements themselves would be impossible.

Outline

Due to the breadth of the field we are unable to give a complete survey and instead highlight a few of the areas where the high flux beam at a neutrino factory allows new measurements:

- A description of a low mass target/detector and typical rates in such a detector.
- Nucleon deep inelastic scattering measurements and a proposed detector design.
- Neutrino cross section measurements, a topic of great interest to the nuclear physics community and also needed to understand normalization at a far neutrino oscillation detector.
- Spin structure functions, which have never been measured in neutrino beams.
- The potential of the neutrino factory as a clean source of single tagged charm mesons and baryons.
- Electroweak measurements in both the hadronic and purely leptonic sectors.
- Use of the very clean initial state to search for exotic interactions.
- Searches for anomalous neutrino interactions with electromagnetic fields.

4.1 Possible detector configurations and statistics

For studies of charged current deep-inelastic scattering on proton targets, the optimal detector system is probably a target followed by precision magnetic tracking systems, an electromagnetic calorimeter and a muon detection system. Such detectors have been used in muon scattering experiments at CERN and FNAL and in the new generation neutrino scattering experiments CHORUS [68] and NOMAD[58]. A low mass target followed by tracking and electromagnetic calorimetry makes the electron anti-neutrinos in the beam a source of additional statistics rather than background, except in the case of neutral current studies.

The target itself should be thin enough that particles produced within it have a small probability of interacting before they reach the tracking systems. In this study we considered liquid hydrogen and deuterium targets – both polarized and unpolarized – and heavier solid nuclear targets. The hydrogen and deuterium targets are 1m long while the polarized target is 50 cm long. All targets are 20 cm in radius, to fit the central beam spot at 50 GeV. For lower beam energies the beam spot grows in size as $\sim 1/E$. Nuclear targets are scaled so that the

Table 10: Charged current muon-neutrino scattering rates in a small target located near a muon storage ring. Rates are per 10^{20} muon decays. The detector is located $(1 \times E_\mu, \text{ GeV})$ meters away from the ring to assure that primary muons have ranged out before the detector.

Machine	Target	Thickness,cm	Events
50 GeV neutrino factory	Liquid H ₂	100	12.1M
	Liquid D ₂	100	29.0M
	solid HD	50	9.3M
	C	5.3	20.7M
	Si	6.3	25.4M
	Fe	2.3	31.6M
	Sn	3.1	39.1M
	W	1.3	44.3M
	Pb	2.4	46.5M
CCFR/NuTeV	Fe	600	$\sim 2\text{M}$

interaction length in the material is constant at 14%. The charged current muon neutrino interaction rates are summarized in table 10.

The numerical estimates in this study use, unless otherwise noted, 10^{20} 50 GeV muon decays in a 600 m straight section.

These are the total event rates for charged current muon-neutrino scattering. The anti-neutrino rates are half as large. Kinematic cuts reduce the statistics by less than a factor of two. We have only considered muon-neutrino charge current scattering for structure function measurements, although for such thin targets, electron neutrino scatters should also be reconstructable with high precision.

4.2 Neutrino Scattering Kinematics

The kinematic variables for neutrino deep inelastic scattering are illustrated in figure 52:

$$\mathbf{q} = \mathbf{k}_\nu - \mathbf{k}_\ell, \quad Q^2 = -\mathbf{q}^2 = 2E_\ell E_\nu - m_\ell^2 - 2E_\nu p_\ell \cos \theta_{lab}, \quad (58)$$

$$\nu = (\mathbf{p}_p \mathbf{q})/M \simeq E_\ell - E'_\ell, \quad (59)$$

$$x = Q^2/2M\nu, \quad (60)$$

$$y = M\nu/(\mathbf{k}_\nu \mathbf{p}_p) = (1 + \cos \theta_{CM})/2 \approx \nu/E_\ell, \quad (61)$$

$$W^2 = 2M\nu + M^2 - Q^2, \quad (62)$$

where the \mathbf{k} are the neutrino and final state four vectors, \mathbf{p}_p is the proton four-vector, M is the target nucleon mass, E_ν is the incoming neutrino energy E_ℓ, p_ℓ are the outgoing lepton energy and momentum θ_{lab} is the lepton angle with respect to the incoming beam. \mathbf{q} is the four-momentum transfer to the target, ν

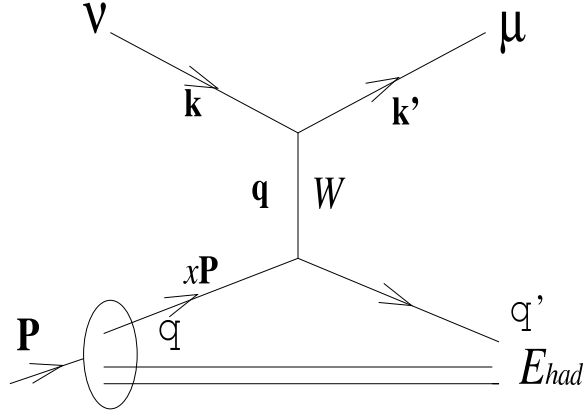


Figure 52: Kinematics of neutrino scattering in the parton model. The energy-momentum transfer from the leptons to the proton is \mathbf{p}_q and the fraction of the proton momentum carried by the struck quark is approximately x .

is the energy transfer, x is the Bjorken x variable, y is the scaled energy transfer and W^2 is the invariant mass of the final state hadronic system squared.

Fig. 53 shows the kinematic region for a neutrino factory as compared to other deep-inelastic scattering experiments.

For $Q \ll E$ and $s \ll M_W$ the unpolarized neutrino (anti-neutrino) scattering cross section is:

$$\begin{aligned} \frac{d\sigma^{\nu(\bar{\nu})}}{dxdy} = & \frac{G_F^2 M E_\nu}{2\pi} \left[[F_2^{\nu(\bar{\nu})}(x, Q^2) \pm x F_3^{\nu(\bar{\nu})}(x, Q^2)] + \right. \\ & [F_2^{\nu(\bar{\nu})}(x, Q^2) \mp x F_3^{\nu(\bar{\nu})}(x, Q^2)] (1-y)^2 - \\ & \left. 2y^2 F_L(x, Q^2) \right], \end{aligned} \quad (63)$$

where the F_i are Structure Functions. $F_L = F_2 - 2xF_1$ is a purely longitudinal structure function. The xF_3 contribution changes sign for anti-neutrino scattering. There are additional structure functions F_4 and F_5 which are suppressed by factors of the lepton mass over the proton mass squared. For ν_τ and ν_μ scattering at very low energies, these terms can become quite important.

If the target is longitudinally polarized with respect to the neutrino polarization, then the cross section difference[80]:

$$\begin{aligned} \frac{d^2(\sigma_{\Rightarrow}^{\leftarrow} - \sigma_{\Leftarrow}^{\leftarrow})^{\nu(\bar{\nu})}}{dxdy} = & \frac{G_F^2 M E_\nu}{\pi} \left\{ \pm y \left(1 - \frac{y}{2} - \frac{xyM}{2E} \right) x g_1 \mp \frac{x^2 y M}{E} g_2 + \right. \\ & \left. y^2 x \left(1 + \frac{xM}{E} \right) g_3 + \left(1 - y - \frac{xyM}{2E} \right) \left[\left(1 + \frac{xM}{E} \right) g_4 + g_5 \right] \right\}, \end{aligned} \quad (64)$$

is described by two parity conserving Polarized Structure Functions g_1 and g_2 , and by three parity violating Polarized Structure Functions g_3, g_4 and g_5 . However, if the nucleon is transversely polarized, the cross section difference is:

Deep Inelastic Scattering Experiments

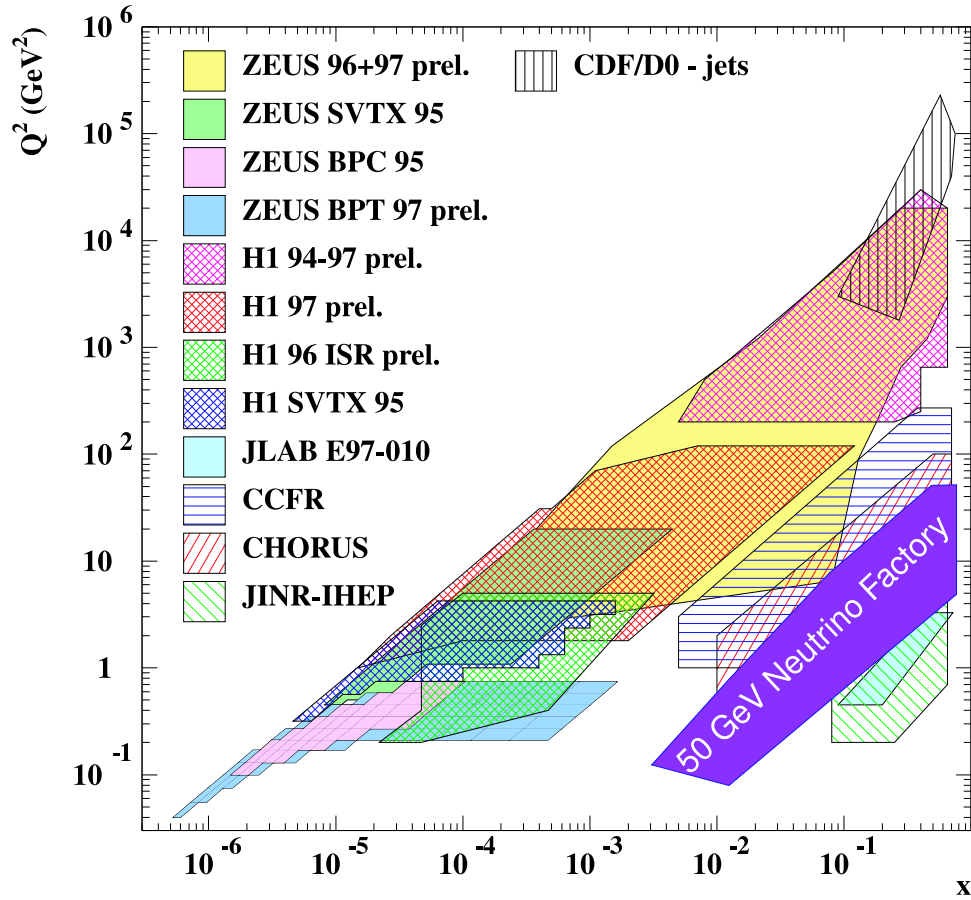


Figure 53: Comparison of kinematic ranges for present DIS experiments with a 50 GeV Neutrino factory.

$$\frac{d^2(\sigma_{\uparrow}^{\leftarrow} - \sigma_{\downarrow}^{\leftarrow})^{\nu(\bar{\nu})}}{dxdy} = \frac{G_F^2 M}{16\pi^2} \sqrt{xyM[2(1-y)E - xyM]} \left\{ \mp 2xy\left(\frac{y}{2}g_1 + g_2\right) \right. \\ \left. + xy^2g_3 + \left(1 - y - \frac{xyM}{2E}\right)g_4 - \frac{y}{2}g_5 \right\}. \quad (65)$$

The transverse cross section is suppressed by M/Q with respect to the longitudinal cross section.

4.3 Total cross section Measurements

A measurement of the total CC neutrino scattering cross section is both of intrinsic interest and essential to precision measurements at a neutrino factory. We currently know the cross sections for neutrino scattering at the 2-3% level [14] at energies above 30 GeV but at energies approaching the resonance region (2 GeV) the uncertainty increases considerably. Because muon decay is so well-understood, the flux and hence the total cross section should be measureable across the full energy spectrum to the 1% level.

The yield Y of neutrino interactions observed in any detector can be written as:

$$Y = n_0(E, r)\sigma(E)\epsilon(E, r)N$$

where n_0 is the flux of incident neutrinos as a function of the neutrino energy E and distance from the center of the detector, r . σ is the cross section, $\epsilon(E, r)$ is the detector efficiency, and N is the number of target particles.

For a far detector, $n_0(E, r) \sim n_0(E)$ is mainly determined by the beam divergence and the muon decay kinematics and can probably be estimated from the machine parameters and decay model with precisions at the 1% level. For a near detector, $n_0(E, r)$ depends mainly on the muon decay kinematics and geometry, with contributions from beam size and divergence at the few percent level.

Without a measurement of the absolute number of neutrinos, the best way to determine the flux is to normalize to a very well-understood process. By comparing the yield of the normalization process and the total event rate, one then has a measurement of the total cross section. Inverse muon decay ($\nu_\mu + e^- \rightarrow \mu^- + \nu_e$ and $\bar{\nu}_\mu + e^- \rightarrow \mu^- + \bar{\nu}_\mu$) provides a clean channel for mapping the beam flux $n_0(E, r)$ at a near detector and for normalizing the total cross section measurement. It has the limitation of an energy threshold of ~ 11 GeV and no corresponding channels for the opposite sign beam. Quasi-elastic scattering is an additional normalization mode since it has a much lower energy threshold and occurs for beams made with muons of either charge. Finally, scattering from atomic electrons is suppressed by a factor of order m_e/m_p relative to the normal

neutrino nucleon interactions, but still yields an event rate of $\simeq 10^4$ interactions per gr/cm^2 for 10^{20} 50 GeV μ^- decays.

If the ratio of flux shapes at far and near detectors can be understood at the 1% level, then measurements of $n_0(E, r)\sigma(E)$ at a near detector can be used to precisely predict the number of events expected in the absence of oscillations at a far detector. Such precise flux measurements are also important for the suite of measurements described in the remainder of this chapter.

4.4 Structure function measurements

In principle, the structure functions can be extracted by fits to the y dependence of the cross section. To date this has proven very difficult as the data must be binned in x , y and Q^2 and no experiment has had sufficient statistics to perform such an analysis with high accuracy[67, 70].

Instead, high statistics experiments[14] such as CHARMII, CCFR and CDHSW have relied on massive targets (Iron, Calcium) which are approximately iso-scalar and have combined neutrino and anti-neutrino information in order to extract average structure functions. The structure functions averages have naive parton model interpretations:

$$\overline{F}_2^N(x, Q^2) \simeq \sum(xq(x, Q^2) + x\overline{q}(x, Q^2)), \quad (66)$$

$$\overline{F}_3^N(x, Q^2) \simeq \sum(xq(x, Q^2) - x\overline{q}(x, Q^2)), \quad (67)$$

where $\overline{F}_2(x, Q^2)$ and $\overline{F}_3(x, Q^2)$ are the average of neutrino and antineutrino structure functions measured on a target which is an average of neutron and proton and $q(x, Q^2)$ and $\overline{q}(x, Q^2)$ represent the parton distribution functions or total probability of finding a quark or antiquark in the proton:

$$q(x, Q^2) = u(x, Q^2) + d(x, Q^2) + s(x, Q^2) + c(x, Q^2) \dots \quad (68)$$

$$\overline{q}(x, Q^2) = \overline{u}(x, Q^2) + \overline{d}(x, Q^2) + \overline{s}(x, Q^2) + \overline{c}(x, Q^2) \dots \quad (69)$$

Given the expectation of 12 M (24 M) events/year in a 1 m hydrogen (deuterium) target at a 50 GeV muon storage ring we can do a complete analysis of each channel $\nu p, \nu n, \overline{\nu} p, \overline{\nu} n$ without averaging. Such an analysis allows a unique extraction of individual quark flavor parton distribution functions.

For example, in the case of νp scattering, a W^+ is exchanged and the reaction is only sensitive to negatively charged quarks. Due to the helicity dependence of the interaction only left-handed d type and right handed \overline{u} quarks will be involved.

The leading order parton model cross section is simply

$$\frac{d\sigma^{\nu p}}{dx dy} \simeq \frac{4G_F^2 M E_\nu}{\pi} x[(d_L(x, Q^2) + s_L(x, Q^2)) + (\bar{u}_R(x, Q^2) + \quad (70)$$

$$\bar{c}_R(x, Q^2))(1 - y)^2], \quad (71)$$

and the different contributions can be extracted from the y dependence of this cross section and the corresponding anti-neutrino cross section. The relative s and d quark contributions can be measured in charm production.

For an unpolarized target $q_L(x) = q_R(x) = \frac{1}{2}q(x)$. For a polarized quark $q_L(x) = \frac{1}{2}(q(x) + \delta q(x))$ and $q_R(x) = \frac{1}{2}(q(x) - \delta q(x))$ where $\delta q(x)$ is the degree to which the quark spin is aligned with the proton spin². Thus a $\sigma_{\nu p}$ measurement on an unpolarized target can determine $d + s$ and $\bar{u} + \bar{c}$ by averaging over the proton spin, while by measuring the polarization asymmetry one can measure $\delta d + \delta s$ and $\delta \bar{u} + \delta \bar{c}$.

Scattering on neutrons can be related to scattering on protons by an isospin transformation which exchanges u and d quarks and anti-quarks. Differences of neutron and proton cross sections can then be used to cancel the u and d components leaving observables sensitive only to s and c distributions.

4.5 Perturbative QCD

Neutrinos do not couple directly to gluons. As a result, QCD effects appear in neutrino scattering as higher order corrections to the leading order parton model. Measurements of the Q^2 dependence of neutrino cross sections are some of the most sensitive measurements of the strong coupling constant α_s [66] and information on the gluon distribution can be obtained from its coupling to the structure functions via the DGLAP[69] evolution equations. The neutrino structure functions can be divided into two types, singlet and non-singlet, depending on their sensitivity to gluon effects in their evolution.

The structure functions $2xF_1$, F_2 and g_1 are singlet functions and are directly coupled to the gluon distribution via the evolution equations. The structure functions $x\bar{F}_3 + xF_3$, $2xg_3$, g_4 and g_5 averaged over neutrino and anti-neutrino are non-singlet functions and their evolution is independent of the gluon distribution. The combination $F_2^p - F_2^n$ also cancels the gluon contributions and is thus non-singlet in nature.

To date, extractions of α_s from non-singlet distributions have been statistics limited and strongly affected by flux uncertainties. The additional factor of 10-100 in statistics and improved flux understanding at a neutrino factory should allow vastly improved measurements of strong interaction parameters in this very clean channel.

² The traditional Δq spin distributions from electron and muon scattering measure the sum $\Delta q = \delta q + \delta \bar{q}$ as photon probes cannot tell quarks and anti-quarks apart.

Once the quark distributions and strong interaction effects have been thoroughly studied in the non-singlet structure function, that knowledge can be used for improved constraints on the gluon distributions via the evolution of the singlet structure functions.

4.6 Nuclear Effects

Experiments at a neutrino factory of nuclear effects in the distribution of partons within nuclei relative to protons and deuterons are of interest to both the nuclear and high energy communities. These nuclear effects have been studied extensively using muon and electron beams but have only been observed in low-statistics bubble chamber experiments[72] using neutrinos. If we consider the behavior of the structure functions $F_2(x, Q^2)$ measured on a nucleus (A) to $F_2(x, Q^2)$ measured on a nucleon as a function of x we pass through four distinct regions in going from $x = 0$ to $x = 1.0$:

Shadowing Region $x < 0.1$

In the shadowing region ($x < 0.1$) there are several effects that should yield a different ratio $R_A \equiv F_{2(A)}/F_{2(N)}$ when using neutrinos as the probe. In the limit $Q^2 \rightarrow 0$, the vector current is conserved and goes to 0. The axial-vector part of the weak current is only partially conserved (PCAC) and $F_2(x, Q^2) \rightarrow$ a non-zero constant as $Q^2 \rightarrow 0$. According to the Adler theorem [73] the cross section of $\nu_\mu - N$ can be related to the cross section for $\pi - N$ at $Q^2 = 0$. This relation can be studied in both proton and in heavy nuclei.

As we increase Q^2 from 0 but keep it under 10 GeV² in the shadowing region we enter the region of vector meson dominance (VMD) in $\mu/e - A$ scattering. The physics concept of VMD is the dissociation of the virtual boson into a quark/antiquark pair, one of which interacts strongly with the ‘surface’ nucleons of the target nucleus (thus the ‘surface’ nucleons ‘shadow’ interior nucleons). In $\nu - A$ scattering there is an additional contribution from axial-vector mesons that is not present in $\mu/e - A$ scattering. Boros et al. [74] predict that the resulting shadowing effects in $\nu - A$ scattering will be roughly 1/2 that measured in $\mu/e - A$ scattering. In a more quantitative analysis, Kulagin [75] used a non-perturbative parton model to predict shadowing effects in $\nu - A$ scattering. At 5 GeV² he predicts equal or slightly more shadowing in $\nu - A$ scattering than in $\mu/e - A$ scattering. He also attempts to determine quark flavor dependence of shadowing effects by separately predicting the shadowing observed in $F_2(x, Q^2)$ (sum of all quarks) and $xF_3(x, Q^2)$ (valence quarks only). Fig. 54 shows the results of a run with 14M events/target using predictions of Kulagin’s model for F_2 and xF_3 . As can be seen, the predicted difference between the shadowing on sea and valence quarks is clearly visible down to $x \simeq 0.03$.

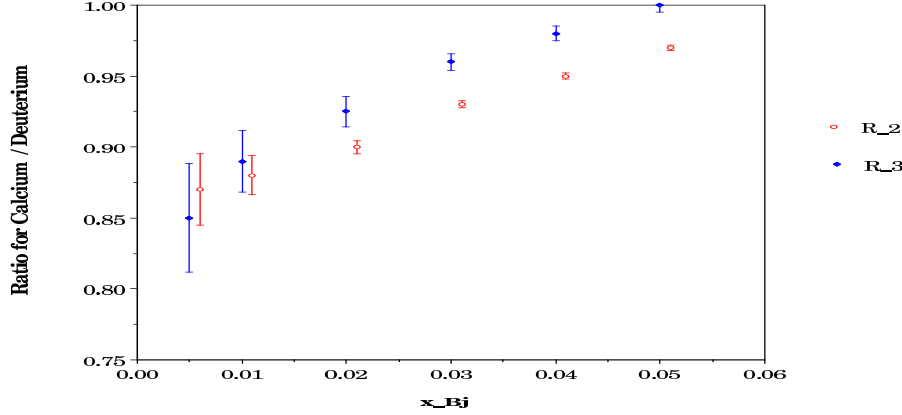


Figure 54: $R_{Ca:D_2}$ for both F_2 and xF_3 as measured with 14 M events on each target.

Anti-shadowing Region ($0.1 < x < 0.2$)

Drell-Yan experiments have also measured nuclear effects. Their results are quite similar to DIS experiments in the shadowing region. However, in the anti-shadowing region, where R_A makes a brief but statistically significant excursion above 1.0 in DIS, Drell-Yan experiments see no effect. This could be an indication of difference in nuclear effects between valence and sea quarks. Eskola et al [76] quantified this difference by using a leading order/leading twist DGLAP model. Taking the work of Kulagin and Eskola together implies that nuclear effects in $xF_3(x, Q^2)$ should be quite dramatic with more shadowing than $F_2(x, Q^2)$ at lower x and then R_A rising fairly rapidly to yield significant antishadowing around $x = 0.1$. With 14 M events on each target we should be able to measure antishadowing effects and the difference between shadowing effects in $F_2(x, Q^2)$ and $xF_3(x, Q^2)$ to the 6σ statistical level.

EMC-effect Region ($0.2 < x < 0.7$)

Determination of individual quark contributions to the EMC-effect will be challenging since the participation of sea quarks, and thus the difference between $F_2(x, Q^2)$ and $xF_3(x, Q^2)$, shrinks rapidly with increasing x . However, Eskola's predictions for this region indicate that the contribution of \bar{u} and \bar{d} to $R_A^{(2)}$ in the Q^2 range of this experiment remains well below unity so that the quantity $(R_A^{(2)} - R_A^{(3)})$ should remain negative well into the EMC-effect region.

Behavior of $F_2(x, Q^2)$ as $x \rightarrow 1$ in a Nuclear Environment

When working in the fermi-motion region it has been shown that we need to add more than the Fermi gas model to a simple nucleon to reproduce the behavior

of $F_2(x, Q^2)$ at high x . Few-nucleon-correlation models and multi-quark cluster models allow quarks to have a higher momentum which translates into a high- x tail. In this region $F_2(x, Q^2)$ should behave as e^{-ax} . There have been analyses of this behavior in similar kinematic domains using $\mu + \text{C}$ and $\nu + \text{Fe}$ interactions. The BCDMS [77] muon experiment finds $a = 16.5 \pm 0.5$ while the CCFR[78] neutrino experiment finds $a = 8.3 \pm 0.7 \pm 0.7$ (systematic). Is the value of a dependent on the nucleus? One would expect any few nucleon correlation or multi-quark effects to have already saturated by Carbon. Is a dependent on the probe?

Summary

There is a rich program of studying nuclear effects with a neutrino probe in a high statistics neutrino factory experiment. The effects could be measured to statistically significant accuracy in a 2 year exposure to the beam in the near-detector experiment described above. The data gathered would allow separate measurements of the effects on valence quarks and sea quarks across much of the x range.

The nuclear community would surely be excited by this valuable tool for nuclear research at a neutrino factory.

4.7 Spin Structure

An intense neutrino beam at a neutrino factory would create significant event rates in compact detectors. This opens the possibility of using a polarized target, and hence a completely new class of neutrino measurements becomes possible. At present we know very little about the spin structure functions $g_1^\nu - g_5^\nu$ introduced in Equations 65 and 66. In particular, the parity violating functions have only been explored via weak-interference measurements of proton form factors by the SAMPLE collaboration [79] with low statistics. A neutrino factory would allow direct high-statistics measurements of all of these structure functions and should be able to answer many unresolved questions about the spin structure of the nucleon.

Formalism

The nucleon spin ($\frac{1}{2}$) can be decomposed in terms of quark and gluon contributions:

$$\frac{1}{2} = \frac{1}{2}\Delta\Sigma + \Delta g + L_q + L_g, \quad (72)$$

where $\Delta\Sigma \equiv \Delta u + \Delta d + \Delta s + \Delta c$ is the net quark helicity and Δg is the net gluon helicity along the nucleon spin direction, while L_i are their relative orbital angular momentum. (We use Δq as a shorthand for the integral $\int \Delta q(x) dx$.)

To date, the only experiments which have studied the spin structure of the nucleon are low energy charged lepton polarized deep-inelastic scattering experiments (PDIS) where only the parity conserving polarized structure functions g_1^l and g_2^l can be measured.

g_1^l can be written in the leading order parton model as a sum of a nonsinglet and singlet part[81]:

$$g_1^l(x, Q^2) = g_{1,NS}^l(x, Q^2) + g_{1,S}^l(x, Q^2) \quad (73)$$

$$= \frac{1}{2} \sum (e_i^2 - \langle e^2 \rangle) \Delta q_i(x, Q^2) + \frac{1}{2} \sum \langle e^2 \rangle \Delta q_i(x, Q^2) \quad (74)$$

The first non-singlet term evolves independently of the gluonic spin contribution while the second is coupled to, and thus depends on, the gluon spin contribution Δg .

The integral structure functions have the following relation to the parton spin contributions:

$$\begin{aligned} \Gamma_1^\ell(Q^2) &= \int dx g_1^l(x, Q^2) \\ &= \Gamma_{1,NS}^\ell(Q^2) + \Gamma_{1,S}^\ell(Q^2) \end{aligned} \quad (75)$$

$$\Gamma_1^{\ell p}(Q^2) = \frac{C_1^{NS}(Q^2)}{6} \left[\frac{1}{2} a_3 + \frac{1}{6} a_8 \right] + \frac{C_1^S}{9} a_0 \quad (76)$$

$$\Gamma_1^{\ell n}(Q^2) = \frac{C_1^{NS}(Q^2)}{6} \left[-\frac{1}{2} a_3 + \frac{1}{6} a_8 \right] + \frac{C_1^S}{9} a_0 \quad (77)$$

Where the C_1 are coefficient functions and the axial charge matrix elements

$$a_3 \equiv F + D \simeq \Delta u - \Delta d \quad (78)$$

$$a_8 \equiv 3F - D \simeq \Delta u + \Delta d - 2\Delta s \quad (79)$$

$$a_0 \equiv \Delta u + \Delta d + \Delta s = \Delta \Sigma \quad (80)$$

$$(81)$$

can be expressed in terms of coupling constants F and D obtained from neutron and hyperon beta decays [83]. Because the interaction between Δg and $\Delta \Sigma$ in the evolution of the singlet (a_0) component, interpretation of Γ_1^ℓ in terms of the quark spin is problematic. Fig. 55 shows NLO QCD predictions for $\Delta \Sigma$ as a function of Δg . The data in the NLO fit are from [82].

Neutrino beams introduce both additional parity violating spin structure functions g_3, g_4 and g_5 and new combinations based on sums and differences of neutrino and anti-neutrino scattering.

For example[80] the sums

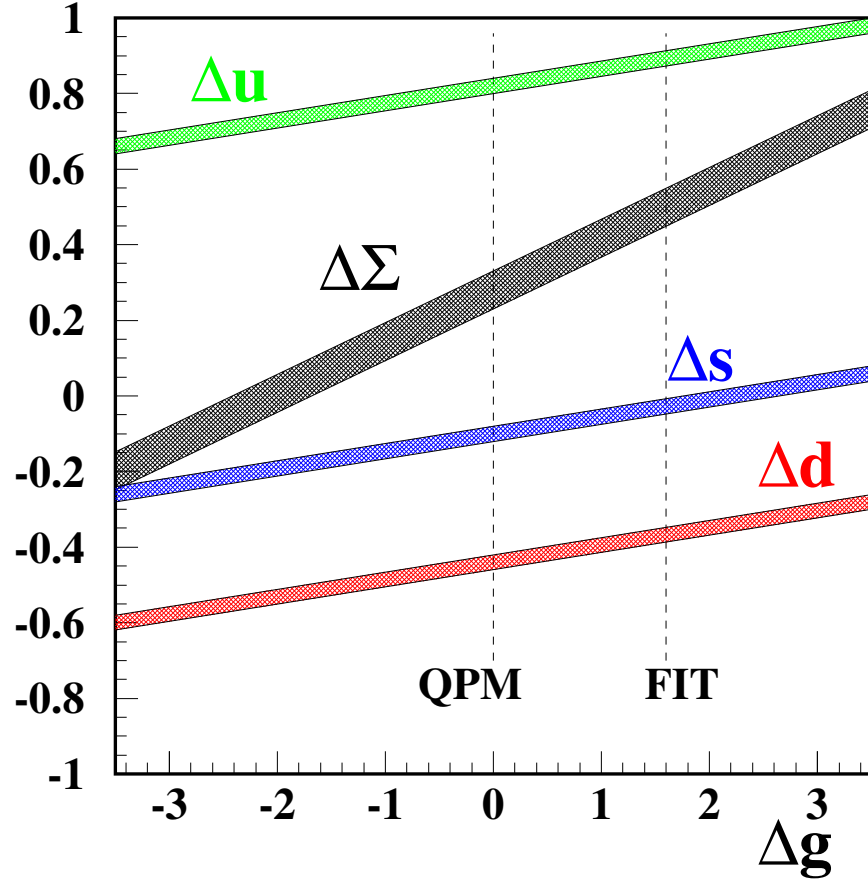


Figure 55: Model dependent decomposition of singlet term into quarks and gluon based on PDIS data, $a_0 \rightarrow \Delta q - 3\frac{\alpha_s}{2\pi}\Delta g$. The QPM expectation and the results from a NLO fit of the Q^2 evolution of most of the available data on g_1^l are also shown. From the fit it was found that $\Delta g = 1.6 \pm 0.3 \pm 1.0$, where the error is dominated by theoretical uncertainties.

$$\Gamma_1^{\nu p} + \Gamma_1^{\bar{\nu} p} = \int dx [g_1^{\nu p}(x, Q^2) + g_1^{\bar{\nu} p}(x, Q^2)] \quad (82)$$

$$\Gamma_1^{\nu n} + \Gamma_1^{\bar{\nu} n} = \int dx [g_1^{\nu n}(x, Q^2) + g_1^{\bar{\nu} n}(x, Q^2)] \quad (83)$$

for both proton and neutron targets are only sensitive to the singlet a_0 term and no input from beta decay is necessary.

The parton model interpretation of these new structure functions is:

$$g_{4+5}^{\nu p}(x, Q^2) = 2xg_3^{\nu p}(x, Q^2) \quad (84)$$

$$= -x[\delta d(x, Q^2) + \delta s(x, Q^2) - \delta \bar{u}(x, Q^2) - \delta \bar{c}(x, Q^2)],$$

$$g_{4+5}^{\bar{\nu} p}(x, Q^2) = 2xg_3^{\bar{\nu} p}(x, Q^2) \quad (85)$$

$$= -x[\delta u(x, Q^2) + \delta c(x, Q^2) - \delta \bar{d}(x, Q^2) - \delta \bar{s}(x, Q^2)].$$

On a deuterium target, the u and d contributions to g_3 can be cancelled leading to a direct measurement of the strange sea contribution to the nucleon spin [80]

$$g_3^{\nu(np)} - g_3^{\bar{\nu}(np)} = -2(\delta s + \delta \bar{s}) + 2(\delta c + \delta \bar{c}), \quad (86)$$

which can also be studied via polarization asymmetries in charm production from strange quarks[84].

The structure functions xg_3, g_4 and g_5 , like F_3 are non-singlet functions in which contribution from gluons cancel. Comparison of the non-singlet functions with the single functions g_1 and F_2 is an indirect way of measuring the contribution of gluons Δg .

Experimental Setup

A promising target technology is the ‘ICE’ target [85], a solid hydrogen-deuterium compound in which the protons or the deuterons can be polarized independently. The expected polarization and dilution are $P_H=80\%$ and $f_H = 1/3$ for H, and $P_D=50\%$ and $f_D = 2/3$ for deuteron. A 7 kg ($\rho_t=1.1$ gr/cm²) polarized target with the qualities mentioned above would be 20 cm in radius and 50 cm thick, similar to the other light targets proposed for structure function studies. Raw event rates in such a detector would be around 20M per 10^{20} muon decays.

If such a data sample is analyzed in 10 in x bins, the error in each x bin would be $\delta g_1 \simeq (f P_T \sqrt{N})^{-1} \sim 1\%$.

If the neutrino beam intensities and polarized target described above are feasible, the physics motivations would be very strong. We will be able to do high precision measurements where we can cleanly separate singlet (gluon-dependent)

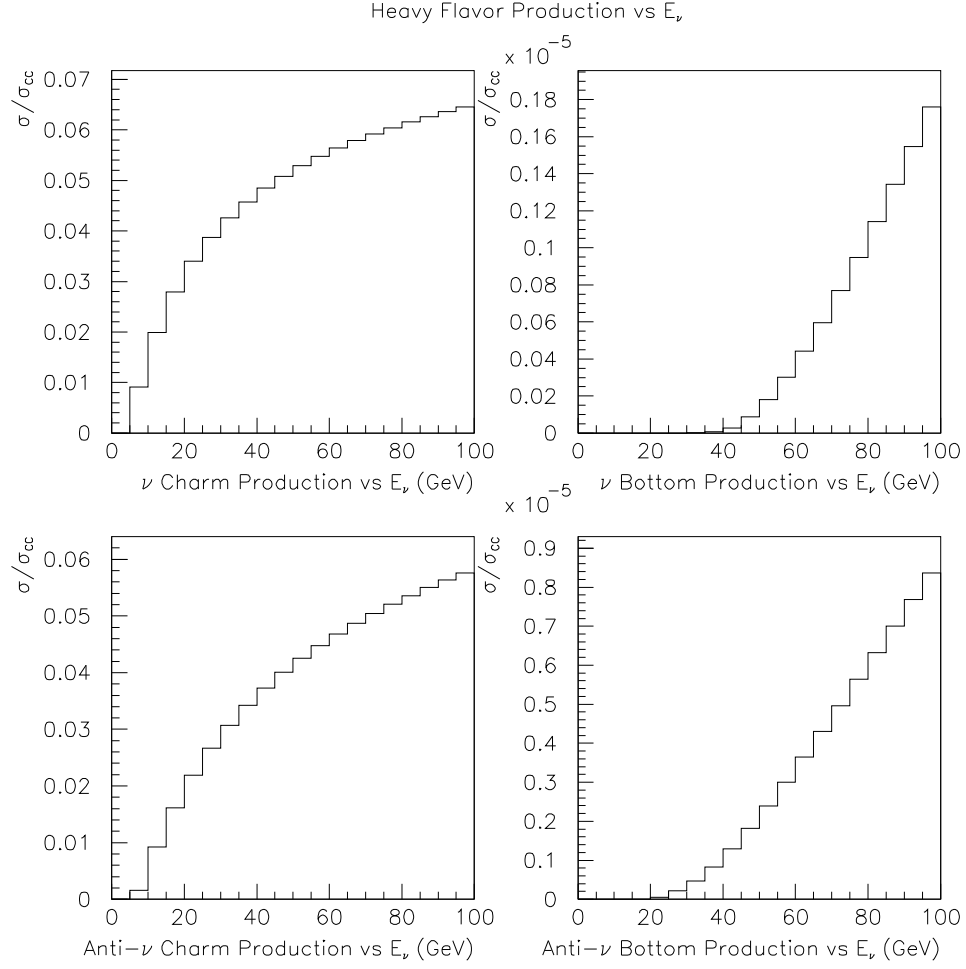


Figure 56: Charm and bottom quark production as a fraction of the total cross-section as a function of E_ν .

from non-singlet (gluon-free) terms. Furthermore, due to the nature of the neutrino charged current interactions it will be possible to perform a measurement of the polarization of the proton's quarks by flavor, with sea and valence contributions separated.

4.8 Charm Production and $D^0 - \bar{D}^0$ Mixing

Neutrino interactions are a very good source of clean, sign-tagged charm particles. Single charm quarks are produced via the processes

$$\nu s \rightarrow \ell^- c \quad \text{Cabbibo favored} \quad (87)$$

$$\nu d \rightarrow \ell^- c \quad \text{Cabbibo suppressed} \quad (88)$$

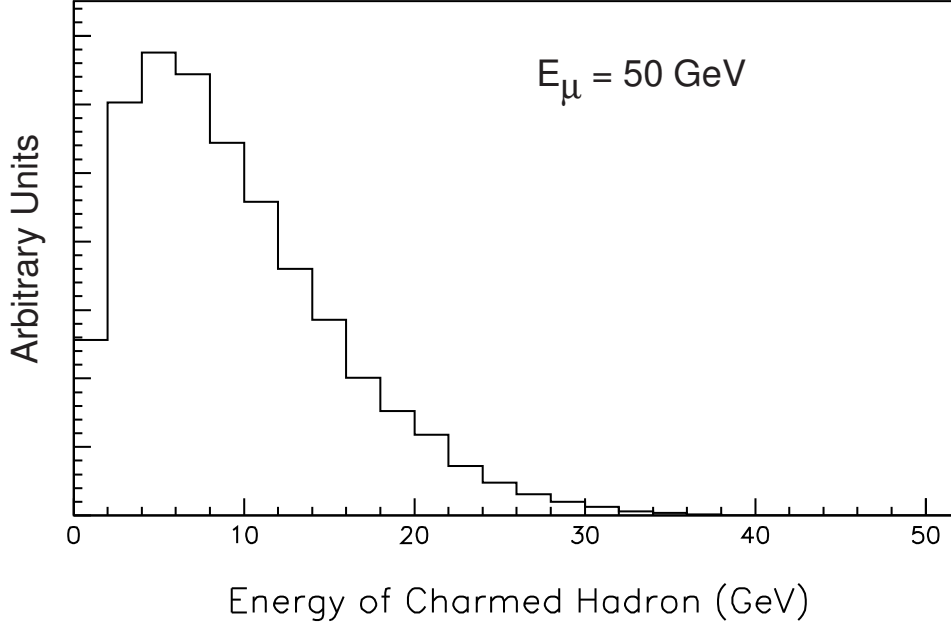


Figure 57: Charmed hadron spectra from neutrino interactions in a near detector from a 50 GeV muon storage ring.

$$\nu\bar{s} \rightarrow \ell^+\bar{c} \quad \text{Cabbibo favored} \quad (89)$$

$$\nu\bar{d} \rightarrow \ell^+\bar{c} \quad \text{Cabbibo suppressed} \quad (90)$$

The fraction of heavy flavor produced as a function of E_ν is shown in Fig. 56. An experiment at a 50 GeV muon storage ring with 10^{20} muon decays and a one ton (fiducial) target made up of silicon strip detectors interleaved with heavier material would observe $\approx 3 \times 10^9$ muon-neutrino charged-current interactions and around 1.2×10^8 charm hadrons with energies above 4 GeV/year. All of these charmed hadrons are flavor tagged at the point of production by the charge of the outgoing primary lepton (c production with ℓ^- and \bar{c} production with ℓ^+).

There are several interesting physics motivations for charm studies at muon storage rings, including measurements of the strange contribution to proton structure and spin; however, the primary motivation for producing charm by this method is the cleanliness of the final state relative to hadroproduction and the flavor tagging in production. This experimental fact compliments the theoretically “clean laboratory” of charm in searches for FCNC, CP asymmetries and $D^0 \rightarrow \bar{D}^0$ oscillations, all of which are small in the standard model because of the lack of coupling of charm to the heavy top quark.

Although this study has concentrated on neutrino energies below 50 GeV, we note that similar arguments hold for bottom production and that for machines with energies above 100 GeV, single B meson production rates can reach 100 per gr/cm^2 of target. Because nuclei mainly consist of u quarks rather than c

quarks, the $u \rightarrow b$ rate will be enhanced and a clean measurement of V_{ub} without final state effects may be possible.

As an example of the physics reach of a neutrino charm factory, consider the example of $D^0 - \overline{D}^0$ mixing measurements. The most sensitive current searches for time-integrated mixing place limits on the process of $\sim 5 \times 10^{-3}$ [90, 91]. BaBar expects to have sensitivity to mixing at the $\sim 5 \times 10^{-4}$ level after several years at design luminosity [92]. These measurements are ultimately limited by tagging mistakes and backgrounds to final state D^0 or \overline{D}^0 identification from doubly-Cabibbo suppressed decays, such as $D^0 \rightarrow K^+\pi^-$ which occur at the few part per thousand level.

At a 50 GeV muon storage ring, with a high mass detector, one could probe $D^0 - \overline{D}^0$ mixing *via*

$$\begin{aligned}\nu N &\rightarrow c\ell^- X \\ &\hookrightarrow \ell^+ X \\ &\hookrightarrow \bar{c} \rightarrow \ell^- X,\end{aligned}$$

and its charge conjugates. The appearance of like-signed leptons would indicate mixing, where opposite-signed leptons are expected. Assuming 50% of the charm produces hadronizes as a D^0 or \overline{D}^0 , this would result in the observation of 2×10^6 tagged neutral charm meson semi-leptonic decays in either the muon or electron channel.

4.9 Precision Electroweak Measurements

Precision measurements of electroweak parameters from neutrino experiments have played an important role in testing the Standard Model and in searching for new physics. Even with the wealth of on-shell W and Z bosons today at colliders, the neutrino data remains important and is complimentary to collider studies. The intense flux of neutrinos from a neutrino factory opens up a new era of precision electroweak measurements previously limited by statistics.

Three interesting precision measurements can be contemplated at a neutrino factory, and each can be cast as a precision measurement of the weak mixing angle, $\sin^2 \theta_W$. The experiment that most dramatically highlights new capabilities at a neutrino factory is the study of neutrino-electron cross sections. The second possible experiment is the extraction of $\sin^2 \theta_W$ from the neutral-current to charged-current deep inelastic scattering (DIS) cross-sections, a measurement which currently is the most precise test of weak interactions in neutrinos and which is currently limited by statistics[86], although difficult theoretical systematics are not far behind. A final possibility is the study of weak boson scattering from photons in the so-called neutrino “trident” process.

Only the first two possibilities are discussed here in detail. Trident processes are not considered here because of the difficult theoretical systematics that will ultimately limit the measurements[87].

Neutrino-electron scattering

Neutrino-electron elastic scattering,

$$\nu e^- \rightarrow \nu e^-, \quad (91)$$

is perhaps the most promising reaction for the precise probe of electroweak unification from neutrino interactions. Because the target particle is point-like, its structure does not introduce uncertainties in extracting parameters of the electroweak interaction from observed cross-sections. These measurements will therefore be limited only by statistical and experimental uncertainties. The best previous measurements of νe scattering come from the CHARM II experiment which observed approximately 5000 events [88].

Two distinct measurements are possible at a muon storage ring because neutrino-electron scattering includes different diagrams for the beams from positive and negative muons. The processes in the $\nu_\mu \bar{\nu}_e$ and $\bar{\nu}_\mu \nu_e$ beams are

$$\begin{aligned} \bar{\nu}_\mu e^- &\rightarrow \bar{\nu}_\mu e^-, & \nu_e e^- &\rightarrow \nu_e e^-, \\ \nu_\mu e^- &\rightarrow \nu_\mu e^-, & \bar{\nu}_e e^- &\rightarrow \bar{\nu}_e e^-, \end{aligned} \quad (92)$$

where the electron-neutrino and electron-antineutrino scattering process includes a charged-current (W^\pm exchange) in the t-channel and s-channel, respectively. The differential cross-section with respect to $y = E_e/E_\nu$ is given by

$$\frac{d\sigma(\nu e^- \rightarrow \nu e^-)}{dy} = \frac{2G_F^2 m_e E_\nu}{\pi} \left[g_L^2 + g_R^2 (1-y)^2 \right], \quad (93)$$

where terms of $\mathcal{O}(m_e/E_\nu)$ are neglected and expressions for the left-handed and right-handed coupling constants, g_L and g_R , for each of the processes shown in Eq. (92) are given in Table 11. The numerical values for the cross-sections after integrating over y are:

$$\sigma(\nu e^- \rightarrow \nu e^-) = 1.72 \times 10^{-41} \times E_\nu [\text{GeV}] \times \left[g_L^2 + \frac{1}{3} g_R^2 \right], \quad (94)$$

where the values for the final term are also given in Table 11. Note that neutrino-electron scattering has a much lower cross-section than DIS, roughly down by the ratio of m_e to m_p . Experimentally, it should be noted that the observed neutrino-electron scattering rate will be summed over both beams since the observed final states are identical.

The experimental signature for $\nu - e$ scattering is a single negatively charged electron with a small transverse momentum relative to the incoming neutrino,

$$p_t^{(e-\nu)} < \sqrt{2m_e E_\nu}. \quad (95)$$

The normalization mode is the appearance of a single muon with similarly low p_t^μ . Of course, the neutrino beam itself has a characteristic divergence from

Table 11: g_L and g_R by $\nu - e$ scattering process

Reaction	g_L	g_R	$g_L^2 + \frac{1}{3}g_R^2$
$\nu_\mu e^- \rightarrow \nu_\mu e^-$	$-\frac{1}{2} + \sin^2 \theta_W$	$\sin^2 \theta_W$	0.0925
$\nu_e e^- \rightarrow \nu_e e^-$	$\frac{1}{2} + \sin^2 \theta_W$	$\sin^2 \theta_W$	0.5425
$\bar{\nu}_\mu e^- \rightarrow \bar{\nu}_\mu e^-$	$\sin^2 \theta_W$	$-\frac{1}{2} + \sin^2 \theta_W$	0.0758
$\bar{\nu}_e e^- \rightarrow \bar{\nu}_e e^-$	$\sin^2 \theta_W$	$\frac{1}{2} + \sin^2 \theta_W$	0.2258

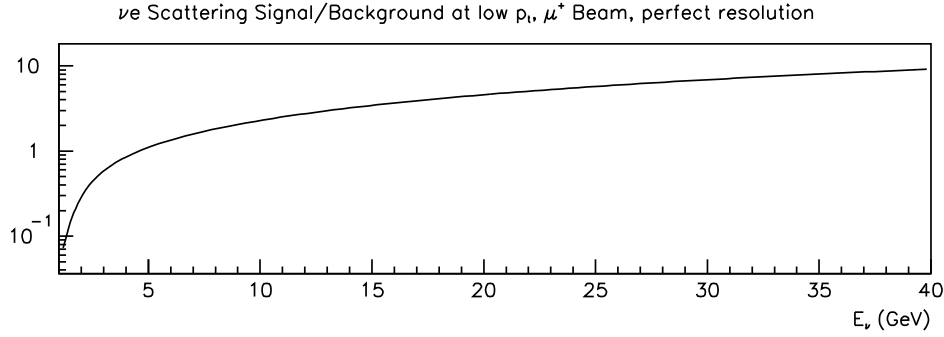


Figure 58: Signal to noise in the low $p_t^{(e)}$ region ($p_t^2 < \frac{\pi^2}{16\gamma_\mu^2} + \frac{m_e E_\nu}{2}$) as a function of E_ν .

decay kinematics of $\frac{\pi}{4\gamma_\mu}$, and therefore the observed lepton $p_t^{(e)}$ relative to the mean beam direction is given by

$$\langle p_t^{(e)} \rangle \approx \sqrt{\frac{\pi^2}{16\gamma_\mu^2} + \frac{m_e E_\nu}{2}}. \quad (96)$$

For a 50 GeV storage ring, this factor is dominated by the fundamental p_t of the interaction and is typically ~ 90 MeV. For a lower energy storage ring of about 15 GeV, these factors become equal.

The primary background to this measurement is from quasi-elastic $\nu_e - N$ or $\bar{\nu}_e - N$ scattering events which occur at $p_t^{(e)}$ up to $\sqrt{m_N E_\nu}$. Fig. 58 shows the estimated signal to background ratios expected in the low p_t region.

Because of the exceptionally low cross section, the target must be very massive. The detector must therefore be capable of resolving the p_t with much better resolution than the background spread. This favors the use of a fully active, high resolution tracking detector with sub-radiation length sampling in order to resolve the p_t of the single electron before it is significantly broadened by shower development. A liquid Argon TPC, such as the one proposed for the ICANOE experiment[41] might be ideal for such a measurement. Another possibility would be a scintillating fiber/tungsten calorimeter.

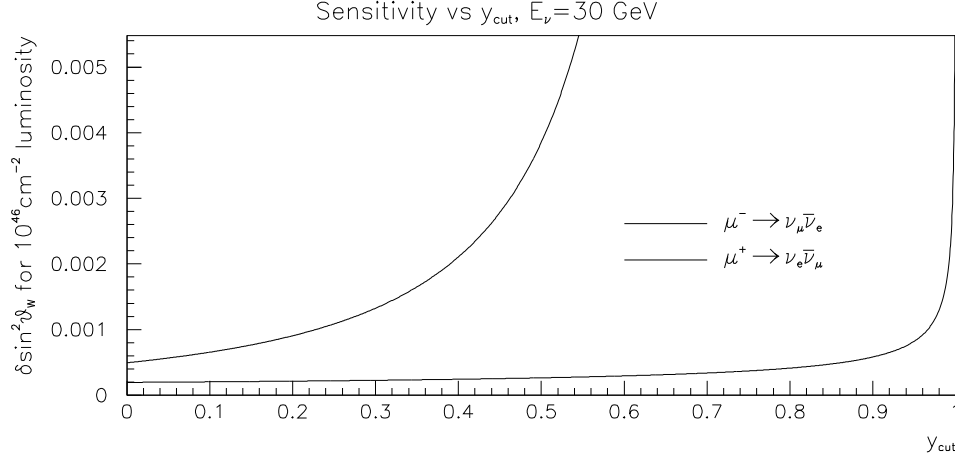


Figure 59: Statistical uncertainty in $\sin^2 \theta_W$ for a luminosity of 10^{46} cm^{-2} as a function of y_{cut} for a 30 GeV neutrino beam. Note that the μ^- produced beam is much less sensitive to $\sin^2 \theta_W$ due to nearly exact cancellation in the $\sin^2 \theta_W$ dependence of the two neutrino species in the beam.

The largest experimental challenge for such a measurement is likely to be the normalization of the absolute neutrino flux. Despite the precise knowledge of muon decays, it would be extremely difficult to predict the precise neutrino flux at the 10^{-4} level merely from monitoring the parent muon beam. Instead, the signal processes will probably have to be normalized to the theoretically predictable processes of inverse muon decay, $\nu_\mu e^- \rightarrow \nu_e \mu^-$, and muon production through annihilation, $\bar{\nu}_e e^- \rightarrow \bar{\nu}_\mu \mu^-$, both of which occur only in the $\nu_\mu \bar{\nu}_e$ beam. Normalization of the ν_e beam may be possible through comparison to neutrino-nucleon scattering, $\nu N \rightarrow l^\pm N'$, in the $\bar{\nu}_\mu \nu_e$ and $\nu_\mu \bar{\nu}_e$ beam.

For a 20 ton detector at a 50 GeV muon storage ring, with $2 \times 10^{20} \mu^-$ decays/year there will be approximately 1.5×10^{10} DIS charged current events and 8.5M $\nu_\mu/\bar{\nu}_e$ -electron scatters per year. This leads to an estimated sensitivity of $\delta \sin^2 \theta_W^{(\text{stat})} \sim 0.0002$

Neutrino-nucleon scattering

There were two dominant systematic uncertainties in present-day measurements of the weak mixing angle in neutrino nucleon scattering, ν_e contamination in the ν_μ beam and the kinematic suppression of scattering from strange quarks in the charged current channel.

For an isoscalar target, the neutral current rates can be related to the charged current rates via [17]:

$$R_\nu - \Delta R_s = \left(\frac{1}{2} - \sin^2 \theta_W + \frac{5}{9} \sin^4 \theta_W \right) [1 - \Delta R_c] +$$

$$\frac{5}{9} \sin^4 \theta_W [r - r \Delta \bar{R}_c] \quad (97)$$

$$R_{\bar{\nu}} - \Delta \bar{R}_s = \left(\frac{1}{2} - \sin^2 \theta_W + \frac{5}{9} \sin^4 \theta_W \right) [1 - \Delta \bar{R}_c] + \frac{5}{9} \sin^4 \theta_W \left[\frac{1}{r} - \frac{1}{r} \Delta R_c \right] \quad (98)$$

where $R_{\nu/\bar{\nu}}$ is the ratio of neutral to charged current cross sections, $r \sim 0.5$ is the ratio of charged current anti-neutrino to neutrino cross sections, and ΔR_s and ΔR_c are small corrections for the kinematic suppression of $s \rightarrow c$ in charged current scattering where the neutral current process $s \rightarrow s$ has no suppression. The charm corrections can be eliminated by a judicious subtraction of neutrino and anti-neutrino rates [97] but with a consequent reduction in statistical power.

Present-day experiments [98, 88, 65] have had integrated fluxes of 10^{15} - 10^{16} neutrinos and have relied on dense nuclear targets. In such targets neutral current events are distinguished from charged current events by the presence or absence of a muon in the final state. In a dense calorimeter, electron neutrino charged current induced events look similar to neutral current events as the electron is lost in the hadronic shower. They are a significant background for precision measurements with conventional beams produced by pion and kaon decay and would be even more significant at a neutrino factory.

The most precise measurement to date is from the NuTeV collaboration [65] of

$$\sin^2 \theta_W = 0.2253 \pm 0.0019(stat) \pm 0.0010(syst). \quad (99)$$

At a neutrino factory, the neutrino flux will be several orders of magnitude higher but the beam will consist of approximately equal numbers of ν_μ and $\bar{\nu}_e$. This makes a detector capable of distinguishing electron charged current events from neutral current events desirable and implies a low density detector such as those considered for the deep-inelastic scattering studies.

We have considered several possible observables for a neutrino factory measurement and propose:

$$R_e^{\mu-} = \frac{\sigma(\nu_\mu, NC) + \sigma(\bar{\nu}_e, NC)}{\sigma(\nu_\mu, CC) - \sigma(\bar{\nu}_e, CC)} = \frac{R^\nu + gr R^{\bar{\nu}}}{1 - gr} \quad (100)$$

or

$$\hat{R}^{\mu-} = \frac{\sigma(\nu_\mu, NC) + \sigma(\bar{\nu}_e, NC) + \sigma(\bar{\nu}_e, CC)}{\sigma(\nu_\mu, CC)} = R^\nu + gr R^{\bar{\nu}} + gr \quad (101)$$

for the $\nu_\mu \bar{\nu}_e$ beam, and

$$R_e^{\mu+} = \frac{\sigma(\bar{\nu}_\mu, NC) + \sigma(\nu_e, NC)}{\sigma(\nu_e, CC) - \sigma(\bar{\nu}_\mu, CC)} = \frac{R^\nu + g^{-1} r R^{\bar{\nu}}}{1 - g^{-1} r} \quad (102)$$

or

$$\begin{aligned}\hat{R}^{\mu+} &= \frac{\sigma(\bar{\nu}_\mu, NC) + \sigma(\nu_e, NC) + \sigma(\nu_e), CC)}{\sigma(\bar{\nu}_\mu, CC)} \\ &= \frac{g}{r}R^\nu + R^\tau + \frac{g}{r}\end{aligned}\quad (103)$$

for the $\bar{\nu}_\mu\nu_e$ beam, where $R_{\nu/\bar{\nu}}$ is the ratio of neutral to charged current cross sections from Eq. (97). The observable R_e^μ requires electron identification while \hat{R}^μ requires only muon identification.

The variable g is the energy-weighted flux ratio between ν_μ and $\bar{\nu}_e$ or, equivalently, between $\bar{\nu}_\mu$ and ν_e :

The flux ratio for neutrinos and anti-neutrinos g is:

$$g \equiv \frac{\int \Phi(E_{\bar{\nu}_e})E_{\bar{\nu}_e}dE_{\bar{\nu}_e}}{\int \Phi(E_{\nu_\mu})E_{\nu_\mu}dE_{\nu_\mu}} = \frac{\int \Phi(E_{\nu_e})E_{\nu_e}dE_{\nu_e}}{\int \Phi(E_{\bar{\nu}_\mu})E_{\bar{\nu}_\mu}dE_{\bar{\nu}_\mu}} \simeq \frac{6}{7}. \quad (104)$$

and is well determined by the muon decay kinematics. However, the relative detection efficiencies for muons and electrons must be known at the 2×10^{-4} level in order to determine $\sin^2 \theta_W$ to 10^{-3} by the first method. In addition, the charm contributions are not cancelled in this observable and must be measured directly in the same experiment.

For the R_e measurement, which requires electron identification, an active target of 20 cm radius, 10 gr/cm² thick consisting of either CCD's or silicon strip detectors (~ 140 300- μ m detectors) spaced over a meter and followed by the tracking, electromagnetic and hadron calorimetry and muon identification proposed above for structure function measurements would yield 15M muon and 8M electron charged current deep-inelastic scattering events/ 10^{20} μ^- decays and would yield a statistical precision of 0.0004 in $\sin^2 \theta_W$. The charm corrections partially cancel in this observable and would also be measured directly via the 2M charm events/year produced in such a detector.

The \hat{R} measurement, which relies only on muon identification can be done with a much denser target, perhaps an iron/silicon sandwich calorimeter. Such a calorimeter 200 gr/cm² thick would have a statistical sensitivity of $\Delta \sin^2 \theta_W \sim 0.0001$ per year at a 50 GeV machine. This method is quite similar to the method used in the NuTeV [65] measurement and would be dominated by systematic errors.

4.10 Heavy Lepton Mixing

A muon storage ring offers ample opportunities to search for new phenomena in yet unexplored physical regions. One such opportunity is the ability to search

for the existence of neutral heavy leptons. Several models describe heavy isospin singlets that interact and decay by mixing with their lighter neutrino counterparts [108, 109]. The high intensity neutrino beam created by the muon storage ring provides an ideal setting to search for neutral heavy leptons with a mass below the muon mass, $105.6 \text{ MeV}/c^2$.

It is postulated that neutral heavy leptons (L_0) could be produced from muon decay when one of the neutrinos mixes with its heavy, isospin singlet partner. Neutral heavy leptons can be produced via one of two channels:

$$\mu^- \rightarrow L_0 + \bar{\nu}_e + e^- \quad (105)$$

$$\mu^- \rightarrow \nu_\mu + L_0 + e^- \quad (106)$$

The branching ratio for each of these reactions is given by:

$$BR(\mu \rightarrow L_0 \mu e) = |U_i|^2 (1 - 8x_m^2 + 8x_m^6 - x_m^8 + 12x_m^4 \ln x_m^2) \quad (107)$$

Here $x_m \equiv m_{L_0}/m_\mu$ and $|U_i|^2$ is the mixing constant between the specific type of neutrino and the neutral heavy lepton: $U_i \equiv \langle L_0 | \nu_i \rangle$. Note that $|U_\mu|^2$ and $|U_e|^2$ need not be identical.

Once produced, a neutral heavy lepton of such low mass can either decay via $L_0 \rightarrow \nu\nu\nu$, $L_0 \rightarrow \nu ee$, or $L_0 \rightarrow \gamma\nu$. The most viable mode for detection is the two-electron channel. For this particular decay mode, the L_0 can decay either via charged current or charged and neutral current interactions. The branching ratio for this decay process has been previously calculated [110]. Since the decay width is proportional to U_j^2 , the number of L_0 's detectable is proportional to $U_i^2 \cdot U_j^2$ in the limit where the distance from the source to the detector is short compared to the lifetime of the L_0 .

Using the above model, one can estimate the number of neutral heavy leptons produced at the muon storage ring which later decay within a given detector:

$$N_{L_0} = N_\nu * BR(\mu \rightarrow L_0 \nu e) * \epsilon * e^{-L/\gamma c\tau} * BR(L_0 \rightarrow \text{detectable}) * (1 - e^{-\delta l/\gamma c\tau}) \quad (108)$$

Here N_ν is the number of neutrinos produced from muon decay, $BR(\mu \rightarrow L_0 \nu e)$ is the branching ratio of muons decaying into neutral heavy leptons versus ordinary muon decay, L is the distance from the beamline to the detector, δl is the length of the detector, ϵ is the combined detector and geometric efficiency, τ is the L_0 lifetime, and $BR(L_0 \rightarrow \text{detectable})$ is the branching ratio for the neutral heavy lepton decaying via a detectable channel (presumably $L_0 \rightarrow \nu ee$).

In estimating the sensitivity to L_0 production at the muon storage ring, we make a few underlying assumptions. We assume that the storage ring utilizes

a pure, unpolarized muon beam with straight sections such that 25 percent of the muons will decay to neutrinos pointing towards the detector. We assume that the fiducial volume is 3 meters in diameter and 30 meters in length, (which is probably compatible with the need for empty space before a conventional detector) and that the detector has sufficient tracking resolution to detect the e^+e^- vertex from the L_0 decay. We assume for now that the background is negligible. These parameters correspond to the fiducial volume of the decay channel used for the L_0 search at E815 (NuTeV) [111, 112].

The sensitivity of the detector has been calculated for a number of different muon energies and beam intensities. Fig. 60 shows limits on the L_0 - ν_μ mixing as a function of L_0 mass. One achieves the best limits from using relatively low energy/high intensity muon beams. This is a major improvement over previous neutral heavy lepton searches, where limits do not reach below 6.0×10^{-6} in the low mass region [113, 109].

The single event sensitivity quoted here depends on having minimal background levels in the signal region. Part of this can be achieved by kinematic cuts which discriminate against neutrino interactions in the detector material. However, it will probably be necessary to reduce the amount of material in the fiducial region compared to NuTeV. We estimate that even if the decay region is composed only of helium gas, the number of neutrino interactions will approach a few thousand. The ideal detector, therefore, would consist of a long vacuum or quasi-vacuum pipe with appropriate segmentation for tracking. The decay pipe could be used in conjunction with larger neutrino detectors adapted for the muon storage ring.

The muon storage ring would to be an ideal location to continue the search for neutral heavy leptons. The high intensity neutrino beam allows for a neutral heavy lepton search to be sensitive to the $10 - 100 \text{ MeV}/c^2$ mass range. In addition, such a neutral heavy lepton program is very compatible with a neutrino detector which uses the same neutrino beam. It is also clear, however, that a neutral heavy lepton search would receive the most benefit at lower muon energies, and thus would yield best results at the earlier stages of the muon storage ring program.

4.11 Neutrino Magnetic Moments

Although neutrino oscillation searches focus on the mass differences between neutrino eigenstates, neutrinos can possess other observable properties such as a magnetic moment. A measurement of the neutrino magnetic moment (NMM) would not only have great impact in the field of cosmology, particularly the development of stellar models, but would also help constrain several Standard Model extensions. An important experimental advantage is that a NMM search can run parasitically as the front-end of a typical long baseline detector.

Despite their lack of charge, neutrinos can possess a non-zero magnetic mo-

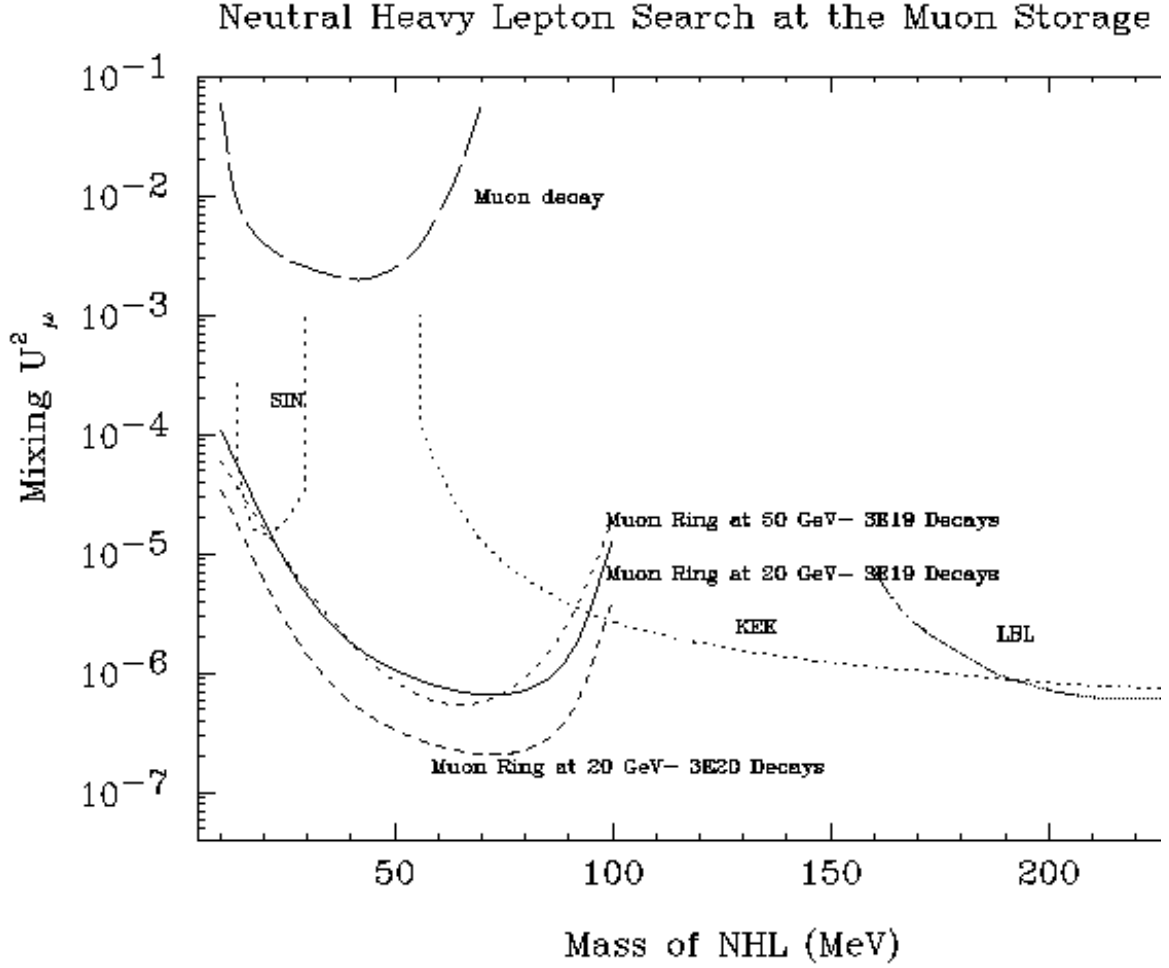


Figure 60: Limits on $|U_{\mu L}|^2$ as a function of L_0 mass for one year of running. The curves show sensitivities for 20 GeV and 50 GeV muon energies. Sensitivities assume no background events in signal region.

ment that can arise through loop diagrams. In the Standard Model, extended to include a right-handed neutrino or with left-handed neutrinos which have mass, the expected magnitude of the [109] neutrino magnetic moment is given by

$$\mu_\nu \simeq 3 \times 10^{-19} \mu_B \cdot \left(\frac{m_\nu}{1 \text{ eV}} \right), \quad (109)$$

where μ_B is the Bohr magneton. Although quite minuscule, several extensions to the Standard Model could dramatically increase μ_ν : supersymmetric models can produce $10^{-14} \mu_B$ to $10^{-12} \mu_B$ [115] and calculations that invoke large extra dimensions easily yield $10^{-11} \mu_B$ or larger [116].

Relative to the Standard Model expectation, the excluded values of NMM are not at all stringent, being seven to nine orders of magnitude larger. The current limits on neutrino magnetic moment from laboratory experiments are $\mu_\nu \leq 1.5$ to $1.8 \times 10^{-10} \mu_B$ for electron neutrinos [117][118] and $\mu_\nu \leq 7.4 \times 10^{-10} \mu_B$ for muon neutrinos [119]. Astrophysical limits are stronger: the slow rate of plasmon decay in horizontal branch stars [120] implies $\mu_\nu \leq 10^{-11} \mu_B$, while the neutrino energy loss rate from supernova 1987a [121] yields $\mu_\nu \leq 10^{-12} \mu_B$. Note, however, that several assumptions are implicit in the astrophysics limits, including the core temperature of the stars; if stellar models omit important processes, these limits might be overestimates. The supernova limit applies only to Dirac neutrinos and not to the Majorana case.

Existing search schemes possess a weakness that sharply limits their ultimate sensitivity: the formulae for the hypothesized effect are quadratic in μ_ν but linear in terms of the experimenter-controlled parameters. In contrast, the following scheme is quadratic in terms of the product of the NMM and a magnetic field strength, $\mu_\nu \cdot B$; hence a carefully designed and executed experiment could improve the limits from current experiments and possibly the limits from astrophysics calculations, or actually detect a NMM.

The energy E of a neutrino with a magnetic moment in a magnetic field B gains a new term $\mu_\nu \cdot B$. Consider a B field along the x -axis, and a neutrino with momentum and helicity along the z -axis at $t = 0$. The eigenstates of the neutrino are projections along the x -axis, and the state of the neutrino is expressed as:

$$|\uparrow\rangle = \frac{e^{-i(E+\mu_\nu B)t}}{\sqrt{2}} |\leftarrow\rangle + \frac{e^{-i(E-\mu_\nu B)t}}{\sqrt{2}} |\rightarrow\rangle. \quad (110)$$

As the neutrino propagates, the relative phase of the two components changes, corresponding to a rotation to a sterile state in the case of a Dirac neutrino or to an antineutrino in the Majorana case. At a far detector, the signal would be a deficit in the number of neutrinos detected or increase in the number of antineutrinos detected with the B field in place compared to the sample detected with no B field turned on.

In this phase rotation scheme, the energy splitting occurs as the neutrino passes through a field gradient and experiences a force $F = \nabla(\mu_\nu \cdot B)$. To preserve

this energy difference, which drives the phase difference in the absence of the B-field, the field must be turned off instead of allowing the neutrino to experience the reverse gradient as it exits the field region. (The principle of changing the energy of neutral dipolar molecules with time-varying electric fields has been demonstrated in the laboratory [122].)

To be successful, there are two basic requirements for the magnetic field:

- 1) The magnetic field must oscillate such that the neutrino experiences only one sign of the gradient. This study assumes that the neutrino bunch length is small compared to the oscillation length. If this assumption is not true, the effects discussed here will be diluted but the basic conclusions will still apply.
- 2) The magnetic field must be as strong as possible.

We have explored the possibility [123] of using two existing technologies for the B field: resonant cavities and kicker magnets. In both cases the maximum magnetic field is too small to yield improved magnetic moment limits given realistic equipment. We are currently exploring configurations involving a series of pulsed current sheets.

The formula for the number of events lost to sterile states may be expressed very simply as:

$$N_{lost} = N * \sin^2(\mu_\nu B t) \quad (111)$$

where t is the neutrino flight time from entering the magnetic field to detection. We note that, in contrast to an oscillation disappearance signal, this effect is explicitly independent of the neutrino energy. Fig. 61 compares the number of events that vanish because of phase rotations to the expected statistical fluctuations in the number of CC events (N) observed in a 50 kton [124] far detector. We see that for a cumulative 10 T field gradient and 10^{19} muon decays we expect a $> 10\sigma$ significance for a NMM of $10^{-11}\mu_B$. With a 3T gradient, the limit drops below two σ . The sensitivity can be greatly increased by increasing the field strength and more weakly by increasing the number of events in the far detector. Because the detector distance determines both t and N in Eqn. 111, the “significance” in the figure is linearly dependent on distance.

To conclude, we have discussed a novel neutrino magnetic moment search technique that uses oscillating magnetic fields at the source of a long baseline detector’s neutrino beam. This is the only technique we know of that is quadratic in both μ_ν and a controllable parameter, and thus has the potential for improved sensitivity as we improve our ability to create oscillating magnetic field gradients.

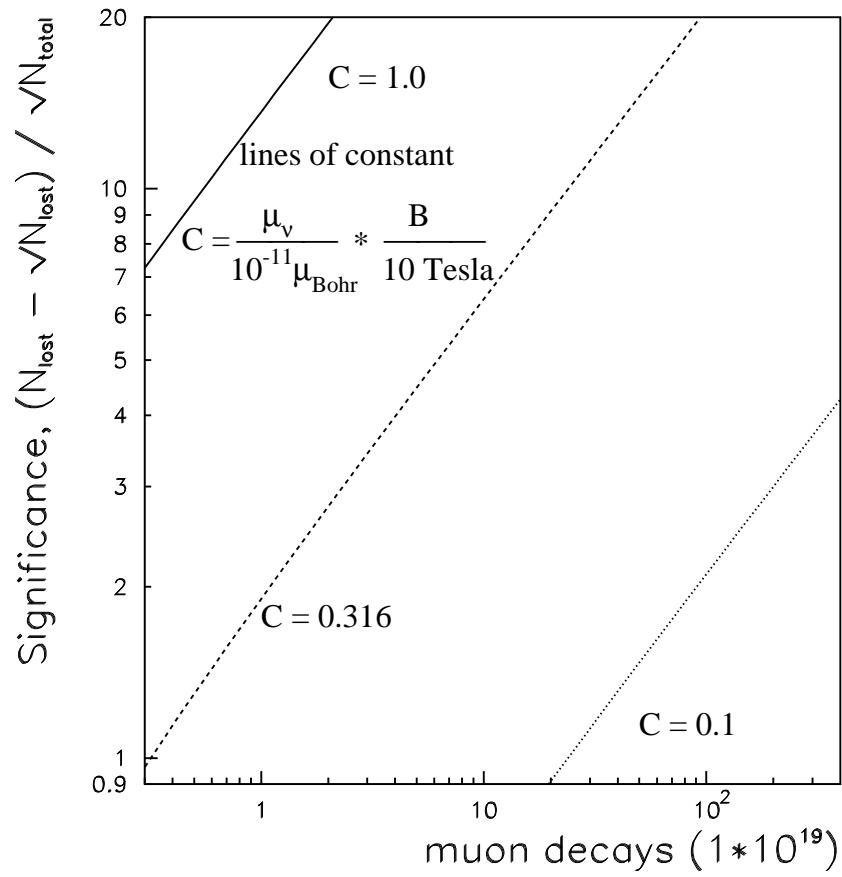


Figure 61: Significance for several scenarios.

4.12 Exotic processes

Neutrino factories offer the possibility of searching for exotic processes resulting in production of e^- , μ^+ , or τ -lepton of either charge. While these searches are interesting in their own right, they are also useful in ruling out exotic contributions to long-baseline neutrino oscillation signals. The neutrino beam from a muon storage ring would consist of a virtually pure combination of $\bar{\nu}_e$ and ν_μ (or charge-conjugate). At very short baselines the $\bar{\nu}_e$ and ν_μ will not have had time to oscillate into other flavors: For a 20 GeV muon storage ring with a 700 m straight section, and neutrino oscillations with $\Delta m^2 = 3.5 \times 10^{-3} \text{ eV}^2$, the oscillation probability is $\approx 5 \times 10^{-9}$.

One could distinguish between exotic processes and the beginning of a neutrino oscillation by exploiting their differing dependence on energy and distance. Specifically, these exotic processes would probably have a flat or rising dependence on the neutrino energy E_ν . In contrast, a neutrino oscillation would have a $1/E_\nu^2$ dependence. Also, if the distance L of the experiment changes, the rate of exotic events would decrease with the flux as $1/L^2$. In contrast, the neutrino oscillation probability would increase as L^2 (for L small compared to the oscillation period), and so the rate of oscillated events would be independent of L .

Current understanding of muon interactions allows for exotic processes in two forms. Anomalous lepton production could occur if muons decay to neutrino flavors other than those in the usual decay $\mu \rightarrow e\bar{\nu}_e\nu_\mu$, and the anomalous neutrinos then interact in the target. Alternatively, they could be produced if a $\bar{\nu}_e$ or ν_μ interacts with the target via an exotic process.

The only direct experimental limit on exotic $\mu \rightarrow e\bar{\nu}_x\nu_y$ decays is $BR(\mu \rightarrow e\bar{\nu}_\mu\nu_e) < 1.3\%$ [125]. Indirect limits are also very weak. The contribution of non- $V - A$ interactions to the muon decay rate has been limited to 8%[125]. Also, the total muon decay rate is one of the main measurements used to constrain electroweak parameters[125]. To first order,

$$\frac{1}{\tau_\mu} = \frac{G_F m_\mu^5}{192\pi^3}. \quad (112)$$

Assuming the standard model, G_F is determined to 1 part in 10^6 from muon lifetime measurements. If there are exotic contributions to the muon lifetime, the measured value of G_F would be shifted from the true value. Since

$$m_W \propto G_F^{-1/2}, \quad (113)$$

the 0.1% uncertainty on m_W corresponds to a 0.4% shift in the muon lifetime. Finally, the CKM matrix element V_{ud} is determined from the rate of nuclear β -decays relative to the muon lifetime. The assumption of unitarity on the CKM matrix gives us the following constraint on the first row:

$$|V_{ud}|^2 + |V_{us}|^2 + |V_{ub}|^2 = 1. \quad (114)$$

The experimental determination is[125]:

$$|V_{ud}|^2 + |V_{us}|^2 + |V_{ub}|^2 = 0.991 \pm 0.005. \quad (115)$$

The uncertainty on this constraint corresponds to a 0.5% shift in the muon lifetime. Additional contributions to the muon decay rate would lead to a downward shift in the determined value of $|V_{ud}|^2$ from the true value. We conclude that exotic decay modes of the muon with branching ratios totaling 0.5% are possible without contradicting current measurements or tests of the standard model.

As a concrete example of such an exotic process we consider R-parity-violating supersymmetric models. These models lead to lepton-number-violating vertices with couplings λ , and muon decay processes such as $\mu \rightarrow e \bar{\nu}_\tau \nu_\tau$ as shown in Fig. 1. The matrix element for these decays turns out to have the same form as for the standard W-exchange. The current constraints on the couplings λ are reviewed in Ref. [126]. These constraints allow a branching ratio of 0.4% for the process in Fig. 62.

Similar processes are allowed for anomalous lepton production as shown for example in Fig. 63. Estimates for allowed rates are in progress [127]. These diagrams involve the λ' couplings. Currently, the best limit on one of these couplings, λ'_{231} , is from ν_μ deep-inelastic scattering, so existing neutrino data is already providing constraints! The search for these types of effects at the muon storage ring could be input into a decision on whether to build a muon-proton collider where they could be studied in more detail.

As a start on estimating the capabilities of an experiment at the neutrino source, we consider the detector concept illustrated in Fig. 64. This concept consists of a repeating sequence of 1.5 mm-thick Tungsten sheets with Silicon tracking, separated by 4 mm. Tungsten, being dense, provides a high target mass while being thin enough for a produced τ to have a high probability of hitting the Silicon. The impact parameter of the τ decay products is typically 90 microns with a broad distribution, so we would like a hit resolution of 5 microns or better. Although there is a lot of multiple scattering in the tungsten, the short extrapolation distance provides for a good impact parameter resolution on the τ decay products. This configuration has been optimized for a 50 GeV muon beam. For lower energy beams, the planes should be spaced more closely, and the Tungsten thickness perhaps reduced. Studies of detectors with passive target mass and tracking with emulsion sheets [128] suggest that we can expect τ reconstruction efficiencies as high as 30%.

We would propose placing such a detector in a magnetic field, and measuring the momentum of muons and hadrons should be straightforward. However, each Tungsten sheet is 0.4 radiation lengths thick, and while we should obtain good energy resolution for electromagnetic showers, it will not be feasible to measure the charge of an electron before it showers.

In summary, with a total mass of 6 tons of Tungsten, 200 m² of Silicon tracking, located close to a muon storage ring with 5×10^{20} muon decays at 50

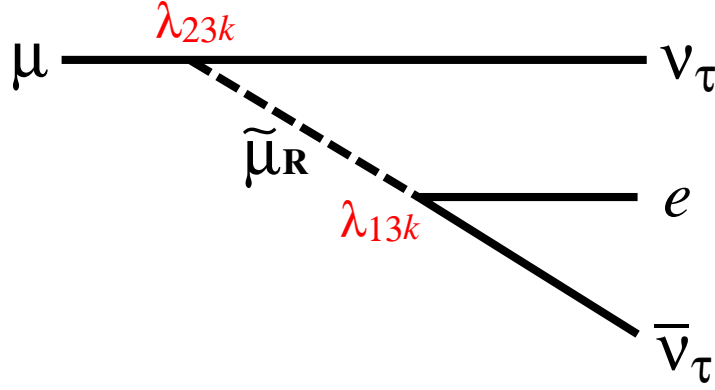


Figure 62: Example of exotic muon decay in R-parity-violating SUSY.

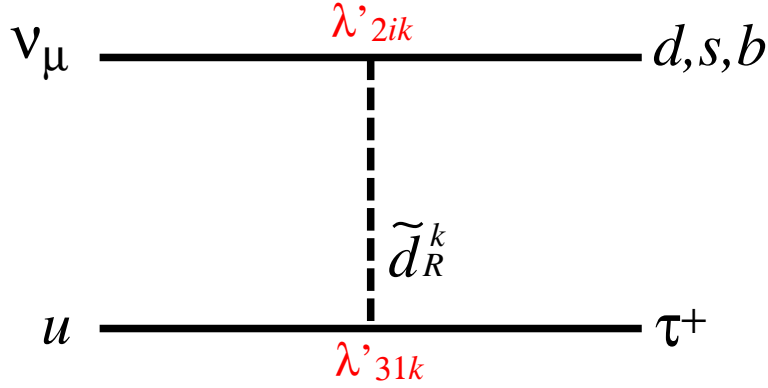


Figure 63: Example of an exotic neutrino interaction in R-parity-violating SUSY.

GeV, we expect a total of 35 billion neutrino interactions, 4 orders of magnitude above present neutrino interaction samples. Thus, there is much potential for detecting very rare exotic processes if we can adequately reduce backgrounds. Detailed simulations and studies of possible Silicon tracking technologies are needed to quantify this.

4.13 Summary

We have investigated possible conventional neutrino physics studies done at a detector located near a muon storage ring. We emphasized novel methods rather than extensions of existing experiments with additional statistics.

For a reference machine with 50 GeV stored muons and 10^{20} muon decays per year we find that it is possible to:

- Measure individual parton distributions within the proton for all light quarks and anti-quarks.
- Determine the effects of a nuclear environment on individual quark species.

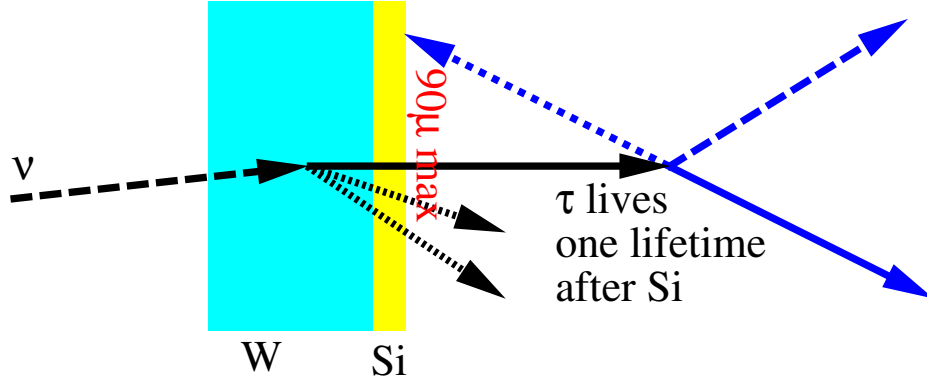


Figure 64: One plane of a detector for τ production.

- Measure the spin contributions of individual quark species, including strange quarks and do precision studies of the QCD evolution of spin effects without a need for data from beta decay measurements.
- Measure charm production with raw event rates of up to 100 million charm events/year with $\simeq 2\text{M}$ double tagged events.
- Measure the Weinberg angle in both hadronic and purely leptonic modes with a precision of 0.0001 to 0.0002.
- Search for the production and decay of neutral heavy leptons with mixing angle sensitivity two orders of magnitude better than present limits in the 30-80 MeV region.
- Search for a neutrino magnetic moment which may be much larger than the Standard Model prediction in some supersymmetric theories.
- Search for anomalous tau production predicted by some R-parity violating supersymmetric models.

We note that the event rates at a near detector increase linearly with neutrino energy. In addition, the acceptance of small detectors is better for the narrower beam produced by higher energy machines. Almost all of the above measurements, with the exception of the neutral heavy lepton search, lose sensitivity if the beam energy is less than 50 GeV and gain if it is greater.

If the storage ring beam energy is lowered to 20 GeV, the statistical power of almost all of the measurements considered here would drop a factor of 2.5 or more. The number of deep-inelastic scattering events with Q^2 high enough for perturbative QCD to be meaningful drops even further and the minimum x rises to 0.05. Measurements involving charm or tau production in the final state would have lower statistics due to threshold effects, as would the inverse muon decay normalization for $\nu - e$ scattering, which has a threshold of ~ 11 GeV.

However, it should be remembered that a 50 GeV neutrino factory will produce neutrino fluxes of order 10^4 higher than existing neutrino beams. At 20 GeV the improvement for most physics processes is still greater than a factor of a thousand.

5 Summary and Recommendations

The main goal of the physics study presented in this report has been to answer the question: Is the physics program at a neutrino factory compelling? The answer is a resounding yes, provided there are 10^{19} or more muon decays per year in the beam forming straight section and the muon beam energy is ~ 20 GeV or greater. Based on our study, we believe that a neutrino factory in the next decade would be the right tool at the right time.

The neutrino oscillation physics program

The recent impressive atmospheric neutrino results from the Super-Kamiokande experiment have gone a long way towards establishing the existence of neutrino oscillations. This is arguably the most dramatic recent development in particle physics. Up to the present era, neutrino oscillation experiments at accelerators were searches for a phenomenon that might or might not be within experimental reach. The situation now is quite different. The atmospheric neutrino deficit defines the δm^2 and oscillation amplitude to which future long baseline oscillation experiments must be sensitive to, namely $\delta m^2 = O(10^{-3}) \text{ eV}^2$ and $\sin^2 2\theta = O(1)$. Experiments that achieve these sensitivities are guaranteed an excellent physics program that addresses fundamental physics questions. Furthermore, should *all* of the experimental indications for oscillations (LSND, atmospheric, and solar) be confirmed, we may be seeing evidence for the existence of sterile neutrinos. This would be a very exciting discovery which would raise many new questions requiring new experimental input.

A neutrino factory would be a *unique facility* for oscillation physics, providing beams containing high energy electron neutrinos (antineutrinos) as well as muon antineutrinos (neutrinos). These beams could be exploited to provide answers to the questions that we are likely to be asking after the next generation of accelerator based experiments.

The oscillation physics that could be pursued at a neutrino factory is compelling. Experiments at a neutrino factory would be able to simultaneously measure, or put stringent limits on, all of the appearance modes $\nu_e \rightarrow \nu_\tau$, $\nu_e \rightarrow \nu_\mu$, and $\nu_\mu \rightarrow \nu_\tau$. Comparing the sum of the appearance modes with the disappearance measurements would provide a unique basic check of candidate oscillation scenarios that cannot be made with a conventional neutrino beam. In addition, for all of the specific oscillation scenarios we have studied, the ν_e component

in the beam can be exploited to enable crucial issues to be addressed. These include:

- (i) A precise determination of (or stringent limits on) all of the leading oscillation parameters, which in a three-flavor mixing scenario would be $\sin^2 2\theta_{13}$, $\sin^2 2\theta_{23}$, and δm_{32}^2 .
- (ii) A determination of the pattern of neutrino masses.
- (iii) A quantitative test of the MSW effect.
- (iv) Stringent limits on, or the observation of, CP violation in the lepton sector.

To be more quantitative in assessing the beam energy, intensity, and baseline required to accomplish a given set of physics goals it is necessary to consider two very different experimental possibilities: (a) the LSND oscillation results are not confirmed, or (b) the LSND results are confirmed.

- (a) LSND not confirmed. A 20 GeV neutrino factory providing 10^{19} muon decays per year is a good candidate “entry-level” facility which would enable either (i) the first observation of $\nu_e \rightarrow \nu_\mu$ oscillations, the first direct measurement of matter effects, and a determination of the sign of δm_{32}^2 and hence the pattern of neutrino masses, or (ii) a very stringent limit on $\sin^2 2\theta_{13}$ and a first comparison of the sum of all appearance modes with the disappearance measurements. The optimum baselines for this entry-level physics program appears to be of the order of 3000 km or greater, for which matter effects are substantial. Longer baselines also favor the precise determination of $\sin^2 2\theta_{13}$. A 20 GeV neutrino factory providing 10^{20} muon decays per year is a good candidate “upgraded” neutrino factory (or alternatively a higher energy facility providing a few $\times 10^{19}$ decays per year). This would enable the first observation of, or meaningful limits on, $\nu_e \rightarrow \nu_\tau$ oscillations, and precision measurements of the leading oscillation parameters. In the more distant future, a candidate for a second (third?) generation neutrino factory might be a facility that provides $O(10^{21})$ decays per year and enables the measurement of, or stringent limits on, CP violation in the lepton sector.
- (b) LSND confirmed. Less extensive studies have been made for the class of scenarios that become of interest if the LSND oscillation results are confirmed. However, in the scenarios we have looked at we find that the $\nu_e \rightarrow \nu_\tau$ rate is sensitive to the oscillation parameters and can be substantial. With a large leading δm^2 scale medium baselines (for example a few $\times 10$ km) are of interest, and the neutrino factory intensity required to effectively exploit the ν_e beam component might be quite modest ($< 10^{19}$ decays per year). If sterile neutrinos play a role in neutrino oscillations, we will have an exciting window on physics beyond the SM, and we anticipate that a neutrino factory would enable crucial measurements to be made exploiting the electron neutrino beam component.

The non-oscillation physics program

A neutrino factory could provide beams that are a factor of $10^4 - 10^5$ more intense than conventional neutrino beams. This would have an enormous impact on the detector technology that could be used for non-oscillation neutrino experiments. For example, the use of silicon pixel targets and hydrogen or deuterium polarized targets would become feasible. Hence, a neutrino factory would offer experimental opportunities that do not exist with lower intensity conventional beams.

We have looked at a few explicit examples of interesting experiments that might be pursued at a neutrino factory:

- Precise measurements of the detailed structure of the nucleon for each parton flavor, including the changes that occur in a nuclear environment.
- A first measurement of the nucleon spin structure with neutrinos.
- Charm physics with several million tagged particles. Note that charm production becomes significant for storage ring energies above 20 GeV.
- Precise measurements of standard model parameters - α_s , the weak mixing angle, and the CKM matrix elements.
- Searches for exotic phenomena such as neutrino magnetic moments, anomalous couplings to the tau and additional neutral leptons.

The non-oscillation measurements benefit from higher beam energies since event rates and the kinematic reach scale with energy, and perturbative calculations become more reliable in the kinematic regions accessed by higher energies.

Recommendations

The physics program we have explored for a neutrino factory is compelling. We recommend a sustained effort to study both the physics opportunities and the machine realities.

- (i) We encourage support for the R&D needed to learn whether a neutrino factory can be a real option in the next decade.
- (ii) We propose further studies of detector technologies optimized for a neutrino factory, including both novel low mass detectors for near experiments and very high mass detectors for long baselines. For long baseline experiments detectors should have masses of a few times 10 kt or more that are able to detect and measure wrong-sign muons, and detectors of a few kt or more able to observe tau-lepton appearance with high efficiency. It is also desirable to identify electrons, and if possible measure the sign of their

charge. Both the detector technologies themselves and the civil engineering issues associated with the construction of such massive detectors need to be addressed.

- (iii) We recommend continued studies to better compare the physics potential of upgraded conventional neutrino beams with the corresponding potential at a neutrino factory, and also studies to better understand the benefits of muon polarization.
- (iv) The present study concentrated on the muon storage ring as a neutrino source and did not cover the additional physics programs which would use the proton driver and the high intensity muon beams. We recommend a further study directed at these other facets of physics at a muon storage ring facility.

Acknowledgments

We would like to thank Mike Witherell, Mike Shaevitz, and Steve Holmes for initiating the two companion 6 month neutrino factory studies, and their continued support that enabled these studies to be productive. We thank Mike Shaevitz in particular for our charge. We would also like to thank the members of the Neutrino Source/Muon Collider Collaboration, whose enthusiastic efforts over the last few years have enabled us to seriously contemplate a facility that requires an intense source of muons. Finally we would like to thank the participants of neutrino factory and related physics studies initiated in Europe and Japan that have given us encouragement and shown interest in the present study.

References

- [1] C. Ankenbrandt et al. (The Muon Collider Collaboration), *Phys. Rev. ST Accel. Beams* **2**, 081001 (1999).
- [2] S. Geer, *Phys. Rev. D* **57** (1998) 6989, *ibid.* **59** (1999) 039903E.
- [3] A. De Rújula, M. B. Gavela, and P. Hernández, *Nucl. Phys.* **B547** (1999) 21 hep-ph 9811390.
- [4] V. Barger, S. Geer, and K. Whisnant, “Long Baseline Neutrino Physics with a Muon Storage Ring Neutrino Source” *Phys. Rev. D* **61**, 053004 (2000).
- [5] Within a growing literature, see, for example, A. Bueno, M. Campanelli, and A. Rubbia, “Long baseline neutrino oscillation disappearance search using a ν beam from muon decays” hep-ph 9808485; “A medium baseline search for $\nu_\mu \rightarrow \nu_e$ oscillations at a ν beam from muon decays” hep-ph 9809252; S. Dutta, R. Gandhi, and B. Mukhopadhyaya, “Tau-neutrino Appearance Searches using Neutrino Beams from Muon Storage Rings” hep-ph 9905475.
- [6] For summaries of the current evidence about neutrino oscillations, see J. M. Conrad, in *Proceedings of the 29th International Conference on High Energy Physics*, Vancouver, edited by A. Astbury, D. Axen, and J. Robinson (World Scientific, Singapore, 1999), p. 25 (hep-ex 9811009), and “Where in the World Is the Oscillating Neutrino?” talk at Inner Space / Outer Space 1999 and PANIC99, available at <http://portia.fnal.gov/~jconrad/isos.html>; P. Fisher, B. Kayser, and K. S. McFarland, “Neutrino Mass and Oscillation,” *Annu. Rev. Nucl. Part. Sci.* **49**, 481 (1999), hep-ph 9906244; L. DiLella, “Accelerator and Reactor Neutrino Experiments,” hep-ex 9912010.
- [7] Y. Fukuda, *et al.* (Super-Kamiokande Collaboration), *Phys. Rev. Lett.* **81** (1998) 1562.
- [8] W. A. Mann, “Atmospheric Neutrinos and the Oscillations Bonanza,” Plenary talk at the XIX Int. Symposium on Lepton and Photon Interactions at High Energies, Stanford, Aug. 1999, hep-ex 9912007.
- [9] C. Athanassopoulos, *et al.* (LSND Collaboration), *Phys. Rev. Lett.* **77** (1996) 3082; *ibid.* **81** (1998) 1774; *Phys. Rev. C* **58** (1998) 2489.
- [10] G. Danby, J. M. Gaillard, K. Goulianos, L. M. Lederman, N. Mistry, M. Schwartz and J. Steinberger, *Phys. Rev. Lett.* **9**, 36 (1962).
- [11] F. J. Hasert *et al.* [Gargamelle Neutrino Collaboration], *Phys. Lett.* **B46**, 138 (1973). *Nucl. Phys.* **B73**, 1 (1974).

- [12] J. M. Conrad, M. H. Shaevitz, and T. Bolton, “Precision Measurements with High Energy Neutrino Beams,” *Rev. Mod. Phys.* **70**, 1341 (1998), hep-ex 9707015.
- [13] See for example: T. K. Gaisser, “Cosmic Rays and Particle Physics,” Cambridge University Press 1990.
- [14] D. MacFarlane et al., (CCFR), *Z. Phys. C* **26**, 1 (1984), J.P. Berge et al., (CDHSW), *Z. Phys. C* **35**, 443 (1987), J.V. Allaby et al., (CHARM), *Z. Phys. C* **38**, 403 (1988), P. Auchincloss et al., (E701), *Z. Phys. C* **48**, 411 (1990), world average from J. Conrad, M. Shaevitz and T. Bolton, *Rev. Mod. Phys.* Vol. 70, no. 4, (1998).
- [15] MINOS Technical Design Report NuMI-L-337 TDR, http://www.hep.anl.gov/ndk/hypertext/minos_tdr.html
- [16] V. Barger, S. Geer, and K. Whisnant, *Phys. Rev. D* **61**, 053004 (2000).
- [17] C.H. Llewellyn Smith, *Nucl. Phys. B* **228**, 205 (1983).
- [18] H.M. Gallagher and M.C. Goodman, Neutrino Cross Sections, NuMI-112, PDK-626, Nov. 10, 1995.
- [19] D. Casper, NUANCE neutrino simulation, private communication.
- [20] C. Crisan and S. Geer, FERMILAB-TM-2101, Feb. 2000.
- [21] Y.Fukuda et al., *Phys. Rev. Lett.* **82**, 1810, 243 (1999).
- [22] M. Gell-Mann, P. Ramond, R. Slansky, in *Supergravity*, edited by P. van Nieuwenhuizen and D. Freedman (North Holland, Amsterdam, 1979), p. 315; T. Yanagida in proceedings of *Workshop on Unified Theory and Baryon Number in the Universe*, KEK, 1979.
- [23] Z. Maki, M. Nakagawa, and S. Sakata, *Prog. Theor. Phys.* **28**, 870 (1962).
- [24] C. Jarlskog, *Phys. Rev. Lett.* **55**, 1039 (1985).
- [25] Parameters of the Preliminary Reference Earth Model are given by A. Dziewonski, Earth Structure, Global, in “The Encyclopedia of Solid Earth Geophysics”, ed. by D.E. James, (Van Nostrand Reinhold, New York, 1989) p. 331; also see R. Gandhi, C. Quigg, M. Hall Reno, and I. Sarcevic, *Astroparticle Physics* **5**, 81 (1996).
- [26] I. Mocioiu, R. Shrock, hep-ph/0002149.
- [27] M. Apollonio et al., *Phys. Lett. B* **420**, 397 (1998); *Phys. Lett. B* **466**, 415 (1999).
- [28] J. Learned, in the Proceedings of the Workshop on the Next Generation Nucleon Decay and Neutrino Detector NNN99, Stony Brook (Sept. 1999).

- [29] Super-Kamiokande Collab., Y. Fukuda et al., Phys. Lett. **B433**, 9 (1998); Phys. Rev. Lett. **81**, 1562 (1998); *ibid.*, **82**, 2644 (1999); Phys. Lett. **B467**, 185 (1999). The fit from the analysis of the current 61 kton-yr of atmospheric data was reported by K. Scholberg (Stony Brook seminar, Feb. 7, 2000).
- [30] G. Barenboim and F. Scheck, Phys. Lett. **B440**, 332 (1998), hep-ph/9808327; I. Stancu, Mod. Phys. Lett. **A14**, 689 (1999), hep-ph/9903552.
- [31] S. M. Bilenky, C. Giunti, and W. Grimus, hep-ph/9812360.
- [32] L. Baudis et al., Phys. Lett. B **407**, 219 (1997); M. Gunther et al., Phys. Rev. D **55**, 54 (1997).
- [33] A. Donini, M.B. Gavela, P. Hernández, and S. Rigolin, hep-ph/9910516.
- [34] Y. Fukuda *et al.* [Super-Kamiokande Collaboration], Phys. Rev. Lett. **81**, 1562 (1998) [hep-ex/9807003].
- [35] T. Kajita, talk at 7th International Symposium On Particles, Strings And Cosmology (PASCOS 99) 10-16 Dec 1999, Granlibakken, Tahoe City, California, <http://pc90.ucdavis.edu/schedule.html>
- [36] M. Apollonio *et al.*, Phys. Lett. **B466**, 415 (1999) [hep-ex/9907037].
- [37] F. Boehm *et al.*, hep-ex/0003022.
- [38] J. Learned, talk at International Workshop On Next Generation Nucleon Decay And Neutrino Detector, 23-25 Sep 1999, Stony Brook, New York.
- [39] Nishikawa, talk at International Workshop On Next Generation Nucleon Decay And Neutrino Detector, 23-25 Sep 1999, Stony Brook, New York.
- [40] OPERA Progress Report, LNGS-LOI 19/99, <http://www.cern.ch/opera/documents.html>
- [41] ICANOE proposal, LNGS-P21/99, <http://pcnometh4.cern.ch/>.
- [42] A. Curioni, talk at International Workshop On Next Generation Nucleon Decay And Neutrino Detector, 23-25 Sep 1999, Stony Brook, New York.
- [43] T. Ypsilantis, talk at International Workshop On Next Generation Nucleon Decay And Neutrino Detector, 23-25 Sep 1999, Stony Brook, New York.
- [44] <http://www-boone.fnal.gov/>
- [45] M. C. Gonzalez-Garcia, P. C. de Holanda, C. Pena-Garay and J. W. Valle, hep-ph/9906469.
- [46] Sudbury Neutrino Observatory, <http://www.sno.phy.queensu.ca/>

- [47] Borexino experiment, <http://almime.mi.infn.it/>
- [48] R.E. Lanou, Jr., Invited talk at 18th International Conference on Neutrino Physics and Astrophysics (NEUTRINO 98), Takayama, Japan, 4-9 Jun 1998, *Nucl. Phys. Proc. Suppl.* **77**, 55 (1999), hep-ex/9808033.
- [49] J. Busenitz *et al.*, “Proposal for US Participation in KamLAND,” March 1999, <http://bkf0.lbl.gov/kamland/>
- [50] A. Bueno, M. Campanelli, A. Rubbia, “Physics Potential at a Neutrino Factory, can we benefit from more than just detecting muons”, hep-ph/0005007.
- [51] V. Barger, S. Geer, R. Raja, K. Whisnant, “Neutrino oscillations at an entry-level neutrino factory and beyond”, Fermilab-PUB 00/049-T, hep-ph/0003184.
- [52] D.A. Harris, J.Yu *et al.*, NuTeV collaboration, hep-ex/9908056. *To appear in Nucl.Instrum.Meth.A.*
- [53] R. Forty, JHEP 9912:002,1999 hep-ex/9910061
- [54] P. Strolin, Nufact’99 Workshop, July 5-9th, Lyon
- [55] D.A. Harris, A. Para, hep-ex/0001035
- [56] W.W. Armstrong *et al*, Atlas Technical Proposal.
- [57] K.Kodama *et al*, CERN-SPSC-98-25, Oct 1998.
- [58] J. Altegoer *et al.* [NOMAD Collaboration], Nucl. Instrum. Meth. **A404**, 96 (1998).
- [59] A. Cervera *et al.*, “Golden measurements at a neutrino factory”, hep-ph/0002108.
- [60] R. Bernstein, in preparation.
- [61] C.H. Albright and S.M. Barr, hep-ph0002155 and hep-ph/0003251.
- [62] V. Barger, S. Geer, R. Raja, K. Whisnant; in preparation.
- [63] V. Barger, S. Geer, R. Raja, K. Whisnant; hep-ph/9911524, submitted to PRD (in press).
- [64] A. Donini *et al.*, hep-ph/9909254 and hep-ph/9910516., A. Kalliomaki, J. Maalampi and M. Tanimoto, hep-ph/9909301
- [65] K.S.McFarland, NuTeV collaboration, to be published in the proceedings of the XXXIIIrd Rencontres de Moriond (1998); J. Yu, NuTeV collaboration, to be published in the proceedings of the DIS98, Brussel, Belgium, Fermilab-Conf-98/200-E (1998)

- [66] W.G. Seligman *et al.*, “Improved determination of $\alpha(s)$ from neutrino nucleon scattering,” Phys. Rev. Lett. **79**, 1213 (1997).
- [67] J. P. Berge *et al.*, Z. Phys. **C49**, 187 (1991).
- [68] P. Annis [CHORUS Collaboration], Nucl. Instrum. Meth. **A409**, 629 (1998).
M. G. van Beuzekom *et al.* [CHORUS Collaboration], Nucl. Instrum. Meth. **A427**, 587 (1999). E. Eskut *et al.* [CHORUS Collaboration], Phys. Lett. **B434**, 205 (1998).
- [69] V. N. Gribov and L. N. Lipatov, Yad. Fiz. **15**, 1218 (1972), G. Altarelli and G. Parisi, Nucl. Phys. **B126**, 298 (1977).
- [70] U. K. Yang *et al.* [CCFR-NuTeV Collaboration], hep-ex/9906042.
- [71] F. Bergsma *et al.* [CHARM Collaboration], Phys. Lett. **B153**, 111 (1985).
- [72] G.T. Jones *et al.*, Z. Phys. C **43**, 527 (1989).
- [73] S. Adler, Phys.Rev.143, (1966), 1144-1155.
- [74] C. Boros *et al.*, hep-ph/9810220, Oct. 1998.
- [75] S.A. Kulagin, hep-ph/9812532, Aug. 1998.
- [76] K.J. Eskola *et al.* hep-ph/9906484, May, 1999.
- [77] A. C. Benvenuti *et al.* [BCDMS Collaboration], Z. Phys. **C63**, 29 (1994).
- [78] M. Vakili *et al.* [CCFR Collaboration], Phys. Rev. **D61**, 052003 (2000) [hep-ex/9905052].
- [79] D.T. Spayde *et al.* nucl-ex/9909010, Phys.Rev.Lett.84:1106-1109,2000
- [80] hep-ph/9810270 Title: Spin Physics and Polarized Structure Functions Authors: Bodo Lampe, Ewald Reya
- [81] R.D. Ball, S. Forte, and G. Ridolfi, Phys. Lett. **B378**, 255 (1996).
- [82] SMC, D. Adams *et al.*, Phys. Rev. D **56**, 5330 (1997).
- [83] J. Ellis and R.L. Jaffe, Phys. Rev. **D9**, 1444(1974); *ibid.* **D10**, 1669 (1974).
- [84] hep-ex/9804010 [abs, src, ps, other] : Title: A Small Target Neutrino Deep-Inelastic Scattering Experiment at the First Muon Collider Authors: Deborah A. Harris (1), Kevin S. McFarland (2) ((1) University of Rochester, (2) Massachusetts Institute of Technology)

- [85] Large Spin-Polarized Solid Hd Targets for Photonuclear Experiments at Brookhaven National Laboratory, with Q. Fan, X. Wei, M. Breuer, J.P. Didelez, M. Rigney, M. Lowry, A. Sandorfi, A. Lewis, S. Whisnant, Twelfth Intl. Symp. on High Energy Spin Physics, Amsterdam, September 1996, "Spin96" Conf. Proceedings, World Scientific, 365.
- [86] K. McFarland *et al.*, Eur. Phys. J. **C1** (1998) 509.
- [87] "The Potential for Neutrino Physics at Muon Colliders and Other Muon Storage Rings", B. King *et al*, to appear in *Physics Reports*.
- [88] P. Vilain *et al*, Phys. Lett. **B335** (1994) 248.
- [89] Bruce King, "High Rate Physics at Neutrino Factories", Proc. 23rd Johns Hopkins Workshop on Current Problems in Particle Theory, hep-ex/9911008.
- [90] E. Aitala *et al*, Phys. Rev. **D57** (1998) 13.
- [91] M. Artuso *et al*, "Search for $D^0 - \overline{D}^0$ Mixing", hep-ex/9908040.
- [92] P. F. Harrison and H. R. Quinn [BABAR Collaboration], "The BaBar physics book: Physics at an asymmetric B factory," SLAC-R-0504.
- [93] Bruce King, "High Rate Neutrino Detectors for Neutrino Factories", Proc. ICFA/ECFA Workshop "Neutrino Factories based on Muon Storage Rings" (nuFACT'99), hep-ex/0001043.
- [94] C.Arroyo, B.J.King *et. al.*, Phys. Rev. Lett. **72**, 3452 (1994).
- [95] K.S.McFarland *et al.*, CCFR, Eur. Phys. Jour. **C1**, 509 (1998)
- [96] R.Bernstein *et. al.*, NuTeV Collaboration, Fermilab-TM-1088 (1994).
- [97] E.A.Paschos and L. Wolfenstein, Phys. Rev. **D7**, 91 (1973)
- [98] A. Blondel *et al.*, Z. Phys. **C45**, 361 (1990).
- [99] H. Schellman, to be published in the proceedings of the Workshop on Physics at the First Muon Collider, Fermilab, Batavia, IL, USA, Nov. 1997.
- [100] D.A.Harris & K.S.McFarland, MIT-LNS-98-276, to be published in the proceedings of the Workshop on Physics at the First Muon Collider, Fermilab, Batavia, IL, USA, Nov. 1997
- [101] B.J.King, to be published in the proceedings of the Workshop on Physics at the First Muon Collider, Fermilab, Batavia, IL, USA, Nov. 1997.
- [102] U.K Yang and A. Bodek, *UR-1543*, Submitted to Phys. Rev. Lett, hep-ex/9809480 (1998)

- [103] U. Baur and M. Demarteau, “Precision Electroweak Physics at Future Collider Experiments,” Fermilab-Conf-96/423 (1996).
- [104] P. Villain *et al.*, Phys. Lett. **B335**:246 (1994). See also Phys. Lett. **B302**:351 (1993) and Phys. Lett. **B281**:159 (1992).
- [105] D. Yu. Bardin and V. A. Dokuchaeva, JINR E2-86-260 (1986).
- [106] U. Baur, “Electroweak Radiative Corrections to W Boson Production at the Tevatron”, SUNY-Buffalo preprint UB-HET-98-02, Sep 1998 (e-Print Archive: hep-ph/9809327).
- [107] E. Sather, Phys. Lett. **B274** (1992) 433.
- [108] M.Gronau, C.N. Leung, and J.L. Rosner, Phys. Rev. **D29**, 2539 (1984).
- [109] R. E. Shrock, Phys. Rev. **D24**, 1232 (1981).
- [110] T. Bolton, L. Johnson, and D. McKay, Phys. Rev. D **56** (1997) 2970.
- [111] A. Vaitaitis *et al.*, Phys. Rev. Lett. **83** (1999) 4943.
- [112] J. Formaggio *et al.*, Phys. Rev. Lett. **XXX** (2000) XXX.
- [113] *Review of Particle Physics* Eur. Phys. J. C. 3,320 (1998).
- [114] B.W.Lee and R.E.Shrock, Phys. Rev. **D16** 1444 (1977).
- [115] M.Frank, Phys. Rev. D60:093005 (1999).
- [116] G.C.McLaughlin and J.N.Ng, hep-ph/9909558.
- [117] J.F.Beacom and P.Vogel, Phys. Rev. Lett. **83**, 5222 (1999).
- [118] A.V.Derbin, Phys. of Atomic Nuclei, **57**, 222 (1994) [Yad. Fiz. **57**, 236 (1994)], and A.I.Derbin *et al.*, JETP Lett. **57**, 768 (1993).
- [119] D.A.Krakauer *et al.*, Phys. Lett. **B252**, 177 (1990); R.C.Allen *et al.*, Phys. Rev. **D47**, 11 (1993).
- [120] MFukugita and S.Yazaki, Phys. Rev. **D36** (1987) 3817.
- [121] R.Barbieri and R.N.Mohapatra, Phys. Rev. Lett. **61** (1988) 27, and J.M. Lattimer and J.Cooperstein, Phys. Rev. Lett. **61** (1988) 23.
- [122] Hendrick L. Bethlem, Giel Berden, and Gerard Meijer, Phys. Rev. Lett. **83**, pg 1558, 23 Aug. 1999. 1999.
- [123] Private discussions with Norbert Holtkamp, Fermilab.

- [124] See Steve Geer's talk at the 2-day meeting. Number of events (5000) was quoted for a 50 kTon detector at L=2800 km and a 20 GeV muon storage ring.
- [125] Review of Particle Properties, C. Caso *et. al.*, Euro. Phys. J. **C3**, 1 (1998).
- [126] H. Dreiner, hep-ph/9707435
- [127] Chris Quigg, private communication
- [128] K. Kodama *et. al.* (OPERA Collaboration), CERN/SPSC 98-25.
A. E. Asratyan *et. al.*, hep-ex/0002019